NMRF/MR/01/2014

MONSOON REPORT

Monsoon-2013:
Performance of NCMRWF Global Assimilation-Forecast Systems

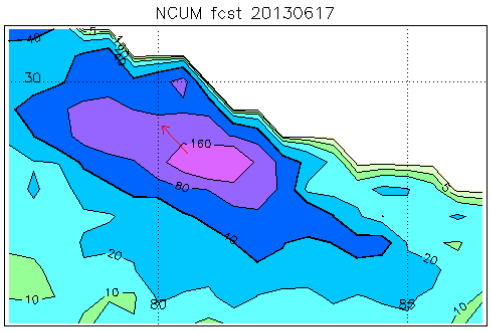

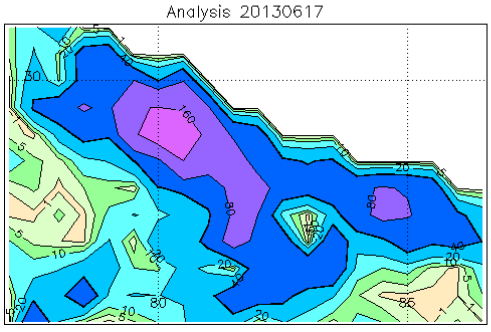

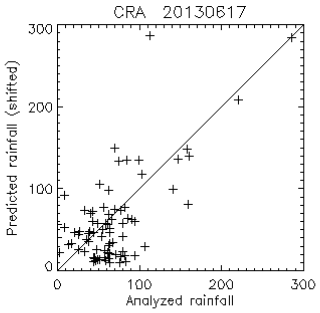

NCUM 72–96 fcst 20130617 n=80
(26.00°,77.50°) to (30.50°,86.00°)
Verif. grid=0.500° CRA threshold=40.0 mm/d

	Analysed	Forecast
# gridpoints ≥40 mm/d	62	51
Average rainrate (mm/d)	67.24	60.31
Maximum rain (mm/d)	285.80	286.80
Rain volume (km³)	14.60	13.09

Displacement (E,N) = [0.50°,−0.50°]

	Original	Shifted
RMS error (mm/d)	52.10	42.12
Correlation coefficient	0.454	0.664

Error Decomposition:

Displacement error	37.5%
Volume error	0.6%
Pattern error	61.9%

February 2014

National Centre for Medium Range Weather Forecasting
Earth System Science Organisation
Ministry of Earth Sciences
A-50, Sector 62, NOIDA – 201 309, INDIA

Please cite this report as given below:

NCMRWF, Ministry of Earth Sciences (MoES), Government of India, (February 2014): "**MONSOON-2013: Performance of the NCMRWF Global Assimilation Forecast Systems**", Report no. NMRF/MR/01/2014, 105 pages, Published by NCMRWF, A-50, Sector- 62, NOIDA, UP, INDIA-201309

Disclaimer:

The geographical boundaries shown in this report do not necessarily correspond to political boundaries.

Front Cover:

Front cover shows Contiguous Rain Areas (CRA) verification of the NCUM model predicted (Day-4) rainfall over Uttarakhand region valid for 03 UTC of 18th June 2013 along with observation.

This report was compiled and produced by:

Gopal R. Iyengar, Raghavendra Ashrit, Kuldeep Sharma and E.N. Rajagopal
NCMRWF/MoES

Acknowledgements:

Acknowledgement is due to NCEP/NOAA for providing the GFS assimilation-forecast system and the GEFS codes. Thanks are also due to the Met Office, UK for providing the forecast data as well as the Unified Model (UM).

For other details about NCMRWF, visit the website: **www.ncmrwf.gov.in**

Ministry of Earth Sciences
Earth System Science Organisation
National Centre for Medium Range Weather Forecasting (NCMRWF)

Document Control Data Sheet

S.No		
1	Name of Institute	National Centre for Medium Range Weather Forecasting (NCMRWF)
2	Document Number	NMRF/MR/01/2014
3	Date of Publication	February 2014
4	Title of the document	Monsoon-2013: Performance of NCMRWF Global Assimilation-Forecast System
5	Type of Document	Monsoon Report (MR), Scientific
6	Number of Pages and Figures	Pages 105 & Figures 78
7	Authors	Compiled by Gopal R. Iyengar, Raghavendra Ashrit, Kuldeep Sharma and E.N. Rajagopal
8	Originating Unit	National Centre for Medium Range Weather Forecasting (NCMRWF), Ministry of Earth Sciences (MoES), Government of India, NOIDA
10	Abstract	The NCMRWF high resolution global model real time forecasts based on the NGFS, NCUM, UKMO and NGEFS are verified during the monsoon season of 2013. The report compiles exhaustive account of the various verification scores taking into account large scale, synoptic and mesoscale processes that interplay during the monsoon season. While both deterministic models, NGFS and NCUM are the state of the art systems, NCUM with the 4DVAR assimilation seems to perform better; particularly in terms of rainfall organization and rainfall amounts. This is adequately supported by the higher forecast skill scores and lower forecast errors in NCUM compared to NGFS. For the first time an object-based spatial verification method, namely Contiguous Rain Areas (CRA) is adopted to quantify the rainfall forecast errors over India.
11	Security Classification	Unclassified
12	Distribution	Unrestricted
13	Key words	Southwest monsoon, Rainfall, monsoon onset, Satellite, Anomaly Correlation, Systematic errors, verification etc.

Executive Summary

The most important rainy period for an agro-economically driven country like India is the ‘southwest monsoon season’. The variability of the Indian summer monsoon rainfall affects the economy of the country significantly. The science pertaining to monsoon has progressed significantly in the last two decades due to an increase in the observations, improvement in understanding of underlying physical and dynamical processes and the availability of enhanced computing power.

NCMRWF constantly strives to imbibe the latest technologies in terms of data assimilation and modeling techniques to capture the monsoon system in a more realistic way. The global high resolution assimilation-forecast system based on Global Forecast System (GFS) of National Centers for Environmental Prediction (NCEP), USA was implemented in 2007 at NCMRWF. Since then real time runs of that system are being carried out initially at T254L64 resolution, upgraded to T382L64 in 2010 and then to T574L64 in 2012. Verification/diagnostics of the analysis - forecast products is a crucial component of research and development activity in NCMRWF.

The NCMRWF version of the Unified Model (NCUM), which also has high resolution (N512L70), is used to produce forecasts out to day-10. The NCUM at a horizontal resolution of about 25 km and 70 levels in the vertical along with its associated 4D-VAR data assimilation scheme is used for generating the initial conditions.

The NCMRWF Global Ensemble Forecast System (NGEFS) is used to generate real time probabilistic forecasts out to Day-10. The 20-member ensemble system has horizontal resolution of T190L28 (~70km).

A comprehensive set of diagnostics not only provides a summary of the model's prediction, but also indicates the suitability of the model for a variety of applications. Performance evaluation reports are generated on a routine basis for comparing the skill of the NCMRWF analysis - forecast system vis-à-vis those of other major global NWP centres.

This report summarizes detailed verification and intercomparison of the NCMRWF model forecasts during monsoon (JJAS) of 2013. The NCMRWF Global Forecast System (NGFS) and the NCMRWF version of the Unified Model (NCUM) are the two deterministic models examined. Additionally the 20 member NCMRWF Global Ensemble Forecast System (NGEFS) is also examined.

- Chapter 1 provides a summary of the systematic errors of the forecast wind, temperature and humidity etc., for lower level (850 hPa), and upper level (200 hPa) is carried out against the respective model analysis. The purpose of the analysis is to characterize, describe and compare the model forecast errors of the above systems using a select set of measures that are widely used world over. Systematic error, Root Mean Square Error (RMSE), Mean Error (ME) are employed to summarize the results.
- Chapter 2 further quantifies the forecast errors and provides the intercomparison of the verification scores among the forecast systems over different regions Global (G2), Tropics (Tro), and RSMC region covering the South Asian monsoon region. The results indicate improved forecast skill in the NGEFS over the NGFS particularly at longer lead time. Among the deterministic systems, NCUM consistently shows higher Anomaly correlation and lower RMSE compared to NGFS particularly at longer lead times.
- Chapter 3 summarizes the rainfall forecast verification. The verification of the model forecast rainfall against IMD-NCMRWF merged daily rainfall data available at 0.5°, (denoted as NMSG) is presented from 1^{st} June through 30^{th} Sept 2013. Verification results are illustrated in terms of standard set of skill scores like Probability of detection (POD), Success Ratio (SR), Threat Score (TS), Equitable Threat Score (ETS) etc. Additionally, for the first time spatial verification of the rainfall forecasts is presented based on the Contiguous Rain Area (CRA) method which helps one to decompose the rainfall forecast errors in to errors due to pattern, displacement and volume errors.
- Chapter 4 presents the verification of the forecast rainfall averaged over meteorological sub-divisions and all over India. The average rainfall over different regions is compared with the reported rainfall amounts and the

anomalies to yield an insight into the model's performance in terms of special aggregated rainfall.

- Chapter 5 presents the dynamical monsoon indices based on the model analysis and the forecasts to provide verification against the observations as well as for intercomparison among the models.
- Chapter 6 documents the performance of the NGFS and NCUM models in predicting the circulation and rainfall associated with the monsoon depressions. The JJAS 2013 features two depressions. Both the cases have been studied using the CRA technique to quantify the forecast rainfall biases especially during the monsoon depressions.

The report compiles exhaustive account of the various verification scores taking into account large scale, synoptic and mesoscale processes that interplay during the monsoon season. While both deterministic models, NGFS and NCUM are the state of the art systems, NCUM with the 4DVAR assimilation seems to perform better; particularly in terms of rainfall organization and rainfall amounts. This is adequately supported by the higher forecast skill scores and lower forecast errors in NCUM compared to NGFS.

Contents

Chapter 1: Systematic Errors

Gopal R. Iyengar and Kuldeep Sharma

1. Introduction

This report summarizes the results of an evaluation of the model forecast errors of the NCMRWF Global Forecasting System (GFS), and the NCMRWF version of the Unified Model (NCUM) over India, during the Southwest Monsoon season (JJAS) of 2013. The GFS (T574L64) has a horizontal resolution of about 22 km and 64 levels in the vertical. The GFS uses 3D-VAR data assimilation scheme for generating the initial conditions. The NCUM (N512L70) has a horizontal resolution of about 25 km and 70 levels in the vertical. The 4D-VAR data assimilation scheme is used for generating the initial conditions in the NCUM.

The purpose of the analysis is to characterize, describe and compare the model forecast errors of the above systems using a select set of measures which are widely used and also well understood. The significant points pertaining to this comparison are given below.

- The comparison is done for 24hr, 48hr, 72hr, 96hr and 120hr forecasts against the analysis from the respective forecast-analysis system for 00UTC. The period of the analysis is 1 June to 30 September (122 days) which is the Southwest Monsoon Season.
- It was carried out on a regular 1^{o} latitude-longitude grid (which is coarser than the model grids) and on standard pressure levels (1000, 925, 850, 700, 600, 500, 400, 300, 250, 200, 150 and 100hPa levels). Grid points lying below altitudes corresponding to a pressure surface were excluded from the analysis (masked). No seasonal trend removal was used in this evaluation.
- The parameters considered are: air temperature (TEMP), relative humidity (RH), zonal wind (U) and the meridional wind (V).
- The scores considered are: Systematic error, Root Mean Square Error (RMSE), Mean Error (ME), Standard Deviation and Time series of daily spatial RMSE.

Though we carried out a comprehensive analysis, it is practically not possible and is not necessary to describe every aspect of the results of the analysis. We include only a limited but the most significant and useful subset of the analysis results.

2. Forecast Errors and Mean Monsoon Circulation

Here we present the model forecast errors expressed in terms of systematic error and Root Mean Square Error (RMSE), with an aim to provide qualitative description of the spatial distribution of errors.

2.1. Systematic errors in wind at 850 and 200hPa

Figures 1-2 (a-d) depict the mean analysis and model forecast systematic errors at 850hPa level from the GFS and NCUM systems respectively. The panel (a) corresponds to the mean analysis and the panels b, c and d correspond to the systematic errors in Day-1, Day-3 and Day-5 forecasts respectively.

The cross equatorial flow (CEF) is one of the main characteristic features of low level monsoon circulation that stands out as the strongest low level flow on the earth during the boreal (northern) summer. The wind speed in the core of the Somali jet exceeds 25 m/s (Findlater, 1969a), the jet core is located about 1.5 km above sea level, 200-400 km east of the east African highlands. This core shifts southward as it approaches and crosses peninsular India to enter the Bay of Bengal. This CEF, which is now referred to as the Somali jet, is an essential component of the Asian monsoon system. It transports moisture from the southern Indian Ocean to south Asia, connects the Mascarene high and Indian monsoon trough, and completes the lower branch of the Hadley cell of the Asian monsoon.

The GFS forecasts show anomalous south-westerlies and westerlies over the north-west parts of India and adjoining areas and southerlies over the eastern parts of the peninsula. These features seem to a form an anomalous anti-cyclonic circulation over the central and peninsular parts of India and suggest that there is a weakening of the whole monsoon flow pattern over India. An anomalous cyclonic circulation is also seen over the northern parts of Bay of Bengal.

The most prominent systematic error seen in the NCUM forecasts at 850hPa is the easterly bias over the equatorial Indian Ocean region. The easterly bias is also seen at 700 and 500 hPa levels (figures not shown). The NCUM forecast also show an anomalous anti-cyclonic circulation over the central and eastern parts of India. This feature is similar to that seen in the GFS, however the magnitude of errors are comparatively smaller in the NCUM forecasts. The NCUM forecasts also show an easterly bias near the foothills and the Arabian Sea.

The strong cross-equatorial low level jet stream with its core around 850 hPa is found to have large intraseasonal variability. Figures 3-4 show the Hovmoller diagram of zonal wind (*u*) of 850 hPa averaged over the longitude band 60–70E for the period 1 June–30 September 2013 for the GFS and NCUM analysis and forecasts respectively. The top panel in each figure shows the analysis and the middle and the lower panel depict the Day-3 and Day-5 forecasts respectively. The active monsoon spells are characterized by strong cores of zonal wind.

The zonal wind attained strength of more than 20 m/s in the second and third week of June and second fortnight week of July. It gradually weakened during the latter half of the season. The presence of the strong core during second and third week of June along with other synoptic features helped in the advance of the monsoon over the entire country by 16th June. The GFS Day-3 and Day-5 forecasts capture reasonably well the variability in the strength of the zonal wind. However the magnitude of the zonal wind is slightly weaker in the Day-5 forecasts as compared to the analyses. The Day-5 forecasts show the appearance of the core a few days later as compared to the analyses. The magnitude of the zonal wind in the NCUM analyses is higher as compared to the GFS analyses. The NCUM forecasts are able to capture better the strong cores of zonal wind as compared to the GFS forecasts.

Figures 5-6 show the Hovmoller diagram of zonal wind (*u*) of 850 hPa averaged over the longitude band 85–90E for the period 1 June–30 September 2013 for the GFS and NCUM analysis and forecasts respectively. The top panel in each figure shows the analysis and the middle and the lower panel depict the Day-3 and Day-5 forecasts respectively.

The GFS and NCUM analysis shows three prominent cases of northward movement of the core of zonal wind: first in the second week of June, second in the

last week of July, associated with the depression over the north-east Bay of Bengal and third in the second week of August associated with the formation of another depression in the north-east Bay of Bengal. However, the strength of the westerlies is high in NCUM compared to GFS.

An extremely important component of the monsoon circulation is the upper level (200hPa) subtropical anticyclone which normally extends from the Middle East region to southeastern Asia along approximately 27.5°N. This 200 hPa anticyclone normally develops during June and reaches full strength in July and August. Accompanying this evolution is a pronounced shift of the mid-latitude westerly winds from south to north of the Tibetan Plateau by mid June.

Figures 7-8 (a-d) depict the mean analysis and model forecast systematic errors at 200hPa level from the GFS and NCUM respectively. The panel (a) corresponds to the mean analysis and panels b, c and d correspond to the systematic errors in Day-1, Day-3 and Day-5 forecasts respectively. GFS analysis shows strong subtropical westerlies over India. Anomalous westerlies are seen over the southern parts of India and adjoining regions in both the models, thereby weakening the Tropical Easterly Jet. NCUM also show strong subtropical westerly jet while the Day-1 forecasts show easterly bias over southern parts of India.

2.2 Systematic errors in temperature at 850 and 200 hPa.

Figures 9-10 (a-c) depict the forecast systematic errors of temperature at 850 hPa level from the GFS and NCUM respectively. The panels a, b and c correspond to the systematic errors in Day-1, Day-3 and Day-5 forecasts respectively. In the Day-1 forecasts, the GFS shows a warm bias in the lower troposphere over the northwest parts and plains of India. This warm bias extends to the eastern parts of India in the Day-3 and Day-5 forecasts. The NCUM forecasts shows a warm bias over the over the northwest parts and plains of India. The NCUM forecasts also show a strong cold and warm bias over the West and East Asian regions respectively.

Figures 11-12 (a-c) depict the mean analysis and model forecast systematic errors of temperature at 200 hPa level from the GFS and NCUM respectively. The panels a, b and c correspond to the systematic errors in Day-1, Day-3 and Day-5

forecasts respectively. The GFS Day-5 forecasts show a warm bias of the order of 1 deg over most parts of India and the eastern Indian Ocean. The NCUM forecasts show a cod bias over most parts of India and the adjoining oceanic regions.

.

2.3 Systematic errors in relative humidity at 850 hPa.

Figures 13-14 (a-c) depict the mean analysis and model forecast systematic errors of relative humidity at 850hPa level from the GFS and NCUM respectively. The panels a, b and c correspond to the systematic errors in Day-1, Day-3 and Day-5 forecasts respectively. The GFS forecasts show a dry bias over the central and southern parts of India. A wet bias is seen over the northern plains near the foothills. The magnitude of the bias is comparable in both the models over India.

3. Root Mean Square Error (RMSE)

The Root Mean Square Error is given by

$$RMSE = \sqrt{\frac{1}{N}\sum_{i=1}^{N}(F_i - O_i)^2}$$

where, Fi and *Oi represent* forecast and observed fields respectively. The RMSE measures the "average" error, weighted according to the square of the error. However, it does not indicate the direction of the deviations. With values ranging from 0 to ∞, *RMSE* puts greater influence on large errors than smaller errors, which may be a good thing if large errors are especially undesirable, but may also encourage conservative forecasting.

The geographical distributions of the RMSE of the forecasts (for each month and the season as a whole) were calculated from the difference at each grid point on each day. Grid points lying below ground were excluded from the computation. These charts are given for all the variables at the pressure levels 850 and 200 hPa. The time series of the spatial root mean square error for a variable over India (68-95°E,5-38°N), as a time series of 1, 2, 3, 4 and 5 day forecasts were computed for all the variables at 850, 700, 500 and 200 hPa levels. In combination with the other scores the time series provides useful information on consistency in the error characteristics of the forecast during the season (day to day variations in forecast errors).

The RMSE of Day-1, Day-3 and Day-5 forecasts of winds (zonal and meridional), geopotential height, temperature and relative humidity for GFS and NCUM forecasts are discussed in detail below.

3.1 RMSE in Zonal wind at 850 and 200 hPa

Panels in Fig. 15 show the RMSE of 850 hPa zonal wind for Day-1, Day-3 and Day-5 forecasts of the NCUM and GFS respectively. The magnitude of RMSE at 850 hPa is of the order of 2-4 m/s in Day-1 forecast in all the model forecasts. The GFS shows a marked increase in the RMSE from Day-1 to Day-5 forecast as compared to NCUM, especially over some parts of central India and northern plains of India. Fig. 16 is same as Fig. 15 but for 200 hPa level. At 200 hPa, the magnitude varies from 2-4 m/s in NCUM and 2-6 m/s in Day-1 forecast of GFS over the Indian region. GFS shows a considerable increase in RMSE from Day-1 to Day-5 forecast and has relatively higher magnitude as compared to NCUM over the Indian mainland. But RMSE in Day-5 forecast of NCUM is considerably high as compared to GFS over the equatorial Indian Ocean.

3.2 RMSE in Meridional wind at 850 and 200 hPa

Panels in Fig. 17 are same as in Fig. 15 but for meridional winds. At 850 hPa, the magnitude of RMSE in meridional component of the wind is of the order of 2-4 m/s in Day1 forecast in both the models over the Indian and neighborhood region. The GFS shows a consistent increase in RMSE from Day-1 to Day-5 forecast with the magnitude of about 4-6 m/s as compared to 2-4 m/s seen in the NCUM. Fig. 18 is same as Fig. 16 but for meridional winds. The magnitude of RMSE is of the order of 2-4 m/s and 2-6 m/s in Day1 forecasts of the NCUM and GFS models respectively over the Indian region. The GFS shows a consistent increase (more than 6 m/s) in RMSE from Day-1 to Day-5 forecast.

3.3 RMSE inTemperature at 850 and 200 hPa

Panels in Fig. 19 show the RMSE of 850 hPa temperature forecasts. At 850 hPa, the magnitude of RMSE is of the order of 1.5-2.5 K in Day-1 forecast over the northwest and plains of India for GFS whereas the magnitude is slightly smaller in

NCUM. There is increase in RMSE from Day-1 to Day-5 forecast in both the model forecasts. The GFS shows consistently higher RMSEs over the northwest parts and plains of India as compared to NCUM. Fig. 20 shows the RMSE of 200 hPa temperature forecasts. At upper level (200 hPa), the magnitude of the errors is less as compared to the lower level (850 hPa). The order of the magnitude at 200 hPa is ~0.5-1 K over the Indian mainland and its neighborhood in NCUM while in GFS it varies from ~0.5-1.5 K.

3.4. RMSE in Relative Humidity at 850 and 200 hPa

Panels in Fig. 21 show the RMSE of 850 hPa relative humidity forecasts. The Day-1 forecasts errors in both the models are similar over the Indian mainland. However, in Day-3 and Day-5 both models show contrasting errors over inland and equatorial Indian Ocean i.e., higher errors over Northern Arabian Sea and North-west parts of India in NCUM whereas GFS shows higher errors over equatorial Indian Ocean. Panels in Fig. 22 show the RMSE of 200 hPa relative humidity forecasts. At 200 hPa, the RMSE in NCUM model is less as compared to the GFS model. The magnitude of RMSE is almost constant up to 5th day forecast for NCUM models over the Indian mainland while it is consistently increasing for GFS models and goes more than 40 % in the Day5 forecasts.

4. Velocity Potential and Divergent wind field

The summer monsoon circulation is generally visualized as a large scale convergence of mass and moisture over India and adjoining Southeast Asia in the lower levels, and a strong upper level divergence aloft. In order to examine the characteristics of the summer monsoon divergent circulation, the mean analyses and Day-5 forecast error of velocity potential and divergent wind field at 850 and 200hPa levels from the GFS are presented in figures 23 and 24 respectively. At 850 hPa, the major centre of the low level convergence is seen over the northern parts of Bay of Bengal and the tropical west Pacific. The 200 hPa velocity potential and divergent wind field is dominated by the outflow from the divergent centre over the summer monsoon region. The GFS shows weakening of the low level convergence/upper level

divergence over the tropical west Pacific. Similar figures (25 and 26) from NCUM show low-level convergence errors over the western equatorial Indian Ocean which is associated with the excessive precipitation over the region.

5. Verification against analyses and observations.

At NCMRWF, a set of standard verification scores suggested by WMO/CBS are generated every month on a routine basis. The verification scores are computed for various regions both against the respective analysis and observations. The verification scores are exchanged among the WMO designated Global Data-Processing and Forecasting System (GDPFS) centers. In addition to the various regions suggested by WMO, another region over India (6-36N, 66-96E) has been added for verification against analysis and observations.

Tables 1 and 2 show the RMSE of Day-3 forecast winds at 850 and 200 hPa against the observations over India from GFS and NCUM during the Southwest Monsoon season (JJAS) of 2013. The NCUM has lower RMSE both at 850 and 200 hPa levels as compared to the GFS.

Table 1: RMSE (m/s) of Day-1 to Day-5 Forecasts of 850 hPa Winds over India

Month		Day-1	Day-2	Day-3	Day-4	Day-5
Jun 2013	GFS	5.1	5.6	6.2	6.6	6.8
	NCUM	5.3	5.6	5.9	6.1	6.2
Jul 2013	GFS	5.8	6.2	6.7	7.0	7.5
	NCUM	5.9	6.3	6.7	6.9	7.0
Aug 2013	GFS	5	5.5	5.9	6.3	6.6
	NCUM	5.2	5.4	5.6	5.7	5.9
Sep 2013	GFS	3.7	4	4.5	4.9	5.2
	NCUM	3.6	3.9	4.2	4.4	4.6

Table 2: RMSE (m/s) of Day-1 to Day-5 Forecasts of 200 hPa Winds over India

Month		Day-1	Day-2	Day-3	Day-4	Day-5
Jun 2013	GFS	7.1	7.5	7.6	7.6	8.2
	NCUM	6.6	6.9	7.2	7.4	7.8
Jul 2013	GFS	6.3	6.3	6.5	6.8	6.9
	NCUM	5.6	5.8	6	6.2	6.5
Aug 2013	GFS	5.7	5.9	6.1	6.4	6.5
	NCUM	5.1	5.3	5.7	5.9	6.0
Sep 2013	GFS	5.1	5.3	5.4	5.9	6.2
	NCUM	6.2	5	5.2	5.5	5.7

6. Improvement in the skill of the forecasts at NCMRWF during 2005-2013

The Figs. 27 (a) and (b) shows the RMSE of the magnitude of the 850hPa wind vector (RMSEV) of the Day-3 forecasts against the radiosonde observations over India from the NCMRWF GFS model since January 2005 (blue) and the NCUM since April 2013 (pink).

The most notable feature of the error variation is its seasonal cycle with the winter months having least error and the Southwest Monsoon having the largest error. The overall decrease in the RMSEV can be attributed to the increase in the resolution of the model, increase in the amount of data being assimilated, improvements in data assimilation techniques.

The comparison of the scores since April 2013 (Fig. 27b) shows that the NCUM forecasts have relatively lower RMSE values as compared to the GFS.

7. Summary

- The systematic errors in the 850 hPa winds in GFS and NCUM forecasts show anomalous anti-cyclonic circulation over the central and peninsular parts of India and suggest that there is a *weakening of the whole monsoon flow pattern* over India.
- The NCUM forecast winds at 850hPa prominently show *easterly bias* over the *equatorial Indian Ocean* region and over the *plains adjoining the Himalayas*.
- The systematic errors in the 850 hPa temperature suggest that the Day-1 forecasts of GFS and NCUM show a *warm bias in the lower troposphere* over the northwest parts and plains of India which extends to the eastern parts of India in the Day-3 and Day-5 forecasts.
- The systematic errors in the 850 hPa relative humidity suggest that the GFS forecasts have a dry bias over the central and southern parts of India. A wet bias is seen over the northern plains near the foothills. The magnitude of the bias is comparable in both the models over India.

- The RMSE of Day-3 forecast winds at 850 and 200 hPa winds against the radiosonde observations over India show that NCUM has lower RMSE both at 850 and 200 hPa levels as compared to the GFS.
- The RMSE in the Day-3 forecast 850 hPa meridional wind (v) shows variation is its seasonal cycle with the winter months having least error and the Southwest Monsoon having the largest error with an overall decreasing trend.
- The overall decrease in the RMSEV can be attributed to the increase in the resolution of the model, increase in the amount of data being assimilated, improvements in data assimilation techniques.
- The comparison of the scores since April 2013 shows that the NCUM forecasts have relatively lower RMSEV values as compared to the GFS.

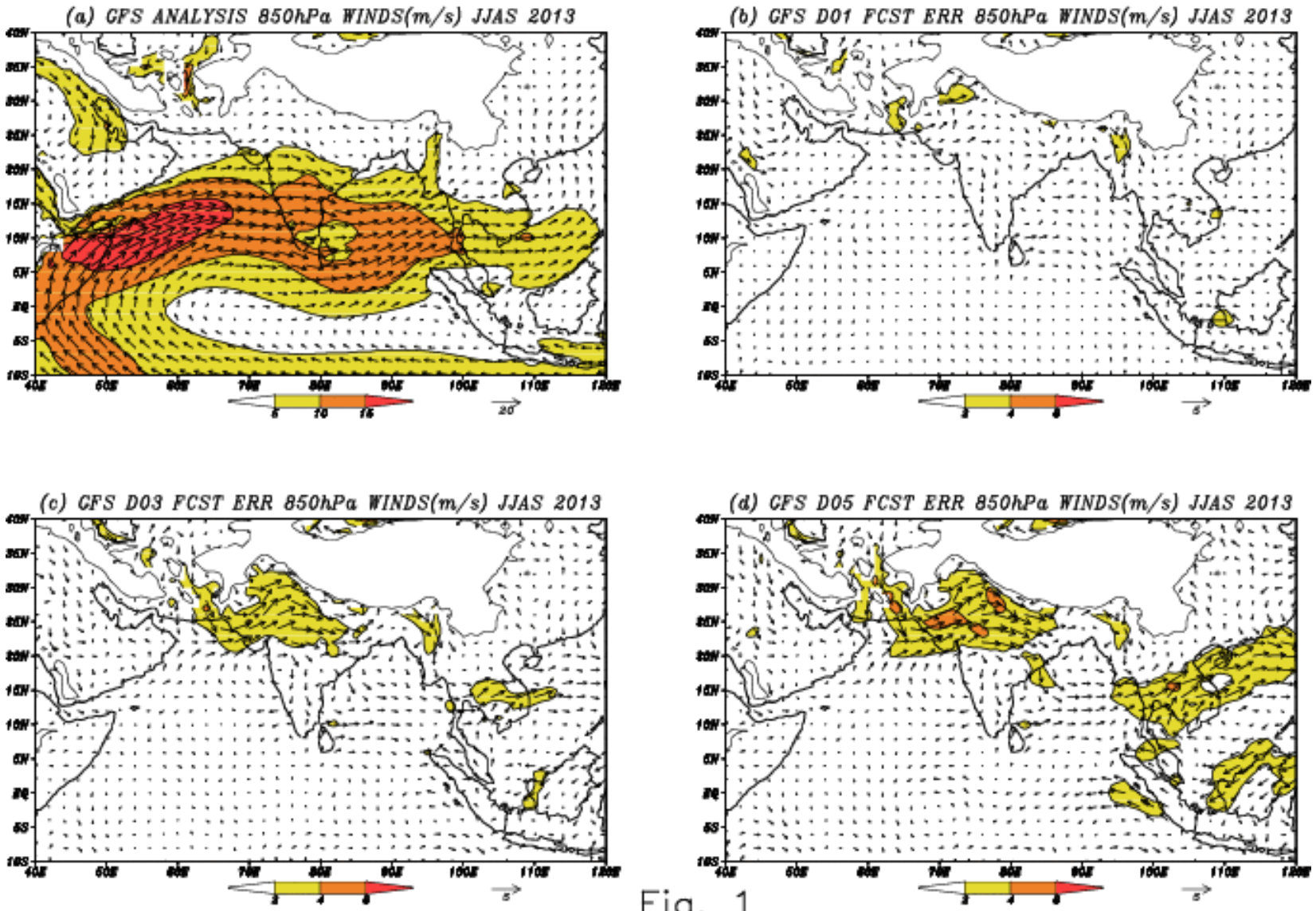
(a) GFS ANALYSIS 850hPa WINDS(m/s) JJAS 2013
(b) GFS D01 FCST ERR 850hPa WINDS(m/s) JJAS 2013
(c) GFS D03 FCST ERR 850hPa WINDS(m/s) JJAS 2013
(d) GFS D05 FCST ERR 850hPa WINDS(m/s) JJAS 2013

Fig. 1

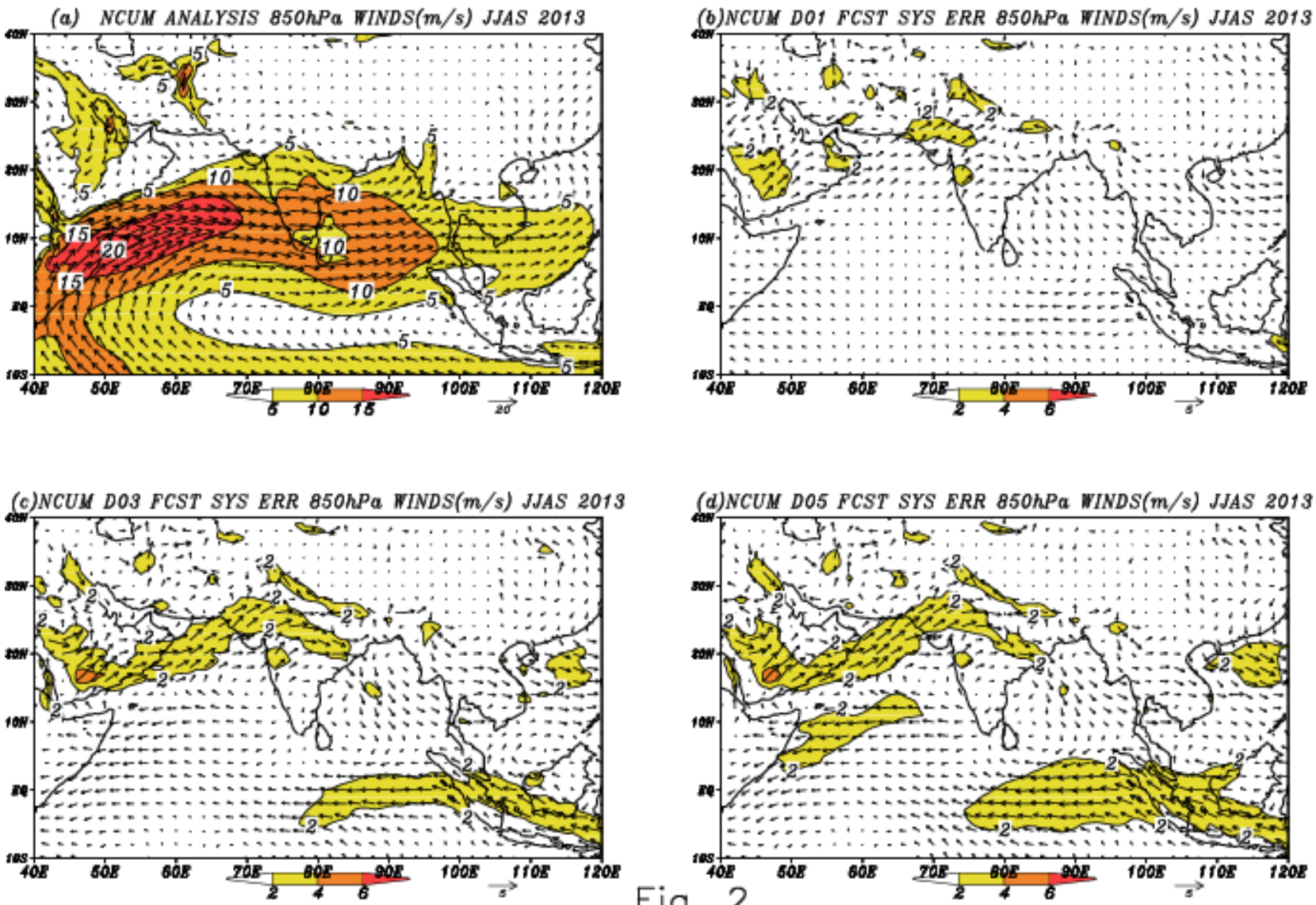
(a) NCUM ANALYSIS 850hPa WINDS(m/s) JJAS 2013
(b)NCUM D01 FCST SYS ERR 850hPa WINDS(m/s) JJAS 2013
(c)NCUM D03 FCST SYS ERR 850hPa WINDS(m/s) JJAS 2013
(d)NCUM D05 FCST SYS ERR 850hPa WINDS(m/s) JJAS 2013
40E
50E
60E
70E
80E
90E
100E
110E
120E
40N
30N
20N
10N
EQ
10S
5 10 15
2 4 6

Fig. 2

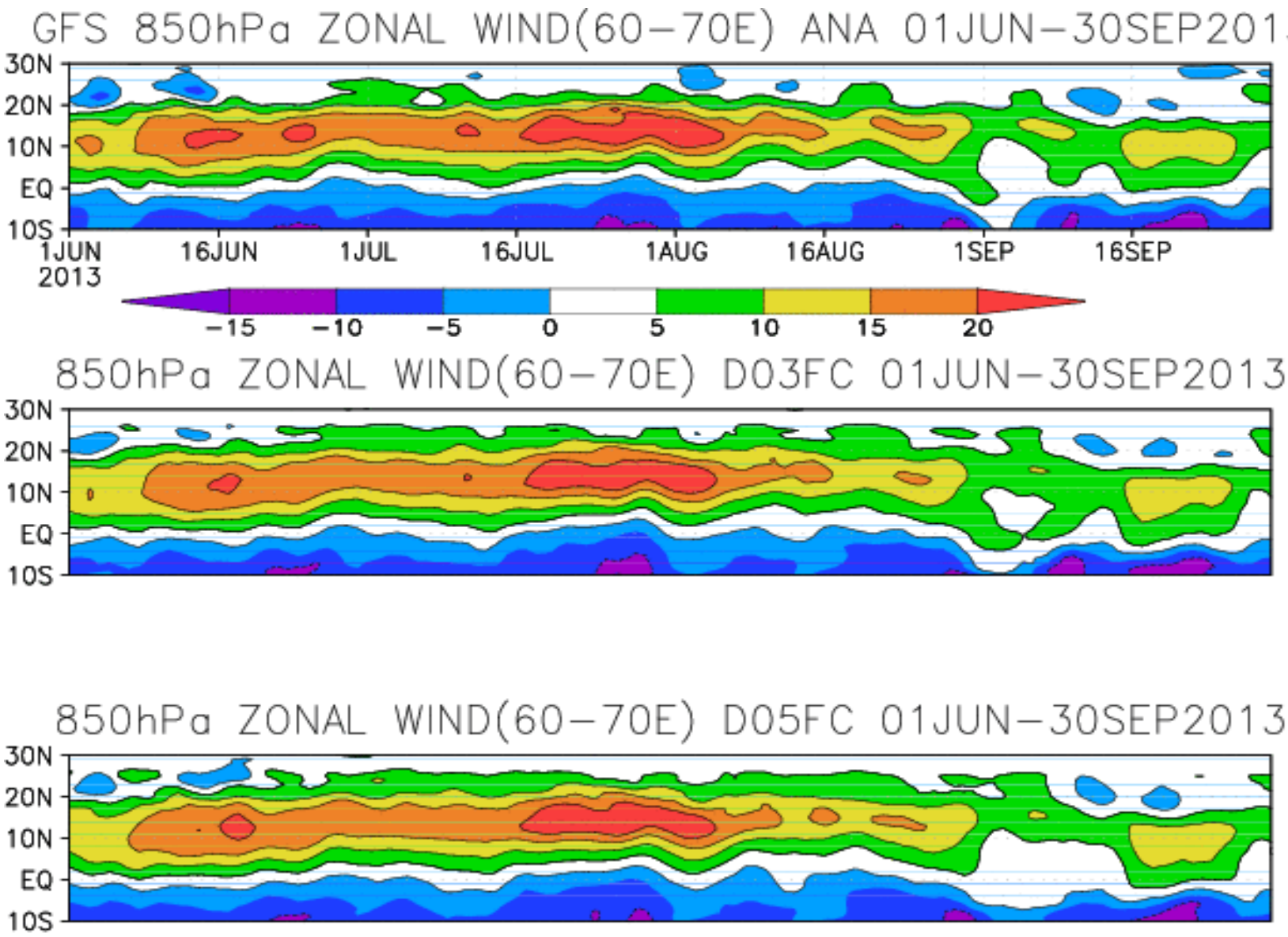
GFS 850hPa ZONAL WIND(60-70E) ANA 01JUN-30SEP2013
30N
20N
10N
EQ
10S
1JUN
2013
16JUN
1JUL
16JUL
1AUG
16AUG
1SEP
16SEP
-15
-10
-5
0
5
10
15
20
850hPa ZONAL WIND(60-70E) D03FC 01JUN-30SEP2013
850hPa ZONAL WIND(60-70E) D05FC 01JUN-30SEP2013

Fig. 3

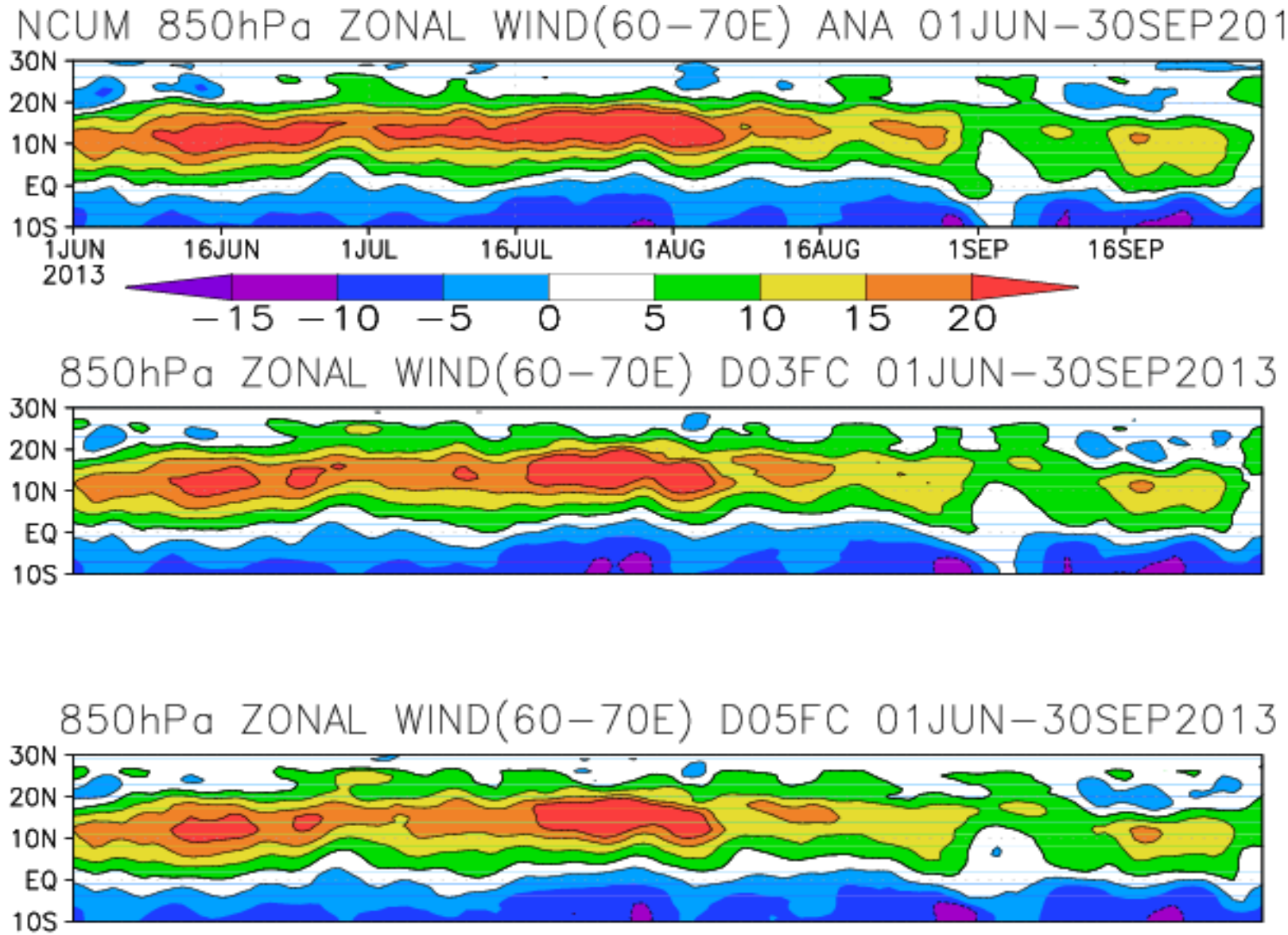
NCUM 850hPa ZONAL WIND(60–70E) ANA 01JUN–30SEP2013
30N
20N
10N
EQ
10S
1JUN
2013
16JUN
1JUL
16JUL
1AUG
16AUG
1SEP
16SEP
−15 −10 −5 0 5 10 15 20
850hPa ZONAL WIND(60–70E) D03FC 01JUN–30SEP2013
850hPa ZONAL WIND(60–70E) D05FC 01JUN–30SEP2013

Fig. 4

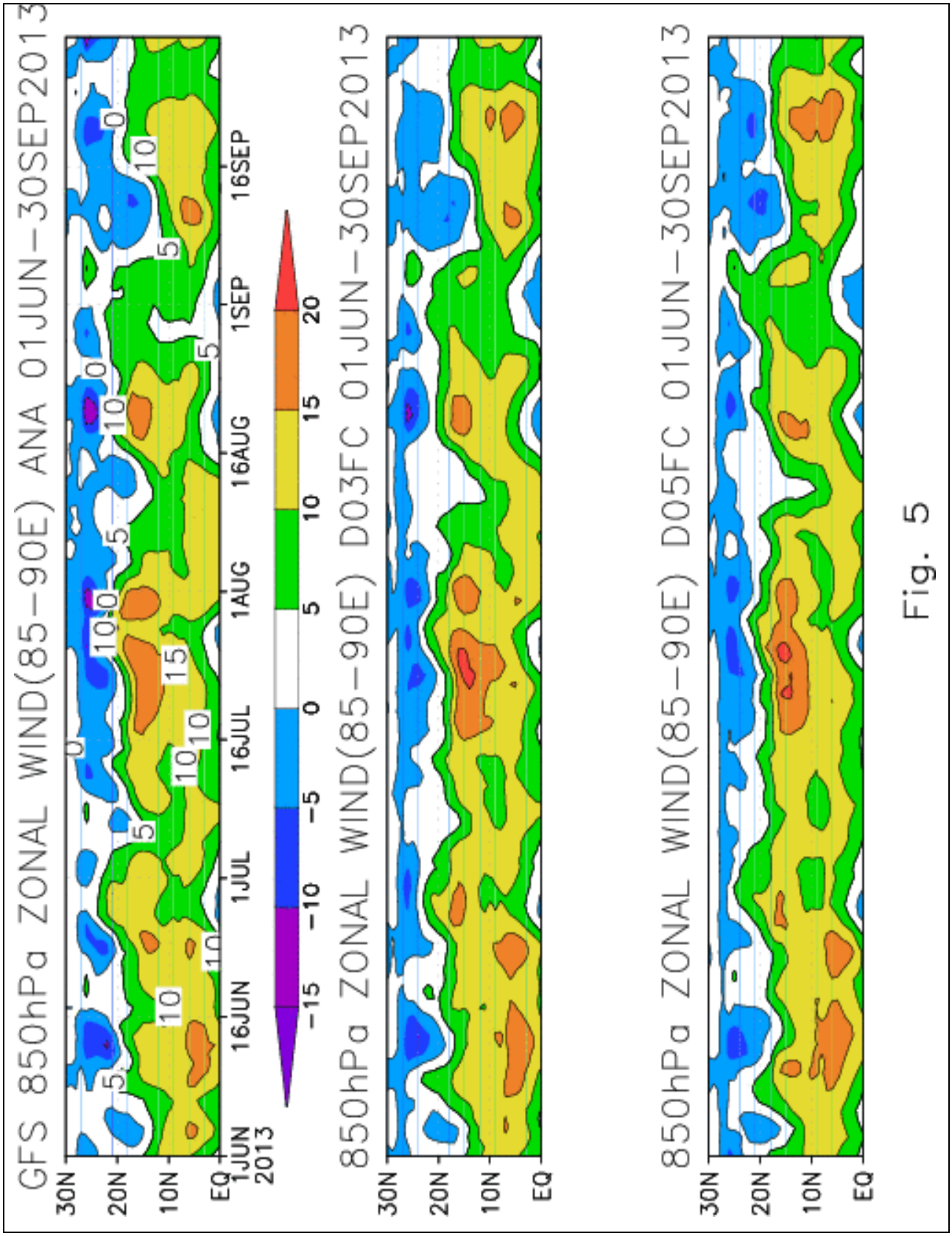
GFS 850hPa ZONAL WIND(85-90E) ANA 01JUN-30SEP2013
850hPa ZONAL WIND(85-90E) D03FC 01JUN-30SEP2013
850hPa ZONAL WIND(85-90E) D05FC 01JUN-30SEP2013
30N
20N
10N
EQ
1JUN 2013
16JUN
1JUL
16JUL
1AUG
16AUG
1SEP
16SEP
-15
-10
-5
0
5
10
15
20

Fig. 5

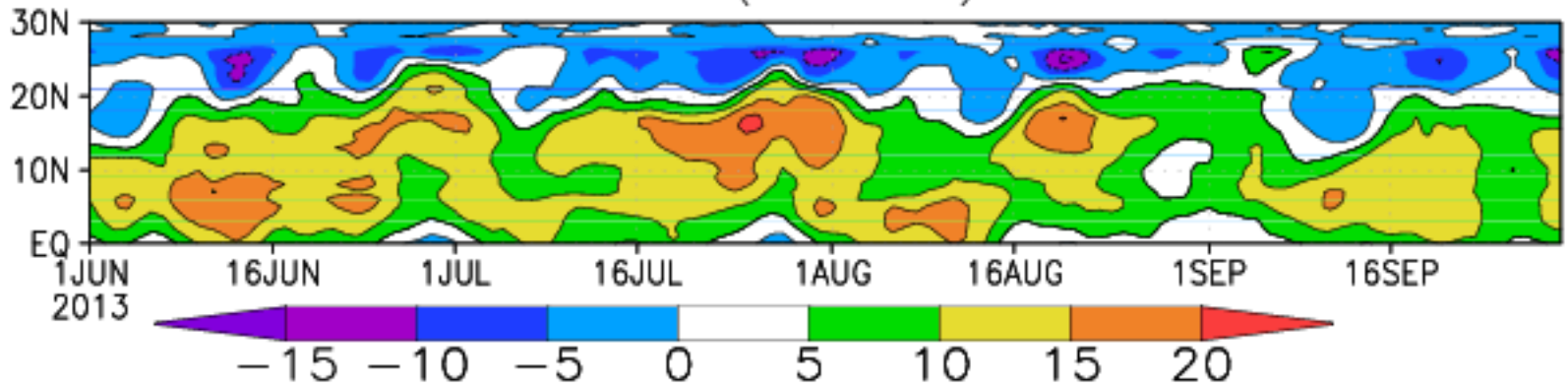
NCUM 850hPa ZONAL WIND(85-90E) ANA 01JUN-30SEP2013
30N
20N
10N
EQ
1JUN
2013
16JUN
1JUL
16JUL
1AUG
16AUG
1SEP
16SEP
-15 -10 -5 0 5 10 15 20

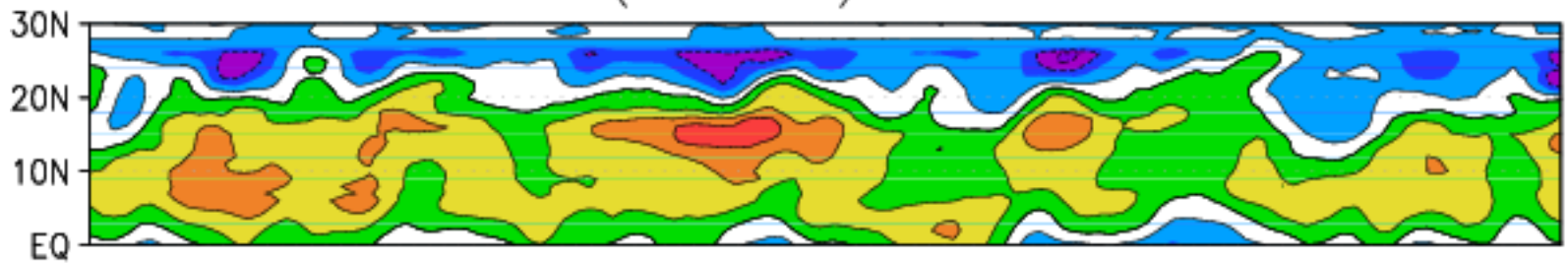
850hPa ZONAL WIND(85-90E) D03FC 01JUN-30SEP2013
30N
20N
10N
EQ

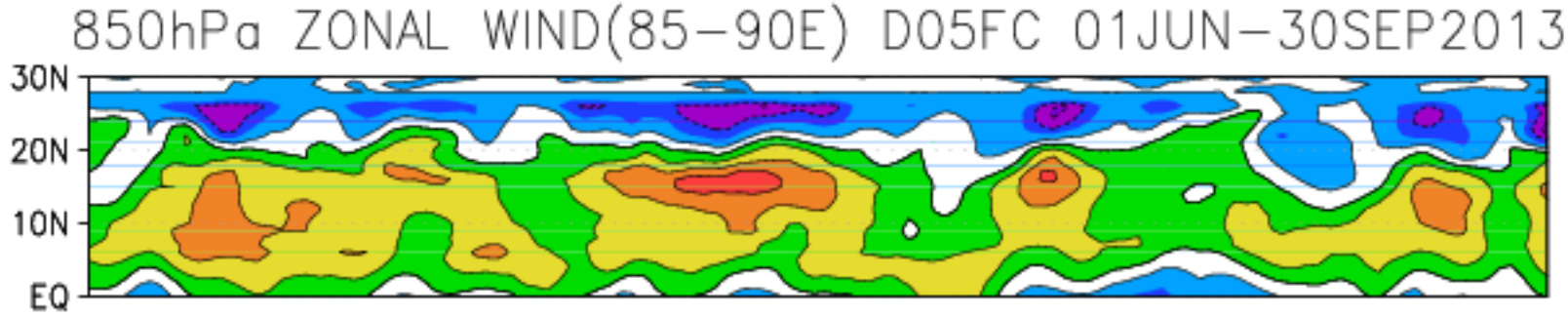
850hPa ZONAL WIND(85-90E) D05FC 01JUN-30SEP2013
30N
20N
10N
EQ

Fig. 6

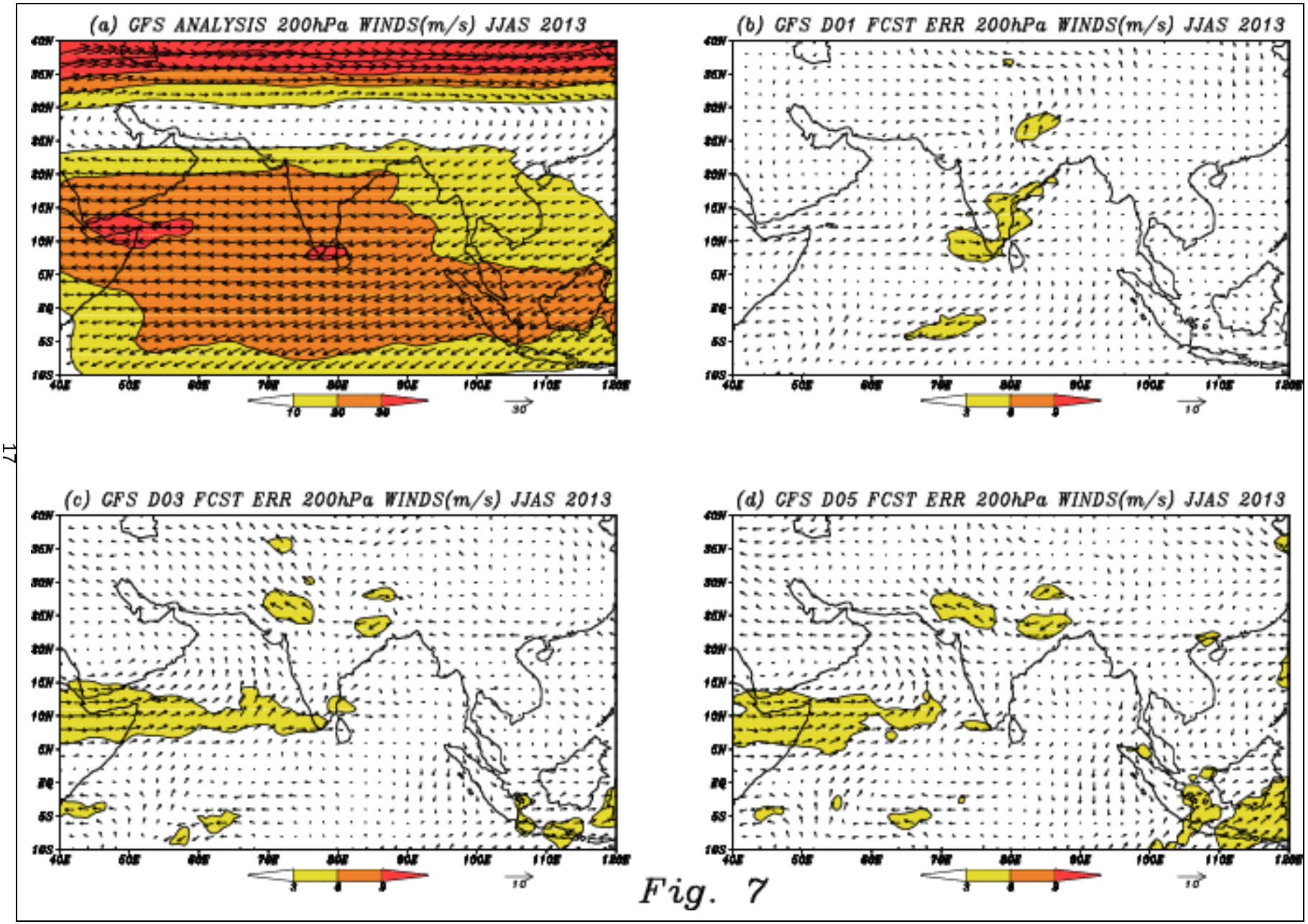
(a) GFS ANALYSIS 200hPa WINDS(m/s) JJAS 2013
(b) GFS D01 FCST ERR 200hPa WINDS(m/s) JJAS 2013
(c) GFS D03 FCST ERR 200hPa WINDS(m/s) JJAS 2013
(d) GFS D05 FCST ERR 200hPa WINDS(m/s) JJAS 2013

Fig. 7

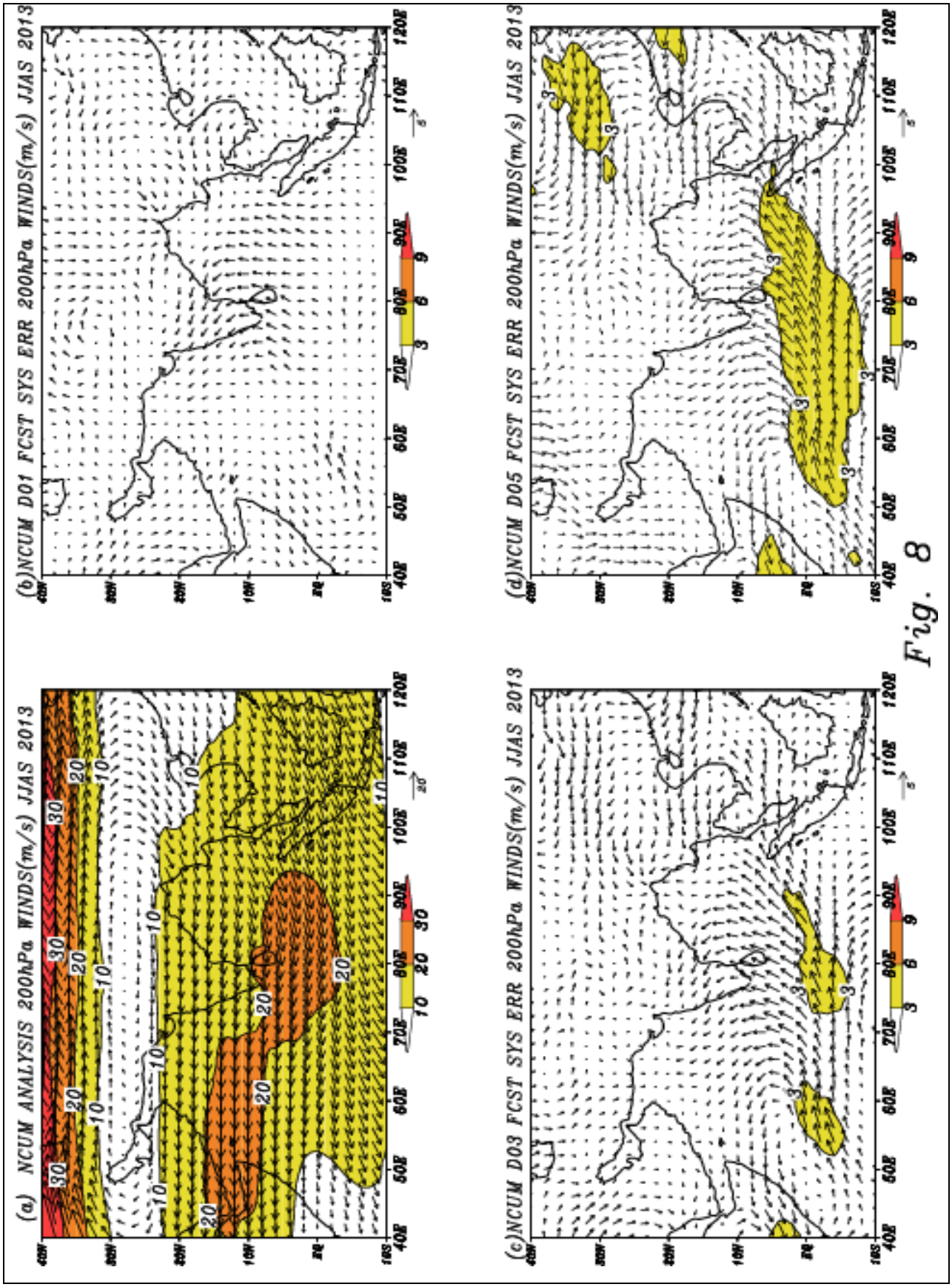
(a) NCUM ANALYSIS 200hPa WINDS(m/s) JJAS 2013
(b)NCUM D01 FCST SYS ERR 200hPa WINDS(m/s) JJAS 2013
(c)NCUM D03 FCST SYS ERR 200hPa WINDS(m/s) JJAS 2013
(d)NCUM D05 FCST SYS ERR 200hPa WINDS(m/s) JJAS 2013

Fig. 8

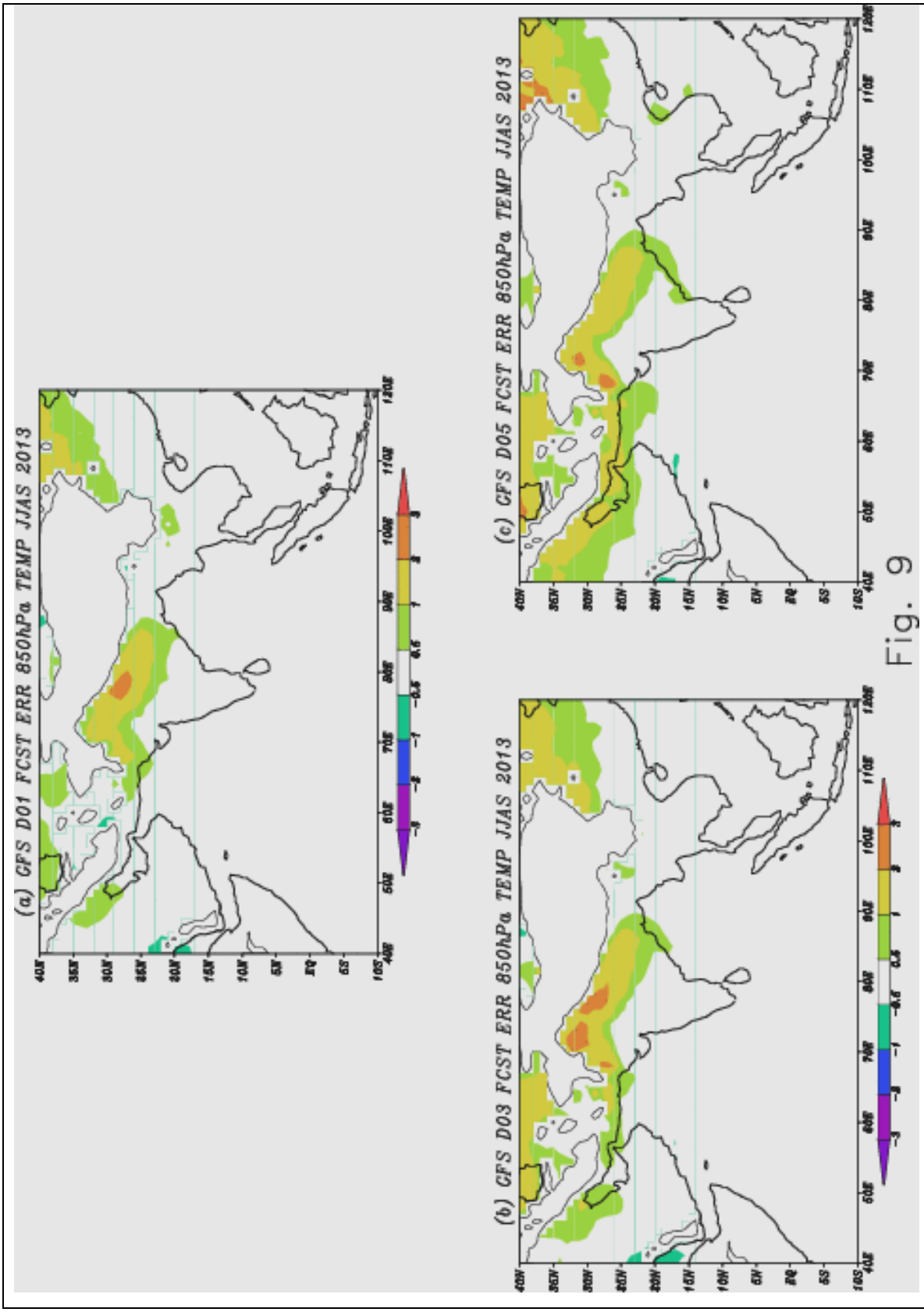
(a) GFS D01 FCST ERR 850hPa TEMP JJAS 2013
(b) GFS D03 FCST ERR 850hPa TEMP JJAS 2013
(c) GFS D05 FCST ERR 850hPa TEMP JJAS 2013

Fig. 9

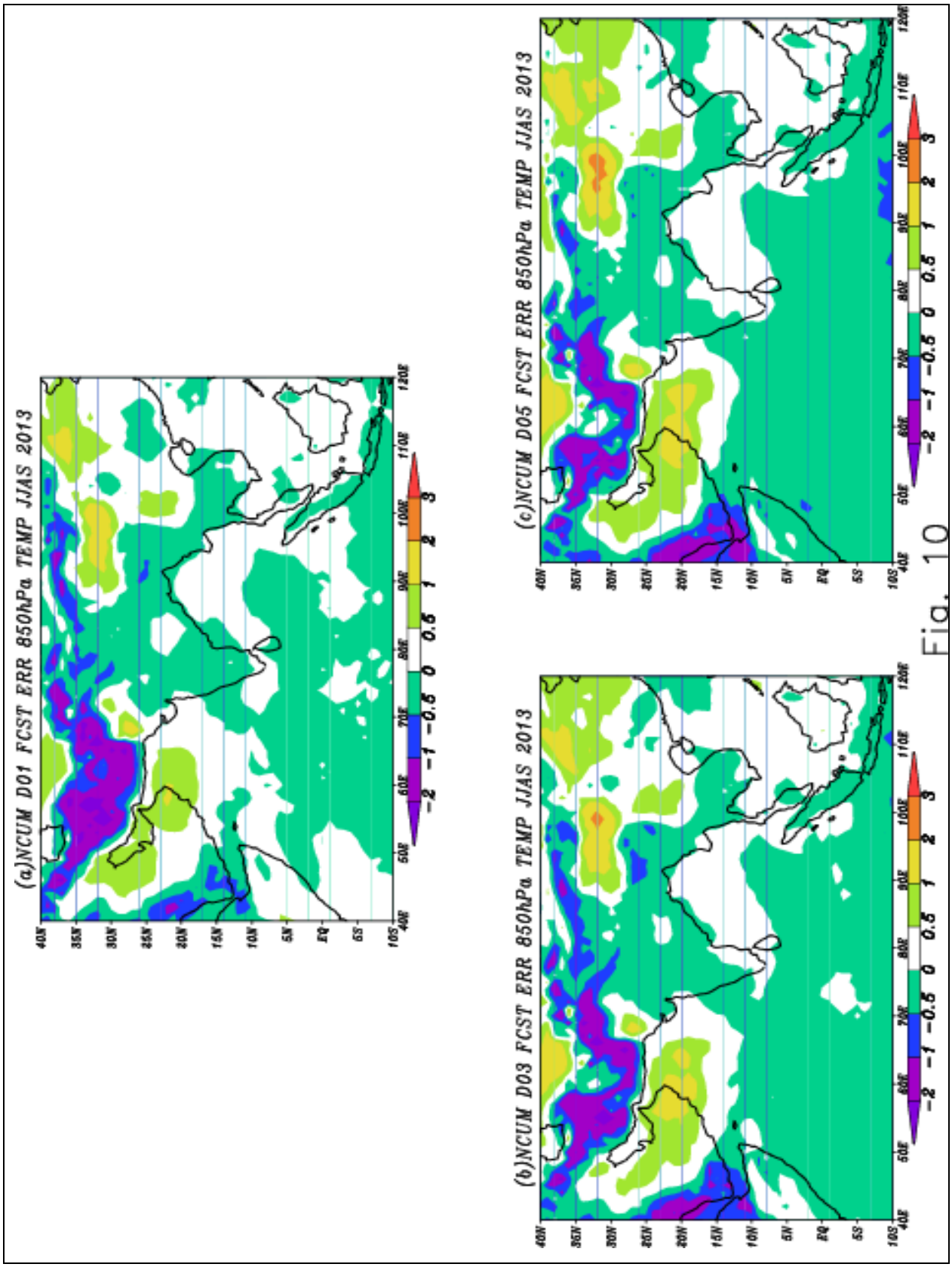
(a)NCUM D01 FCST ERR 850hPa TEMP JJAS 2013
(b)NCUM D03 FCST ERR 850hPa TEMP JJAS 2013
(c)NCUM D05 FCST ERR 850hPa TEMP JJAS 2013
-2 -1 -0.5 0 0.5 1 2 3

Fig. 10

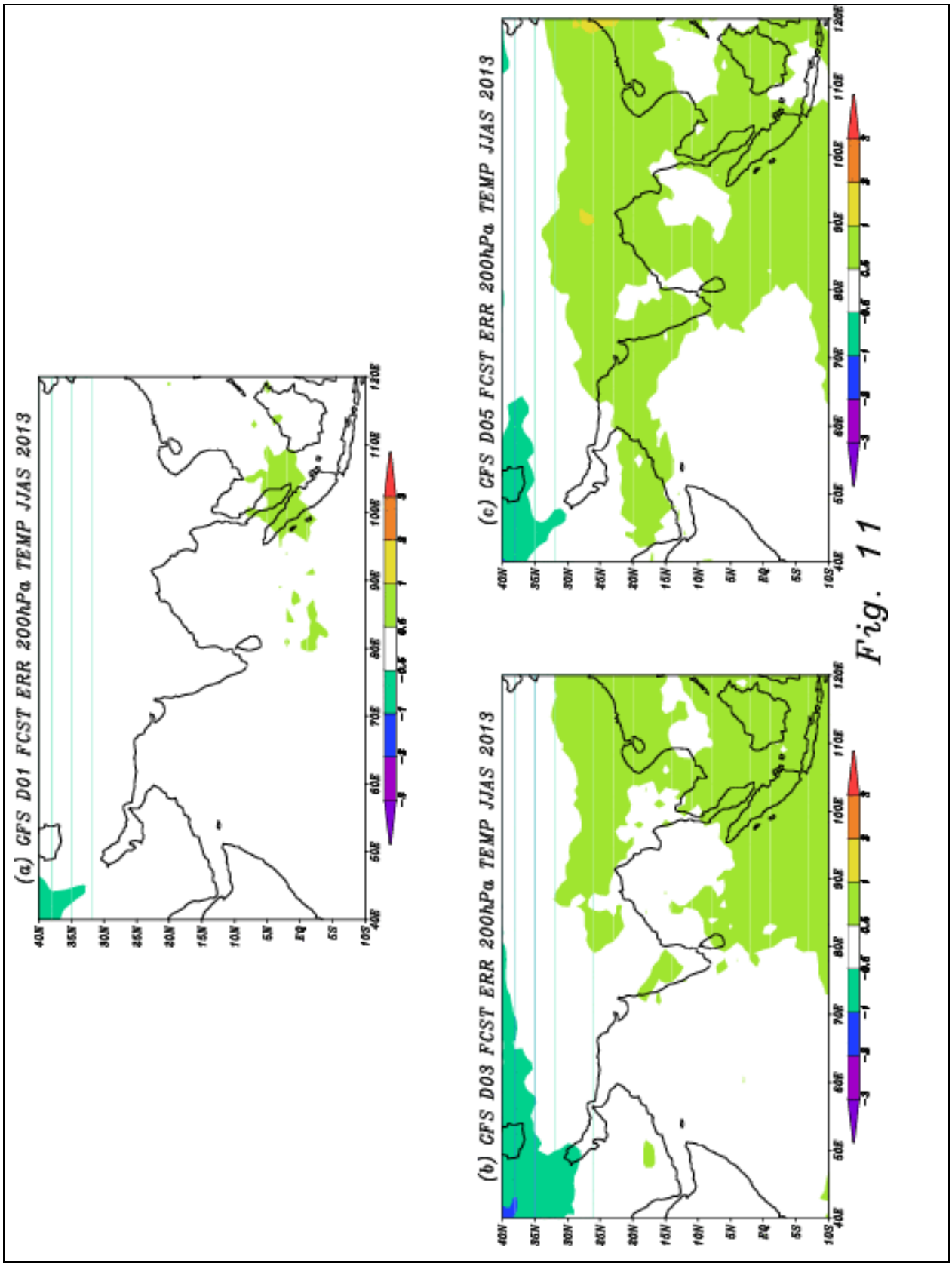
(a) GFS D01 FCST ERR 200hPa TEMP JJAS 2013
(b) GFS D03 FCST ERR 200hPa TEMP JJAS 2013
(c) GFS D05 FCST ERR 200hPa TEMP JJAS 2013

Fig. 11

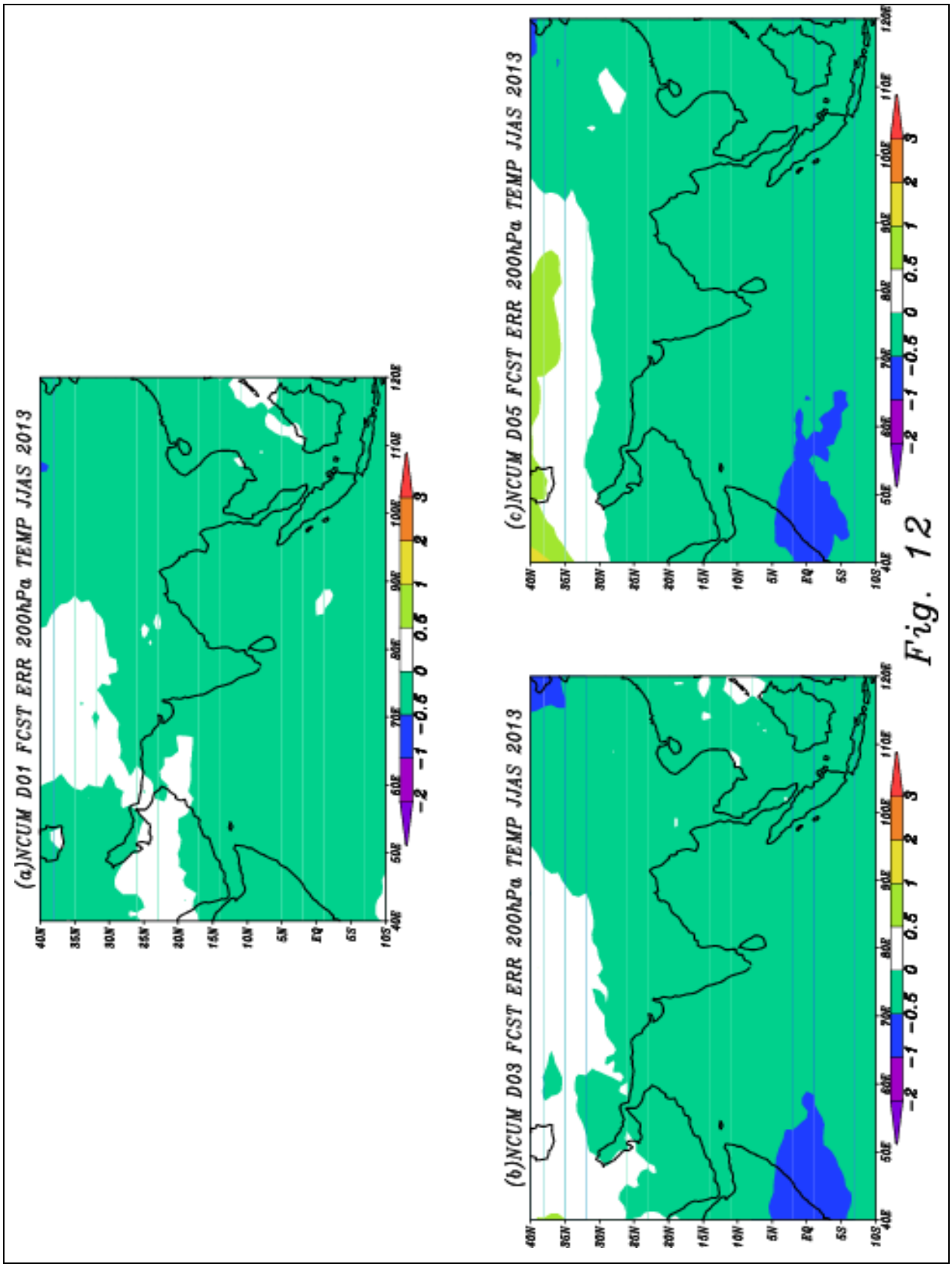
(a)NCUM D01 FCST ERR 200hPa TEMP JJAS 2013
(b)NCUM D03 FCST ERR 200hPa TEMP JJAS 2013
(c)NCUM D05 FCST ERR 200hPa TEMP JJAS 2013
-2 -1 -0.6 0 0.6 1 2 3

Fig. 12

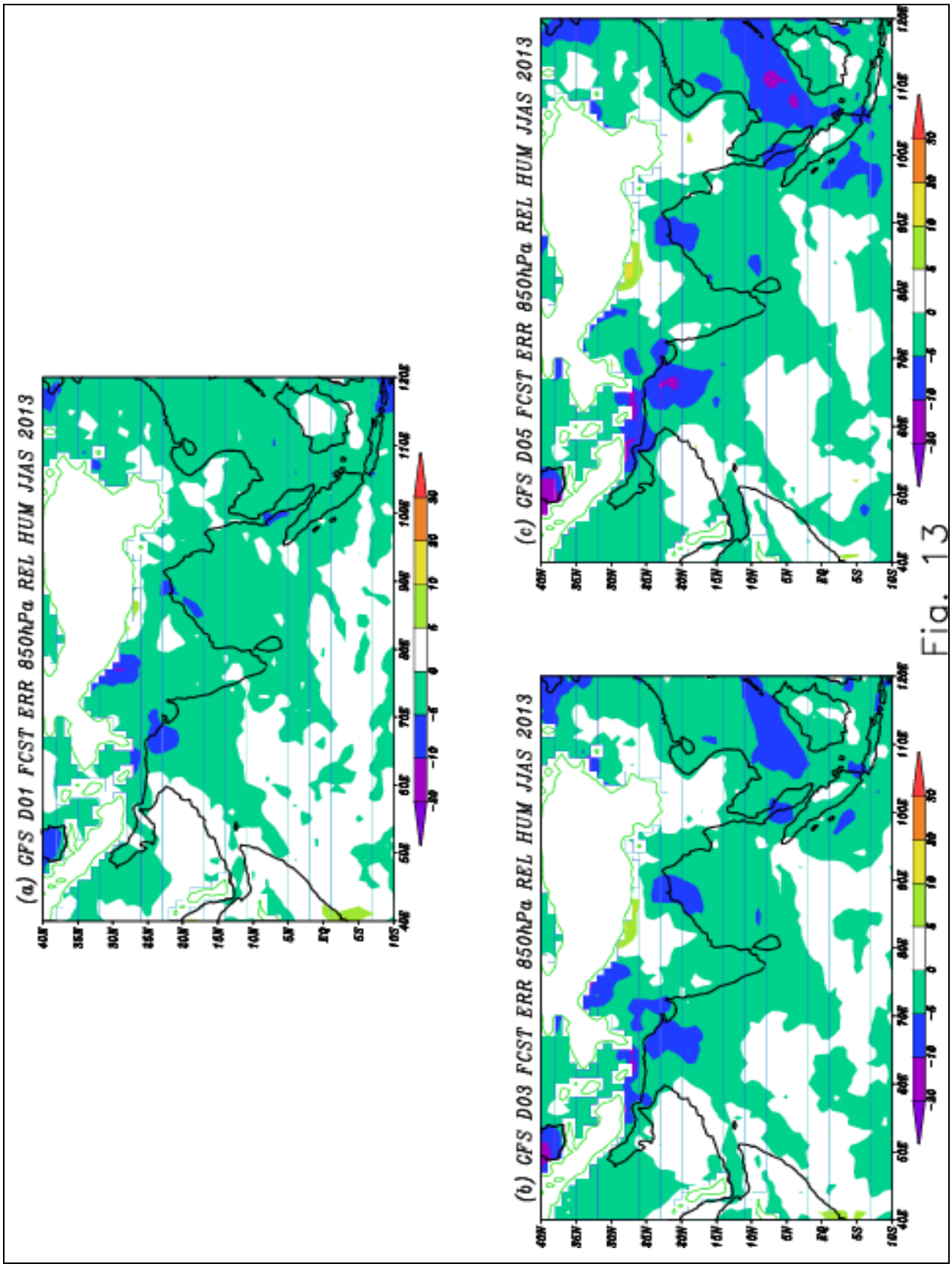
(a) GFS D01 FCST ERR 850hPa REL HUM JJAS 2013
(b) GFS D03 FCST ERR 850hPa REL HUM JJAS 2013
(c) GFS D05 FCST ERR 850hPa REL HUM JJAS 2013

Fig. 13

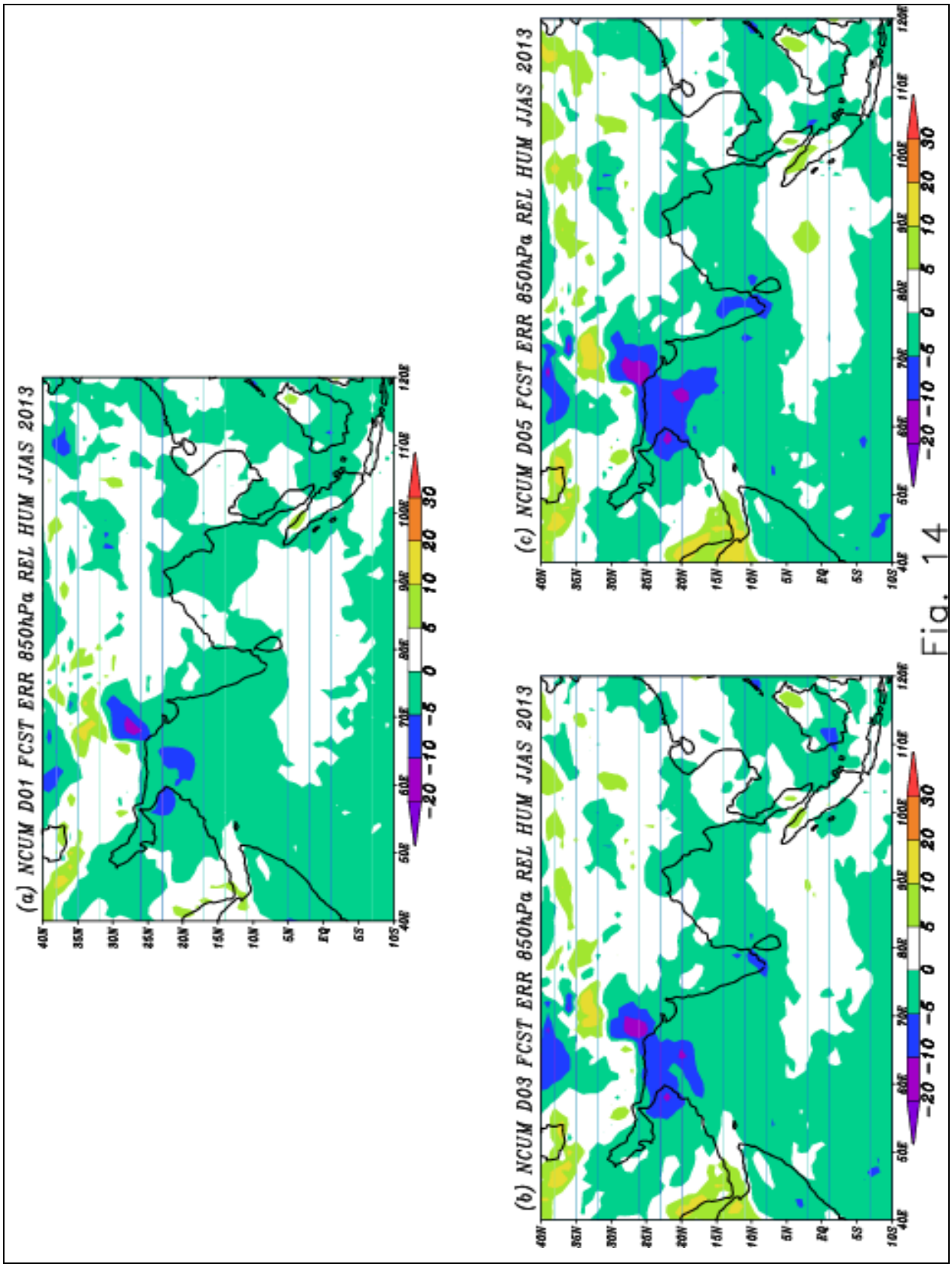
(a) NCUM D01 FCST ERR 850hPa REL HUM JJAS 2013
(b) NCUM D03 FCST ERR 850hPa REL HUM JJAS 2013
(c) NCUM D05 FCST ERR 850hPa REL HUM JJAS 2013
-20 -10 -5 0 5 10 20 30

Fig. 14

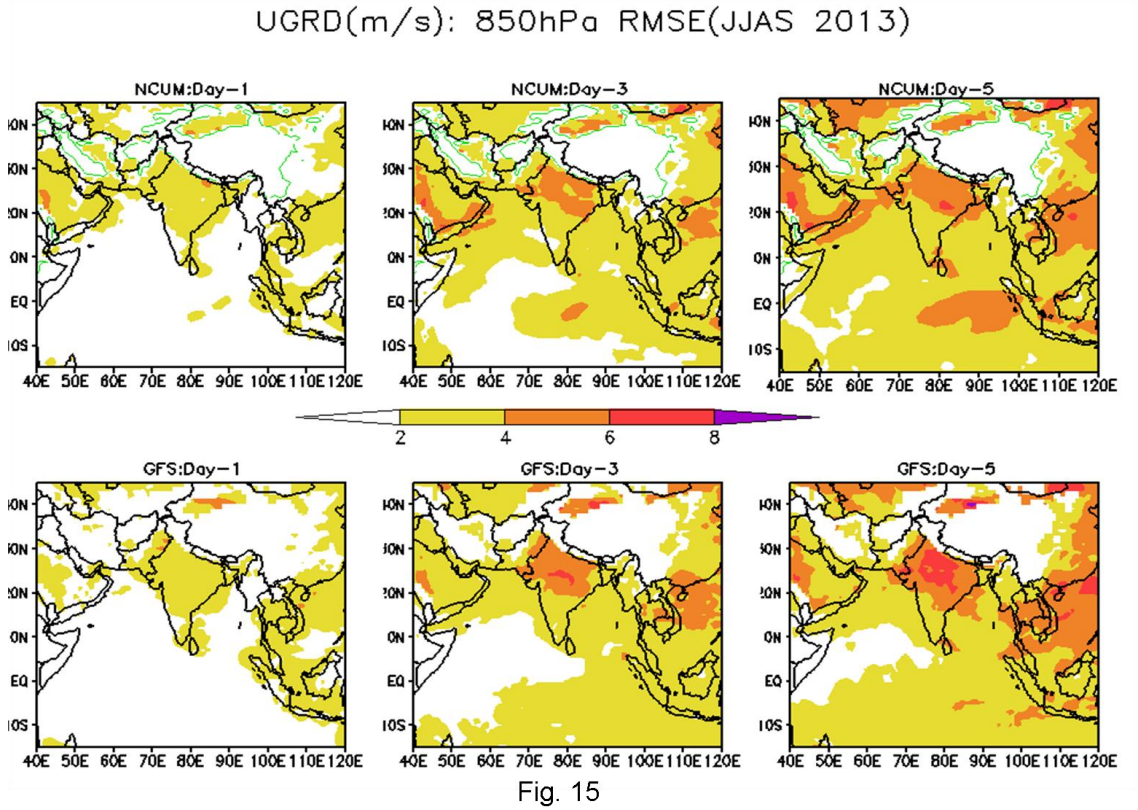
UGRD(m/s): 850hPa RMSE(JJAS 2013)
NCUM:Day-1
NCUM:Day-3
NCUM:Day-5
GFS:Day-1
GFS:Day-3
GFS:Day-5
2
4
6
8

Fig. 15

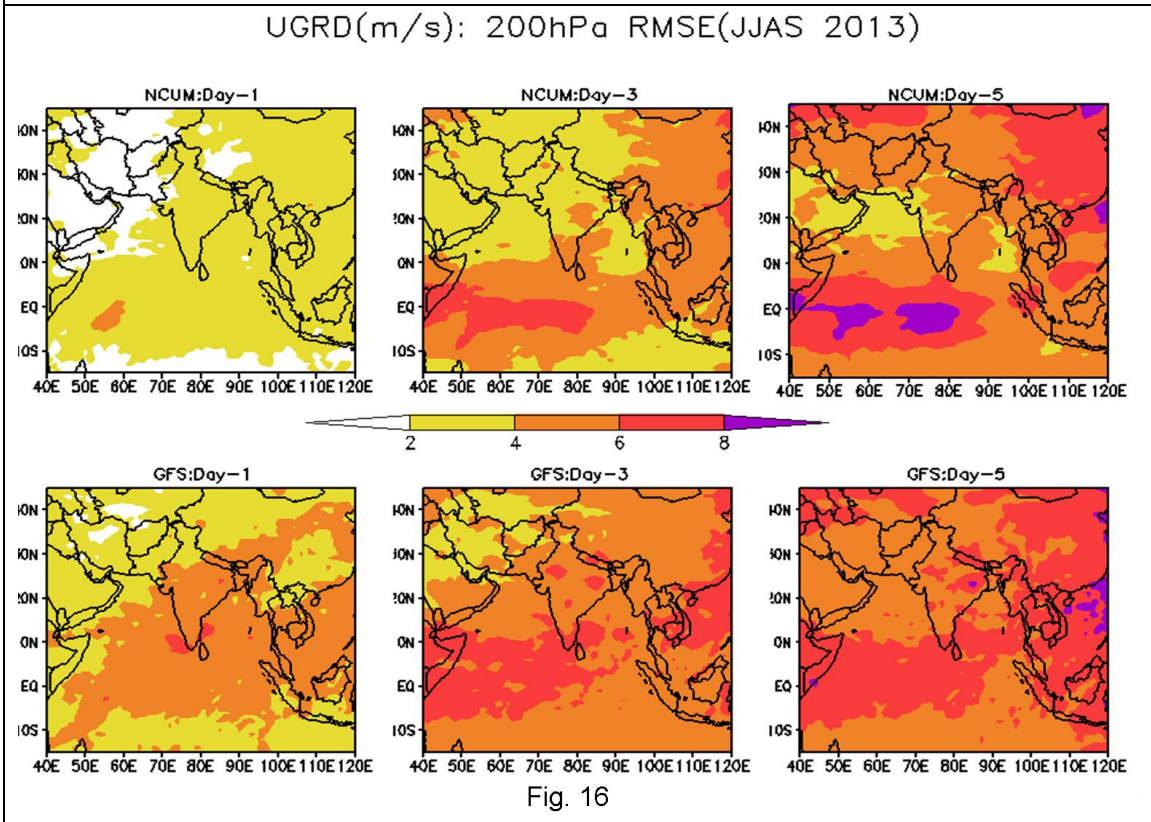
UGRD(m/s): 200hPa RMSE(JJAS 2013)
NCUM:Day-1
NCUM:Day-3
NCUM:Day-5
GFS:Day-1
GFS:Day-3
GFS:Day-5
2
4
6
8

Fig. 16

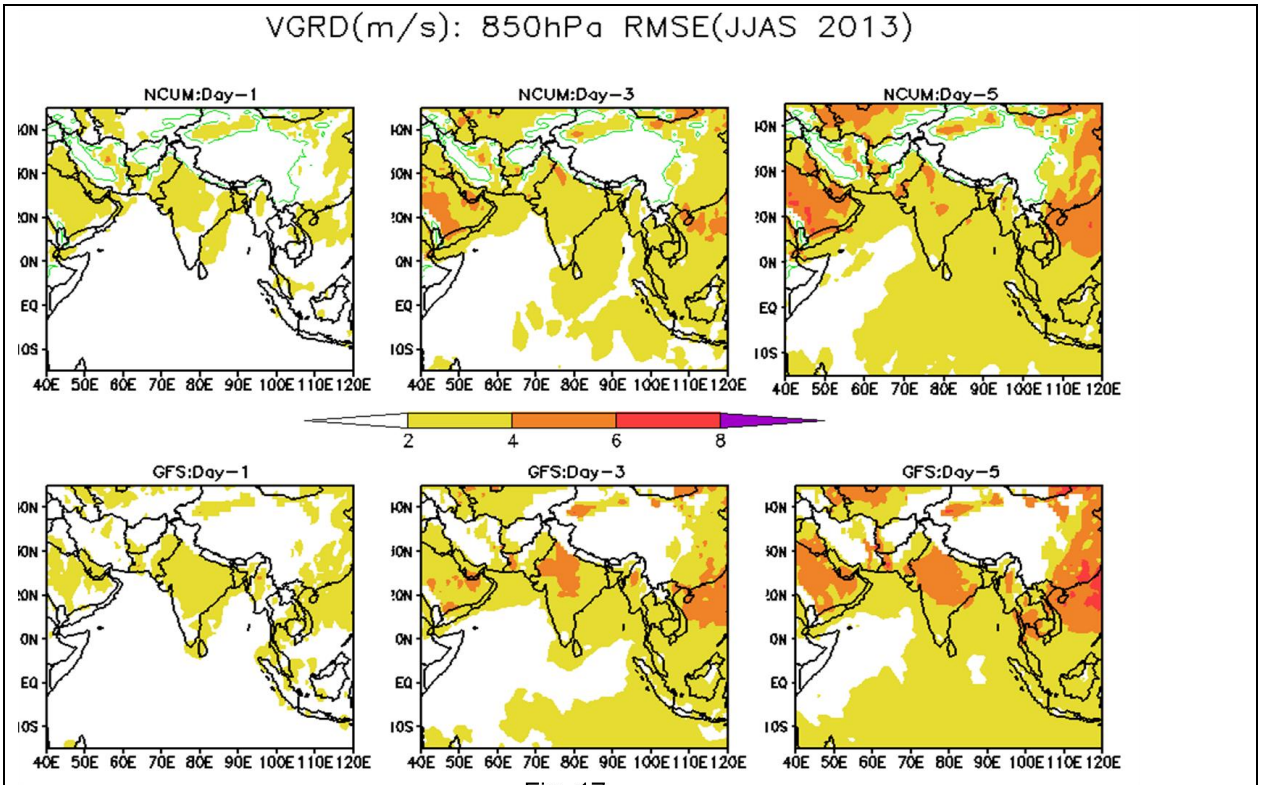
VGRD(m/s): 850hPa RMSE(JJAS 2013)
NCUM:Day-1
NCUM:Day-3
NCUM:Day-5
GFS:Day-1
GFS:Day-3
GFS:Day-5
2
4
6
8

Fig. 17

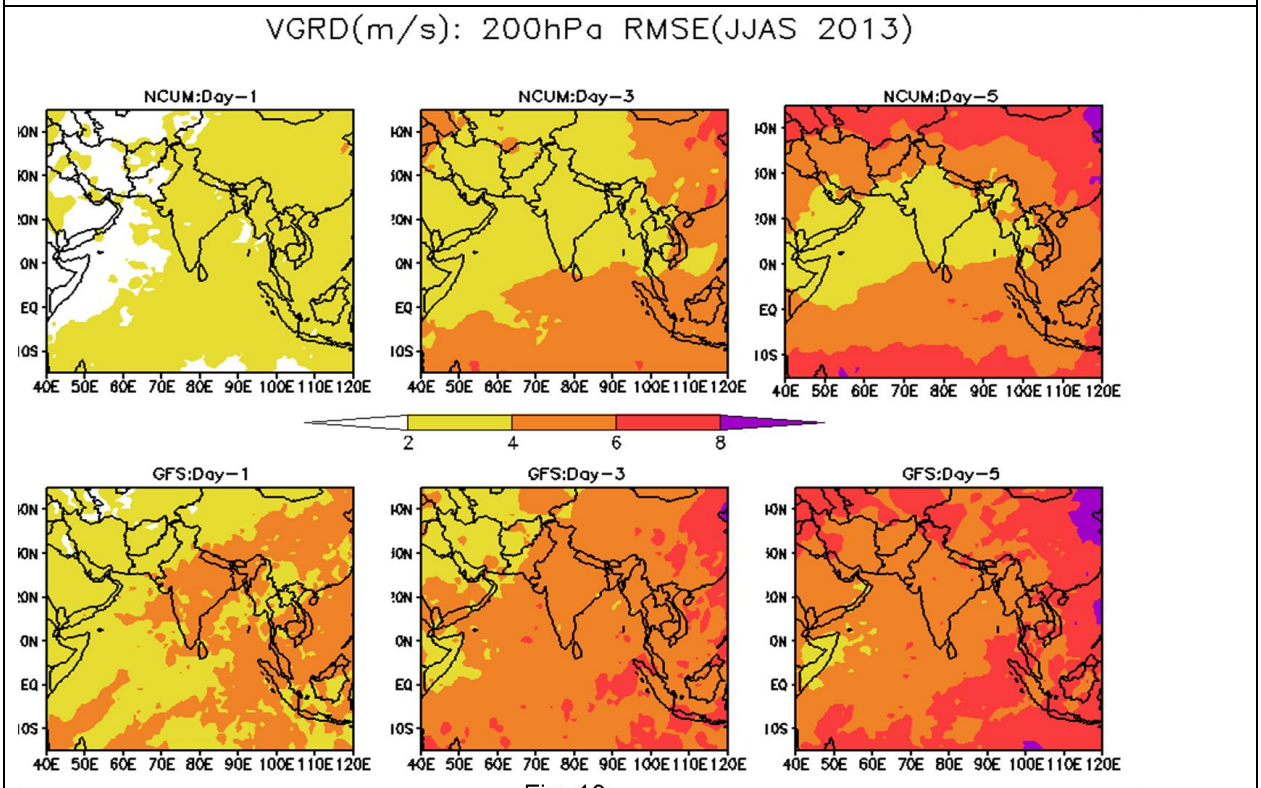
VGRD(m/s): 200hPa RMSE(JJAS 2013)
NCUM:Day-1
NCUM:Day-3
NCUM:Day-5
GFS:Day-1
GFS:Day-3
GFS:Day-5
2
4
6
8

Fig. 18

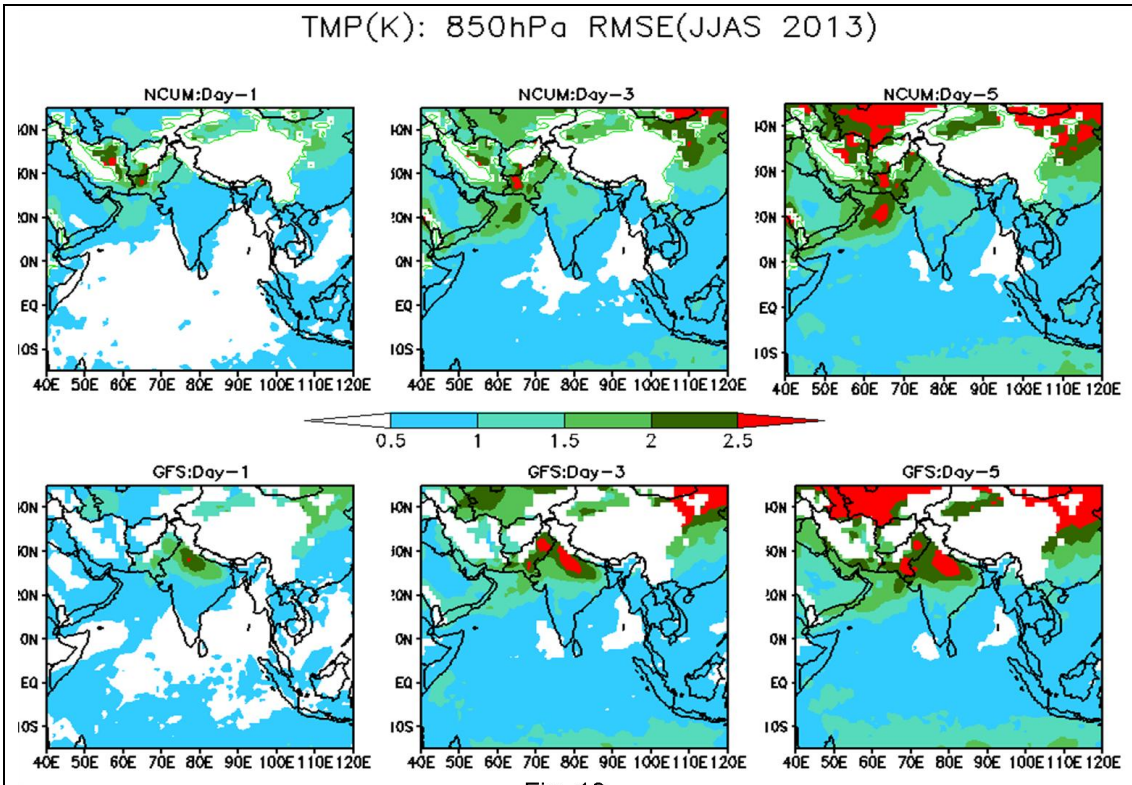
TMP(K): 850hPa RMSE(JJAS 2013)
NCUM:Day-1
NCUM:Day-3
NCUM:Day-5
GFS:Day-1
GFS:Day-3
GFS:Day-5
0.5
1
1.5
2
2.5

Fig. 19

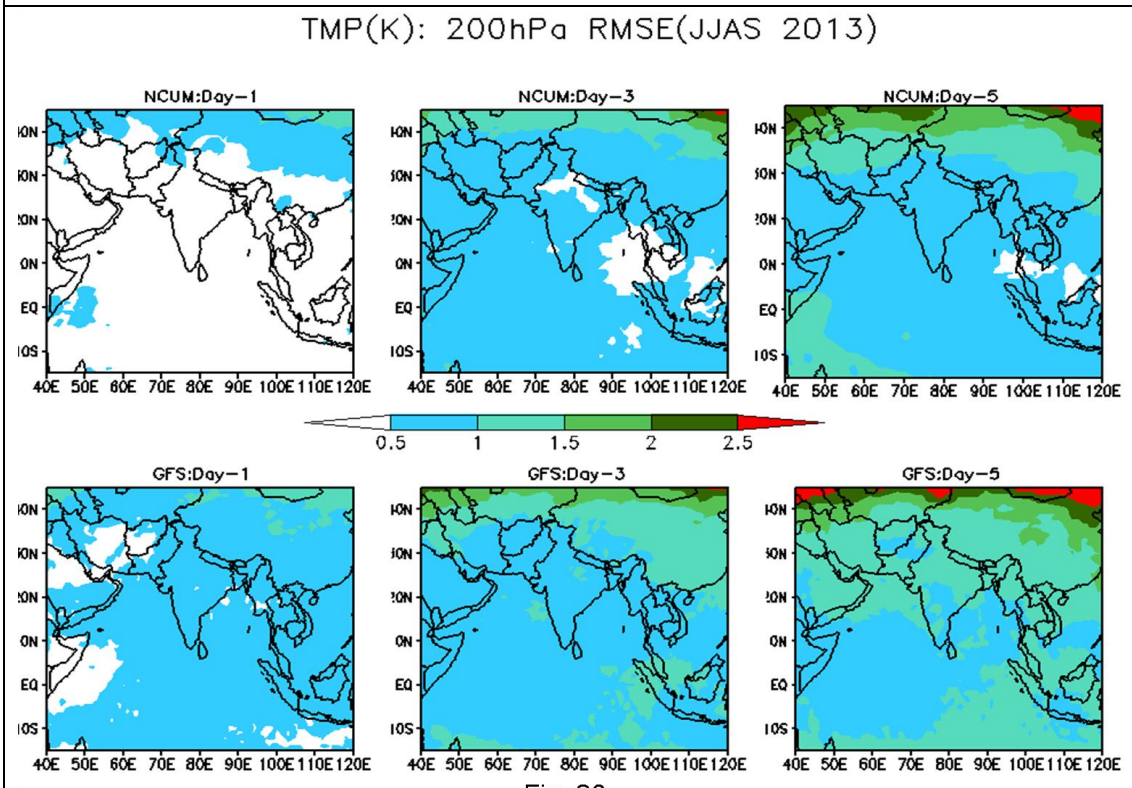
TMP(K): 200hPa RMSE(JJAS 2013)
NCUM:Day-1
NCUM:Day-3
NCUM:Day-5
GFS:Day-1
GFS:Day-3
GFS:Day-5
0.5
1
1.5
2
2.5

Fig. 20

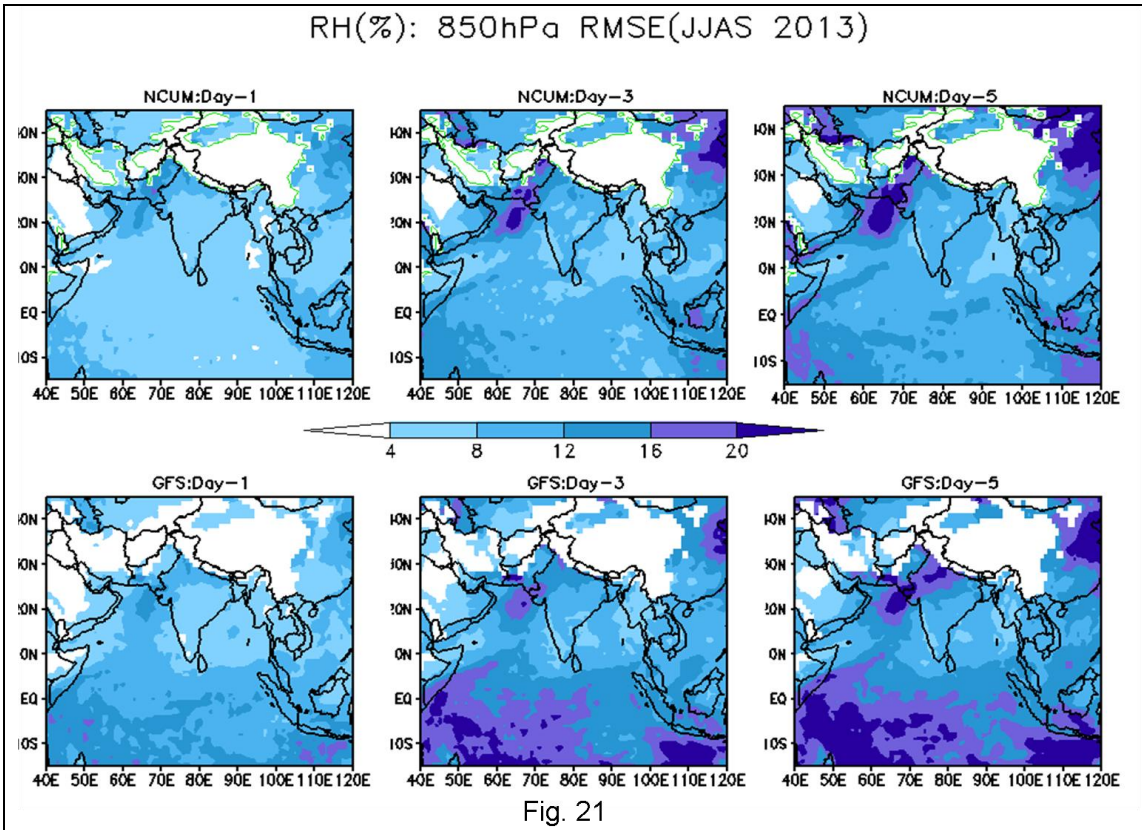
RH(%): 850hPa RMSE(JJAS 2013)
NCUM:Day-1
NCUM:Day-3
NCUM:Day-5
GFS:Day-1
GFS:Day-3
GFS:Day-5
4
8
12
16
20

Fig. 21

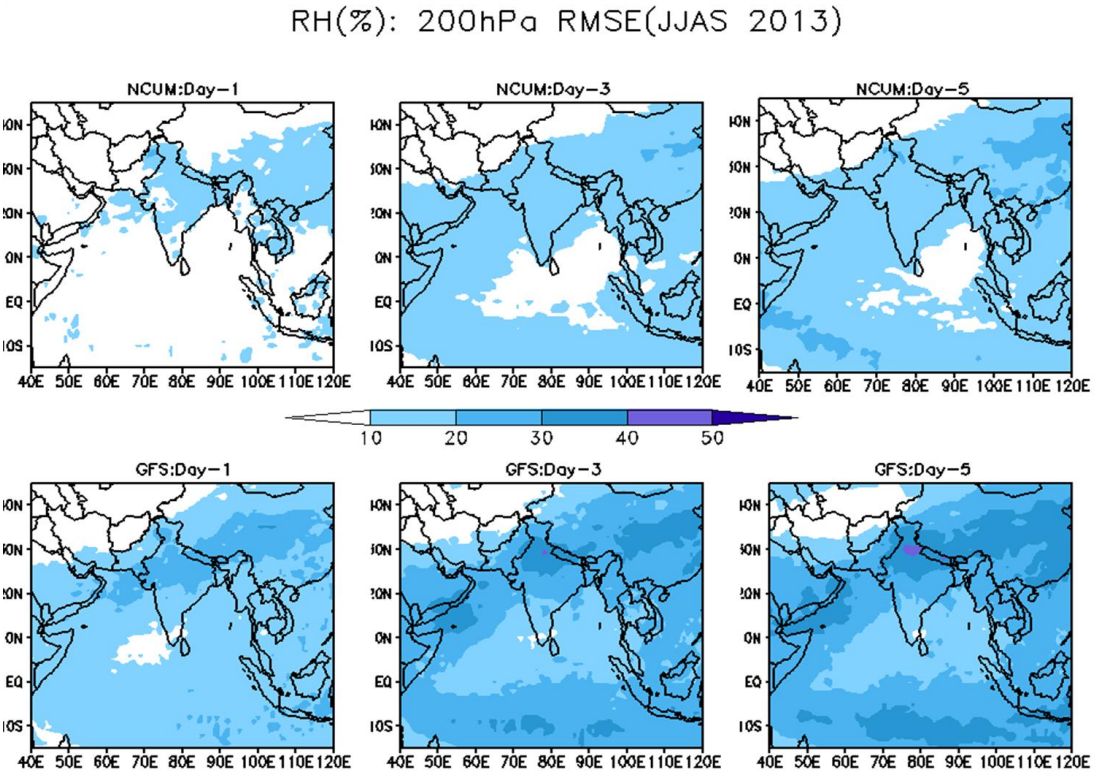
RH(%): 200hPa RMSE(JJAS 2013)
NCUM:Day-1
NCUM:Day-3
NCUM:Day-5
GFS:Day-1
GFS:Day-3
GFS:Day-5
10
20
30
40
50

Fig. 22

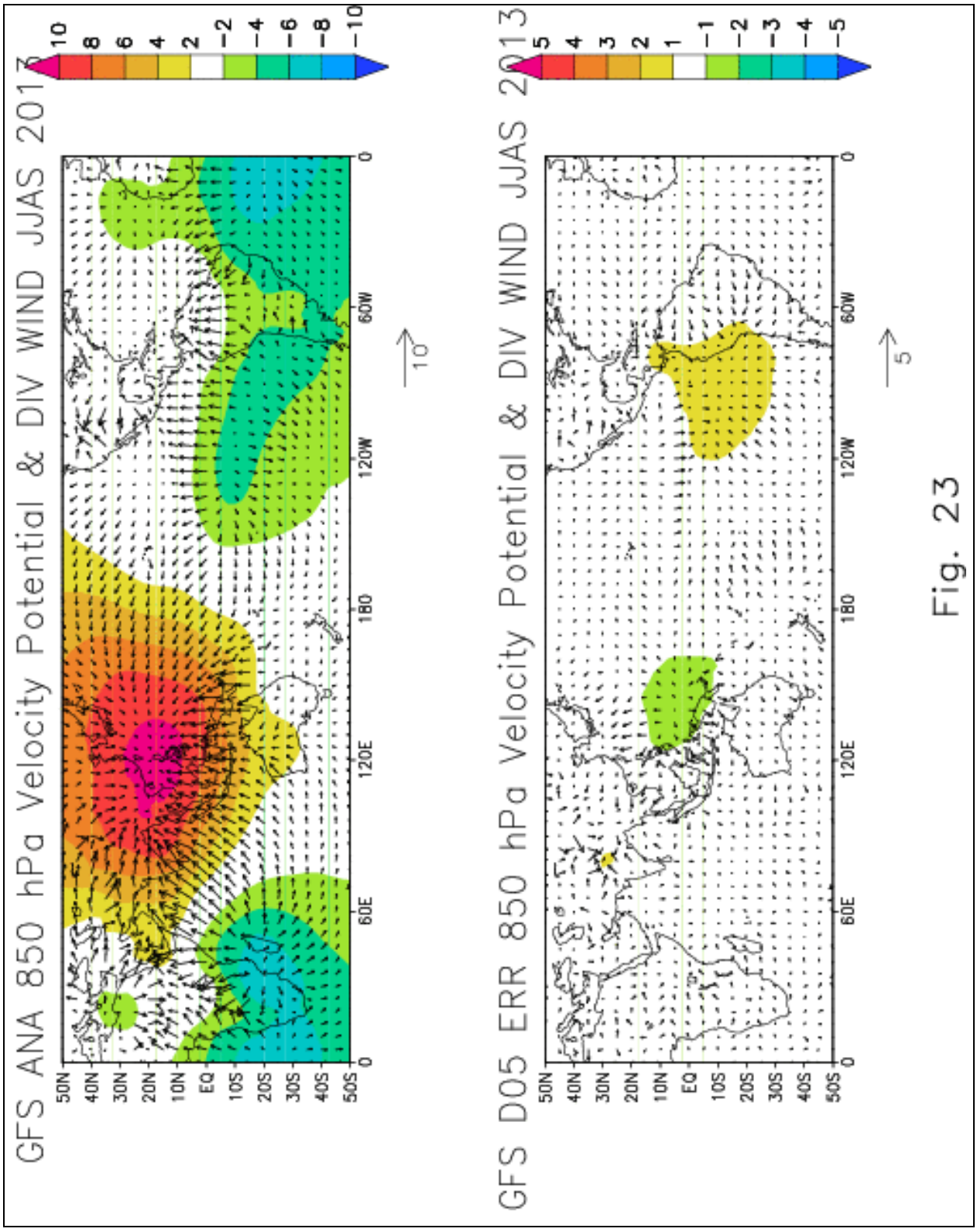
GFS ANA 850 hPa Velocity Potential & DIV WIND JJAS 2013
10 8 6 4 2 −2 −4 −6 −8 −10
50N 40N 30N 20N 10N EQ 10S 20S 30S 40S 50S
0 60E 120E 180 120W 60W 0
10
GFS D05 ERR 850 hPa Velocity Potential & DIV WIND JJAS 2013
5 4 3 2 1 −1 −2 −3 −4 −5
50N 40N 30N 20N 10N EQ 10S 20S 30S 40S 50S
0 60E 120E 180 120W 60W 0
5

Fig. 23

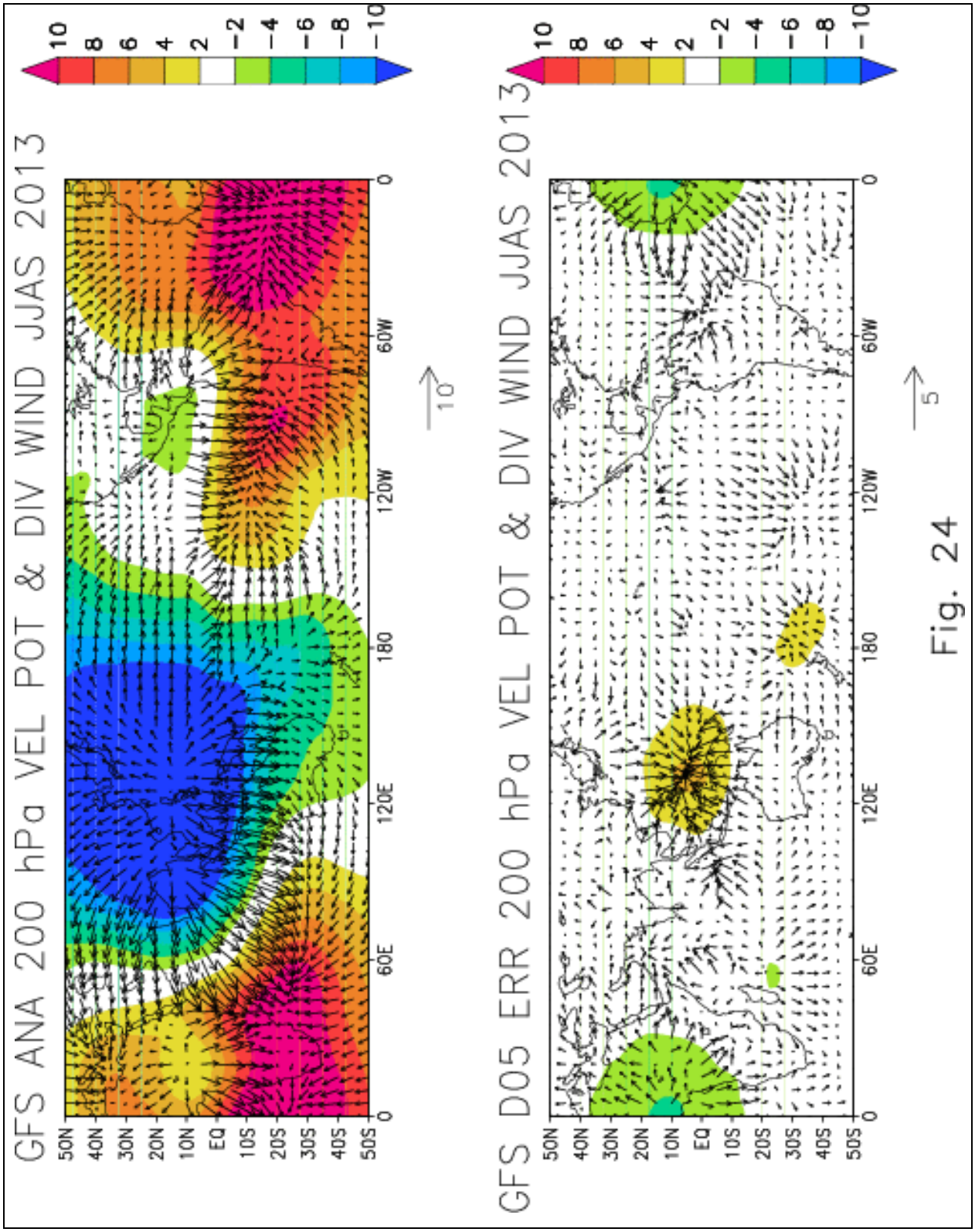
GFS ANA 200 hPa VEL POT & DIV WIND JJAS 2013
10 8 6 4 2 −2 −4 −6 −8 −10
50N 40N 30N 20N 10N EQ 10S 20S 30S 40S 50S
0 60E 120E 180 120W 60W 0
10
GFS D05 ERR 200 hPa VEL POT & DIV WIND JJAS 2013
10 8 6 4 2 −2 −4 −6 −8 −10
50N 40N 30N 20N 10N EQ 10S 20S 30S 40S 50S
0 60E 120E 180 120W 60W 0
5

Fig. 24

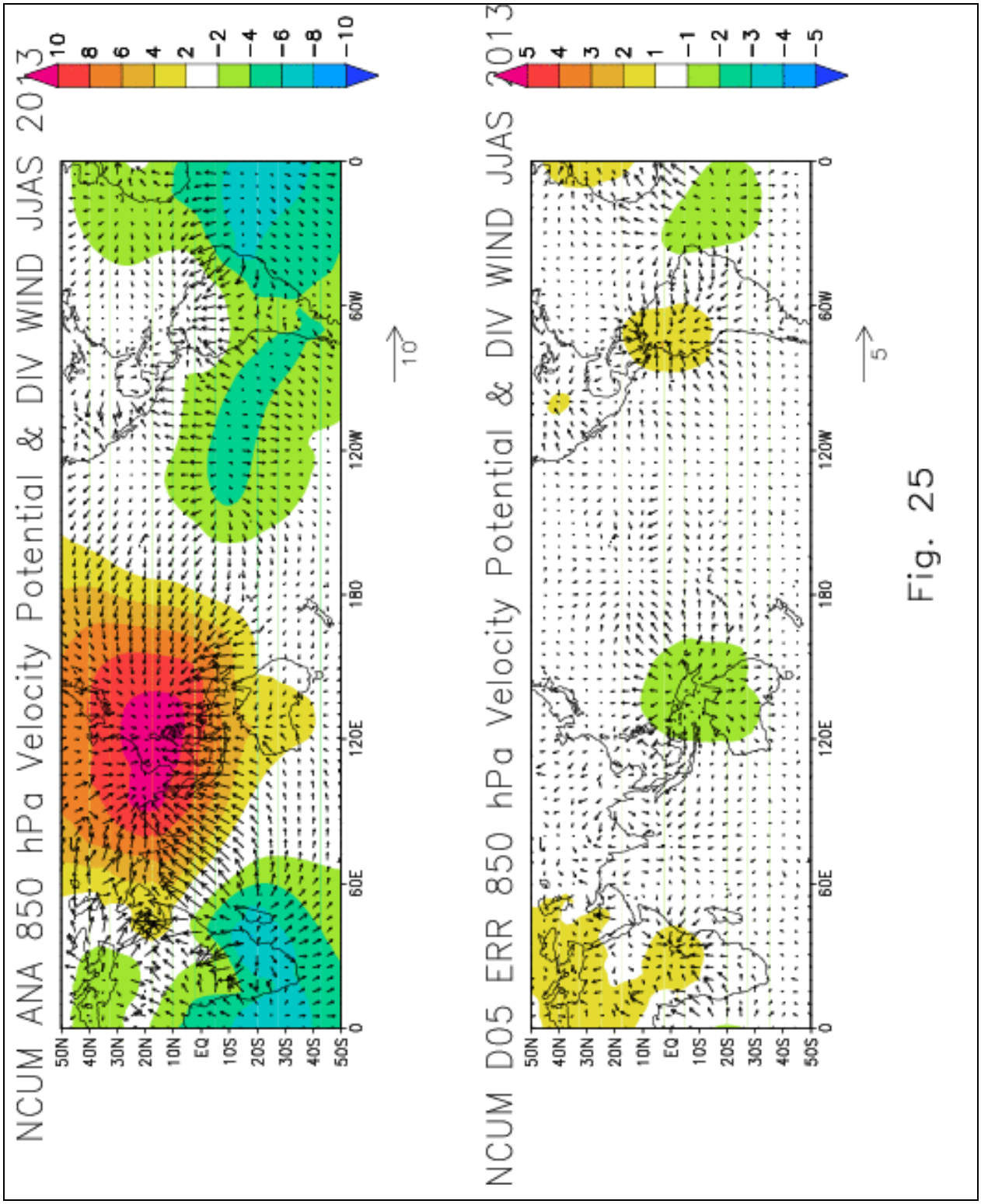
NCUM ANA 850 hPa Velocity Potential & DIV WIND JJAS 2013
10 8 6 4 2 −2 −4 −6 −8 −10
50N 40N 30N 20N 10N EQ 10S 20S 30S 40S 50S
0 60E 120E 180 120W 60W 0
10
NCUM D05 ERR 850 hPa Velocity Potential & DIV WIND JJAS 2013
5 4 3 2 1 −1 −2 −3 −4 −5
50N 40N 30N 20N 10N EQ 10S 20S 30S 40S 50S
0 60E 120E 180 120W 60W 0
5

Fig. 25

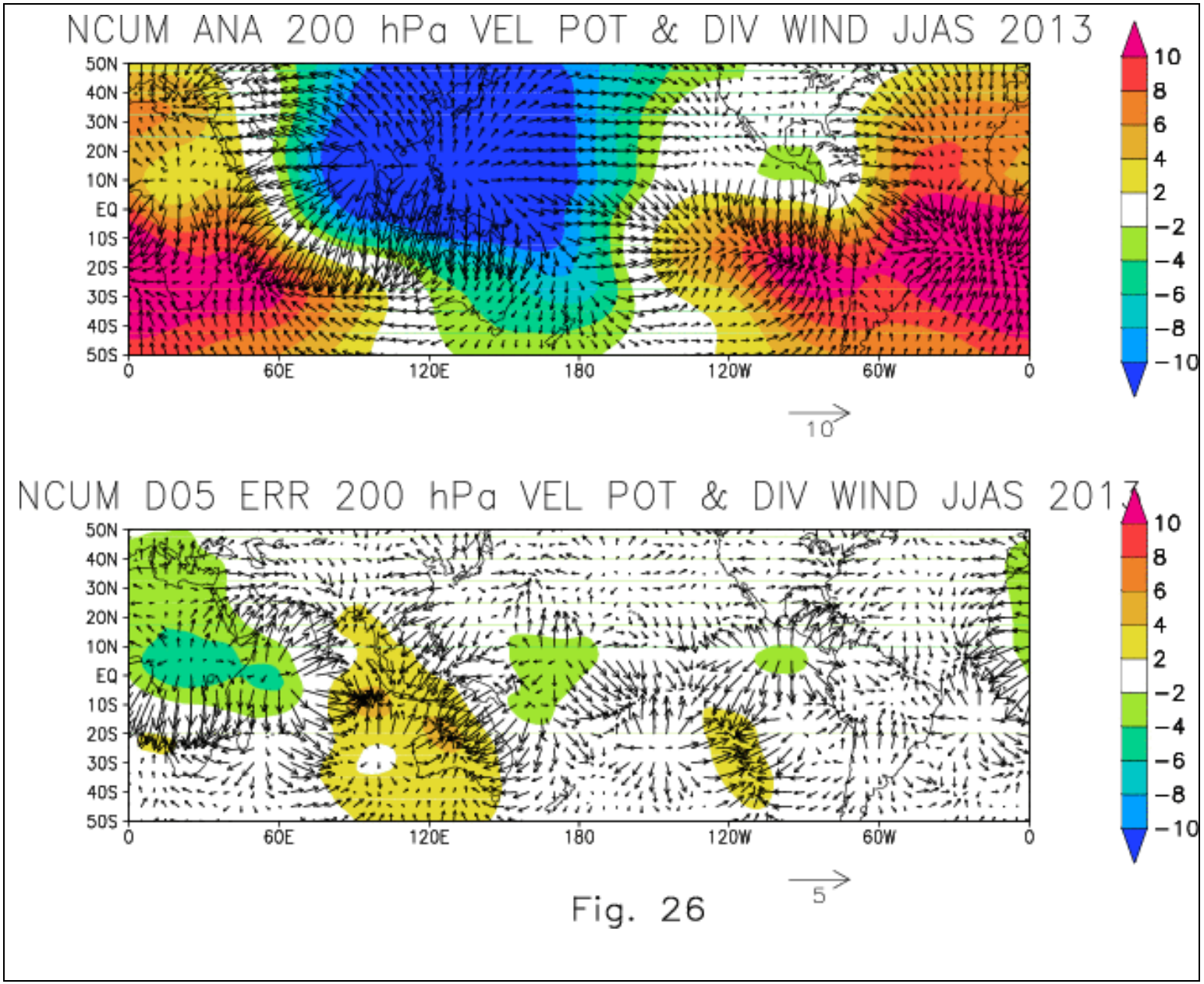
NCUM ANA 200 hPa VEL POT & DIV WIND JJAS 2013
50N
40N
30N
20N
10N
EQ
10S
20S
30S
40S
50S
0
60E
120E
180
120W
60W
0
10
10
8
6
4
2
−2
−4
−6
−8
−10
NCUM D05 ERR 200 hPa VEL POT & DIV WIND JJAS 2013
50N
40N
30N
20N
10N
EQ
10S
20S
30S
40S
50S
0
60E
120E
180
120W
60W
0
5
10
8
6
4
2
−2
−4
−6
−8
−10

Fig. 26

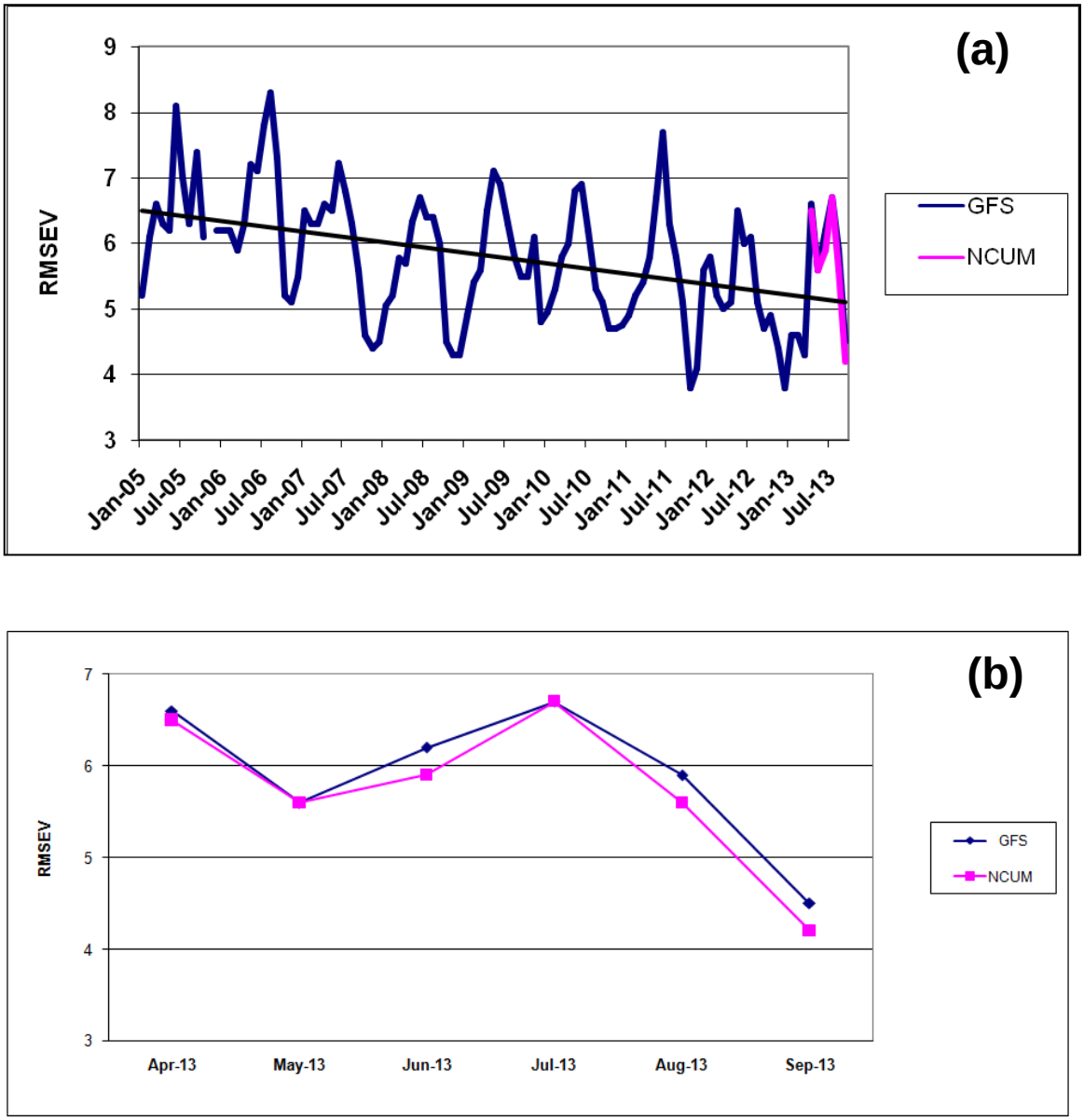

Fig. 27: RMSE of the 850hPa wind vector (RMSEV) of the Day-3 forecasts against the radiosonde observations in GFS and NCUM (a) during 2005-2013. (b) April-September 2013.

Chapter 2: Anomaly Correlation and RMSE

V. S. Prasad and C. J. Johny

1. Model Verification Scores

The verification of model forecasts with respect to their respective analyses is conducted over five regions viz. G2-Globe, NHX-Northern Hemisphere (20^0N-80^0N), SHX-Southern Hemisphere (20^0S-80^0S), TRO-Tropics (20^0S-20^0N) and RSMC-India and surrounding region (20^0S-45^0N, 30^0E-120^0E). The performance of forecasts from GFS (T574L64), GEFS (Global Ensemble Forecast System), UM_NCMRWF (Unified Model at NCMRWF) and UM_UKMO (Unified Model at UKMO) is analyzed in terms of the parameters Geo-Potential Height, Temperature and Vector Wind. The 850/700, 500 and 250 hPa are considered as the representative of the lower, middle and upper atmosphere.

2. Anomaly Correlation

Anomaly correlation for Global, Tropics and RSMC regions at lower (850/700 hPa), middle (500 hPa) and upper (200 hPa) troposphere for forecasts valid at Day-1, 3 and 5 are tabulated respectively in Table 1 (a, b & c) for temperature, Table 2 (a, b & c) for vector wind and Table 3 (a, b & c) for geo-potential height. UM_NCMRWF is found to have higher Day-1 temperature anomaly correlation over Global domain and tropics. Over RSMC region at 500 and 250 hPa pressure levels UM_NCMRWF shows higher correlation values while at 850 hPa pressure level T574 shows higher Day-1 temperature anomaly correlation. In the case of Day-3 temperature anomaly correlation UM_UKMO has higher values over global domain and UM_NCMRWF shows higher values over RSMC region while in tropics at 200 and 850 hPa UM_NCMRWF is the best and at 500 hPa T574 has the highest correlation values. In the case of Day-5 temperature anomaly correlation at 850 hPa GEFS performs better over all the three domains while at 500 hPa UM_UKMO is best over global domain, in tropics T574 is the best and over RSMC region GEFS performs better. At 200 hPa UM_NCMRWF has higher Day-5 temperature anomaly correlation in tropics and RSMC region while UM_UKMO has higher values over global domain.

UM_NCMRWF has higher vector wind anomaly correlation in Day-1 forecast over all the three domains. In Day-3 forecast UM_UKMO has higher vector wind anomaly correlation over global domain and RSMC region while in tropics UM_NCMRWF has higher correlation values. In Day-5 forecast UM_UKMO has higher vector wind anomaly correlation over all the three domains. UM_UKMO shows higher anomaly correlation values of geo-potential height for Day-3 and Day-5 forecast over all the three regions. In Day-1 forecast UM_UKMO has higher geo-potential height anomaly correlation values in global domain and at 700 and 500 hPa pressure levels in RSMC region while over tropics UM_NCMRWF has higher correlation values.

3. Root Mean Square Error

Figures (1 – 9) depict the RMSE of temperature, vector wind and geo-potential height forecasts for Day 1 -10 with respect to their respective analysis over Global, Tropics and RSMC region at 850, 500 and 200 hPa pressure levels. In the lower part of the figures the difference of the RMSE's from GEFS, UM_NCMRWF and UM_UKMO with respect to the RMSE from T574 is presented. The colour of the histograms corresponds to the same colour of the line depicting the forecast RMSE and the RMSE differences. The RMSE differences outside the histograms are statistically significant at 95% level of significance. UM_NCMRWF forecasts are depicted till Day-7 and that of UM_UKMO till Day-6 as these models were being run only up to Day-7 and Day-6 respectively during the monsoon season.

Temperature RMSE over globe (Figure 1) is lowest for UM_NCMRWF up to Day-2 forecast at all levels while in Day-3 forecast RMSE is lowest for UM_UKMO at all levels and for forecasts beyond Day-3 GEFS perform better except at 200 hPa pressure level where UM_UKMO show lowest RMSE values. The difference is significant at 95% level of confidence. At all levels beyond Day-2 forecast T574 has highest temperature RMSE. Over tropics (Figure 2), UM_NCMRWF has lowest RMSE values at 500 and 200 hPa pressure levels and up to Day-2 forecast at 850 hPa. At 850 hPa GEFS has lowest RMSE values for forecasts beyond Day-2. Over RSMC region (Figure 3), UM_NCMRWF has an edge over the other forecasts at 200 hPa and up to Day-3 forecast at 500 hPa whereas GEFS performs better for forecasts beyond

Day-3 at 500 hPa and for forecasts beyond Day-2 at 850 hPa level. At 850 hPa T574 performs better up to forecasts of Day-2 compared to other forecasts.

Vector wind RMSE over globe (Figure 4) is lowest for GEFS at all the three levels (850, 500 and 200hPa) beyond Day-4 forecasts. Over tropics (Figure 5) UM_NCMRWF performs up to forecasts of Day-4 while GEFS performs better beyond forecasts of Day-4. Over RSMC region (Figure 6) UM_NCMRWF has lowest RMSE values in 500 and 200 hPa up to Day-3 forecasts while GEFS performs better beyond Day-4 forecasts. At 850 hPa UM_UKMO has lowest RMSE values up to Day-4 forecast and beyond that GEFS performs better.

Geo-potential height RMSE (Figure 7) is lowest for UM_UKMO over Globe at 850, 500 and 200hPa pressure levels. Over tropics (Figure 8) UM_NCMRWF has lowest RMSE in 850 and 500 hPa levels while at 200 hPa UM_UKMO performs better up to Day-3 forecast and GEFS performs better beyond Day-3 forecasts. Over RSMC (Figure 9) region, the performances of all the four forecast systems are giving mixed results.

From the model verification score, performance of Unified Model (UM) is found to be better compared to that of GFS (T574). Table 4 lists the count of the observations that are provided to the T574, UM_NCMRWF and UM_UKMO assimilation systems for a given typical assimilation cycle. It can be seen that number of observations ingested into GFS and UM_NCMRWF are comparable but the same is much higher in UM_UKMO.

4. Summary

- The RMSE in the temperature field globally averaged is lowest for UM_NCMRWF up to Day-2 forecast at all levels while in Day-3 forecast RMSE is lowest for UM_UKMO at all levels and for forecasts beyond Day-3 GEFS perform better except at 200 hPa level where UM_UKMO show lowest RMSE values.

- The RMSE in the vector wind averaged over the tropics indicate that UM_NCMRWF performs better up to Day-4 forecast while GEFS performs

better beyond Day-4 forecasts. Over the RSMC regions UM_NCMRWF has lowest RMSE values in middle and upper levels up to Day-3 forecasts while GEFS performs better beyond Day-4 forecasts. At lower level UM_UKMO has lowest RMSE values up to Day-4 forecast and beyond that GEFS perform better.

- From these model verification scores, performance of Unified Model (UM) is found to be better than that of GFS (T574)

	Table: 1a **Temperature Anomaly Correlation – Day 1 Forecast**											
Level hPa	***Global***				***Tropics***				***RSMC***			
	T574	**GEFS**	**UM NCMR**	**UM UKMO**	**T574**	**GEFS**	**UM NCMR**	**UM UKMO**	**T574**	**GEFS**	**UM NCMR**	**UM UKMO**
850	0.961	0.958	0.976	0.968	0.926	0.9	0.938	0.878	0.948	0.943	0.94	0.924
500	0.973	0.974	0.983	0.974	0.926	0.899	0.93	0.841	0.945	0.94	0.948	0.915
250	0.959	0.961	0.978	0.969	0.851	0.858	0.916	0.83	0.944	0.945	0.97	0.947
	Table: 1b **Temperature Anomaly Correlation – Day 3 Forecast**											
Level hPa	***Global***				***Tropics***				***RSMC***			
	T574	**GEFS**	**UM NCMR**	**UM UKMO**	**T574**	**GEFS**	**UM NCMR**	**UM UKMO**	**T574**	**GEFS**	**UM NCMR**	**UM UKMO**
850	0.877	0.894	0.903	0.913	0.804	0.817	0.837	0.778	0.875	0.873	0.878	0.869
500	0.891	0.906	0.901	0.914	0.803	0.787	0.8	0.724	0.855	0.861	0.861	0.837
250	0.84	0.864	0.871	0.885	0.665	0.704	0.767	0.699	0.867	0.88	0.915	0.898
	Table: 1c **Temperature Anomaly Correlation – Day 5 Forecast**											
Level hPa	***Global***				***Tropics***				***RSMC***			
	T574	**GEFS**	**UM NCMR**	**UM UKMO**	**T574**	**GEFS**	**UM NCMR**	**UM UKMO**	**T574**	**GEFS**	**UM NCMR**	**UM UKMO**
850	0.743	0.791	0.786	0.757	0.733	0.764	0.757	0.709	0.807	0.816	0.813	0.811
500	0.743	0.786	0.75	0.791	0.702	0.687	0.68	0.631	0.768	0.783	0.764	0.758
250	0.669	0.734	0.704	0.742	0.549	0.592	0.652	0.6	0.8	0.825	0.849	0.8

	Table: 2a **Vector Wind Anomaly Correlation – Day 1 Forecast**											
Level hPa	***Global***				***Tropics***				***RSMC***			
	T574	**GEFS**	**UM NCMR**	**UM UKMO**	**T574**	**GEFS**	**UM NCMR**	**UM UKMO**	**T574**	**GEFS**	**UM NCMR**	**UM UKMO**
850	0.937	0.938	0.96	0.958	0.912	0.876	0.929	0.906	0.897	0.861	0.912	0.903
500	0.951	0.958	0.976	0.974	0.932	0.926	0.965	0.942	0.908	0.904	0.941	0.932
250	0.957	0.964	0.98	0.977	0.872	0.894	0.954	0.931	0.882	0.902	0.951	0.936
	Table: 2b **Vector Wind Anomaly Correlation – Day 3 Forecast**											
Level hPa	***Global***				***Tropics***				***RSMC***			
	T574	**GEFS**	**UM NCMR**	**UM UKMO**	**T574**	**GEFS**	**UM NCMR**	**UM UKMO**	**T574**	**GEFS**	**UM NCMR**	**UM UKMO**
850	0.807	0.832	0.823	0.858	0.778	0.754	0.794	0.785	0.764	0.748	0.789	0.798
500	0.838	0.868	0.863	0.889	0.801	0.814	0.854	0.832	0.767	0.788	0.82	0.823
250	0.859	0.882	0.888	0.904	0.724	0.769	0.822	0.809	0.767	0.804	0.84	0.839
	Table: 2c **Vector Wind Anomaly Correlation – Day 5 Forecast**											
Level hPa	***Global***				***Tropics***				***RSMC***			
	T574	**GEFS**	**UM NCMR**	**UM UKMO**	**T574**	**GEFS**	**UM NCMR**	**UM UKMO**	**T574**	**GEFS**	**UM NCMR**	**UM UKMO**
850	0.619	0.687	0.641	0.699	0.666	0.67	0.684	0.687	0.645	0.654	0.686	0.696
500	0.664	0.731	0.692	0.744	0.675	0.709	0.727	0.723	0.63	0.672	0.697	0.711
250	0.694	0.75	0.726	0.77	0.598	0.657	0.683	0.691	0.674	0.727	0.728	0.741

	Table: 3a **Geo-Potential Correlation – Day 1 Forecast**											
Level hPa	***Global***				***Tropics***				***RSMC***			
	T574	**GEFS**	**UM NCMR**	**UM UKMO**	**T574**	**GEFS**	**UM NCMR**	**UM UKMO**	**T574**	**GEFS**	**UM NCMR**	**UM UKMO**
700	0.992	0.99	0.995	0.996	0.959	0.931	0.966	0.958	0.972	0.949	0.969	0.973
500	0.993	0.993	0.996	0.997	0.961	0.933	0.977	0.972	0.974	0.962	0.982	0.983
250	0.994	0.994	0.997	0.997	0.953	0.938	0.978	0.967	0.983	0.982	0.992	0.991
	Table: 3b **Geo-Potential Anomaly Correlation – Day 3 Forecast**											
Level hPa	***Global***				***Tropics***				***RSMC***			
	T574	**GEFS**	**UM NCMR**	**UM UKMO**	**T574**	**GEFS**	**UM NCMR**	**UM UKMO**	**T574**	**GEFS**	**UM NCMR**	**UM UKMO**
700	0.945	0.947	0.955	0.97	0.836	0.844	0.91	0.91	0.876	0.869	0.911	0.92
500	0.95	0.952	0.959	0.972	0.856	0.853	0.922	0.923	0.873	0.889	0.926	0.933
250	0.957	0.957	0.963	0.975	0.862	0.878	0.903	0.904	0.931	0.942	0.955	0.962
	Table: 3c **Geo-Potential Anomaly Correlation – Day 5 Forecast**											
Level hPa	***Global***				***Tropics***				***RSMC***			
	T574	**GEFS**	**UM NCMR**	**UM UKMO**	**T574**	**GEFS**	**UM NCMR**	**UM UKMO**	**T574**	**GEFS**	**UM NCMR**	**UM UKMO**
700	0.819	0.842	0.839	0.885	0.741	0.778	0.835	0.848	0.747	0.765	0.836	0.854
500	0.827	0.849	0.845	0.888	0.764	0.798	0.841	0.859	0.750	0.779	0.823	0.843
250	0.843	0.86	0.859	0.897	0.758	0.795	0.818	0.83	0.862	0.873	0.878	0.896

Table: 4 ***Observation Data Count***			
	GFS	**UM_NCMRWF**	**UM_UKMO**
AIRCFT	87152	84922	97366
ASCAT Winds	74394	82183	228936
GPSRO	531	550	
AMV	149888	134080	542620
Sonde	1144	1048	3956
Surface	39263	38421	67649

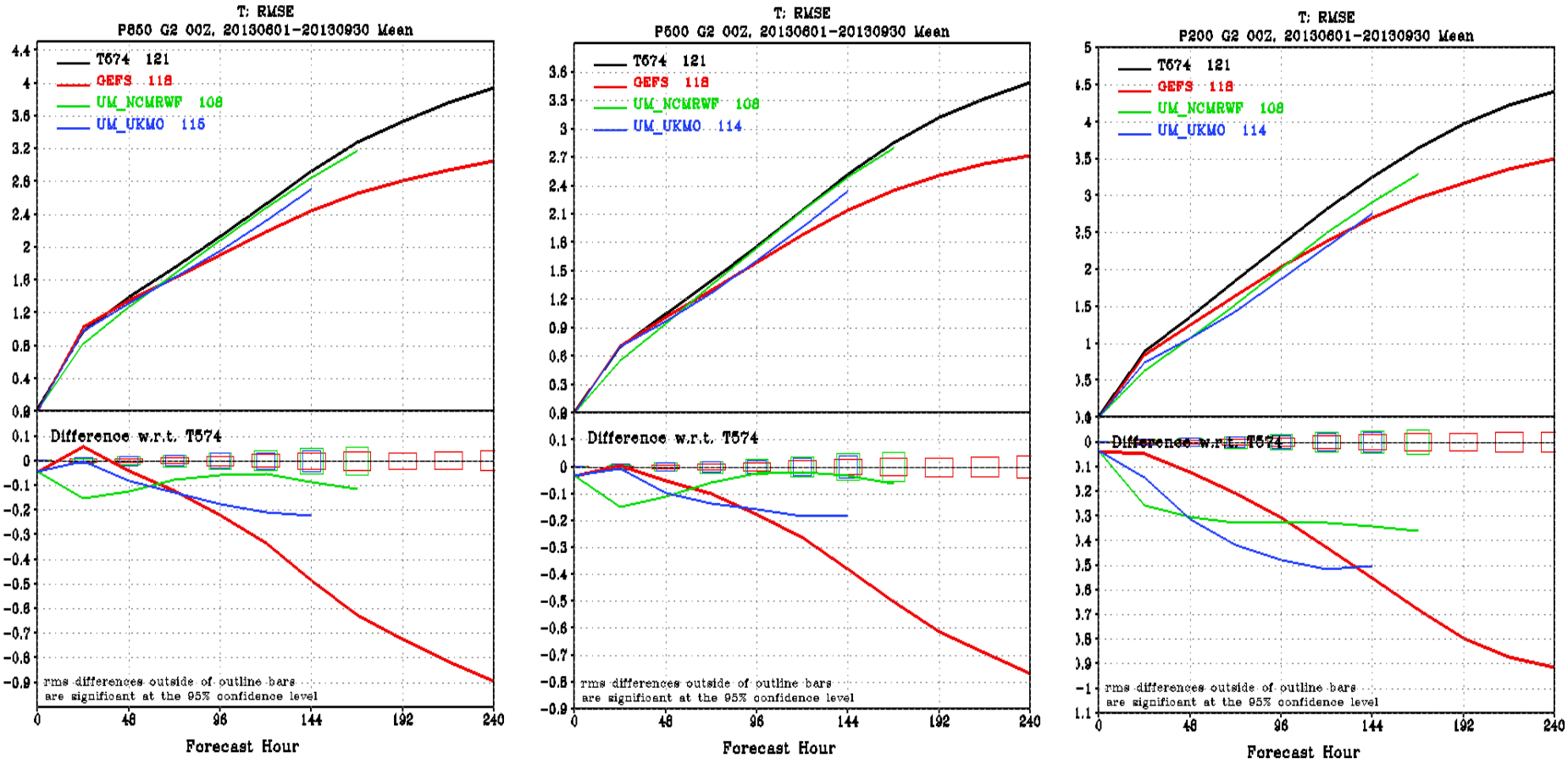

Figure 1: Root Mean Square Error (RMSE) of Temperature at 850, 500 & 200hPa pressure level (upper part) and difference of Mean (RMSE) w.r.t T574L64 and its statistical significance (lower part) over Globe.

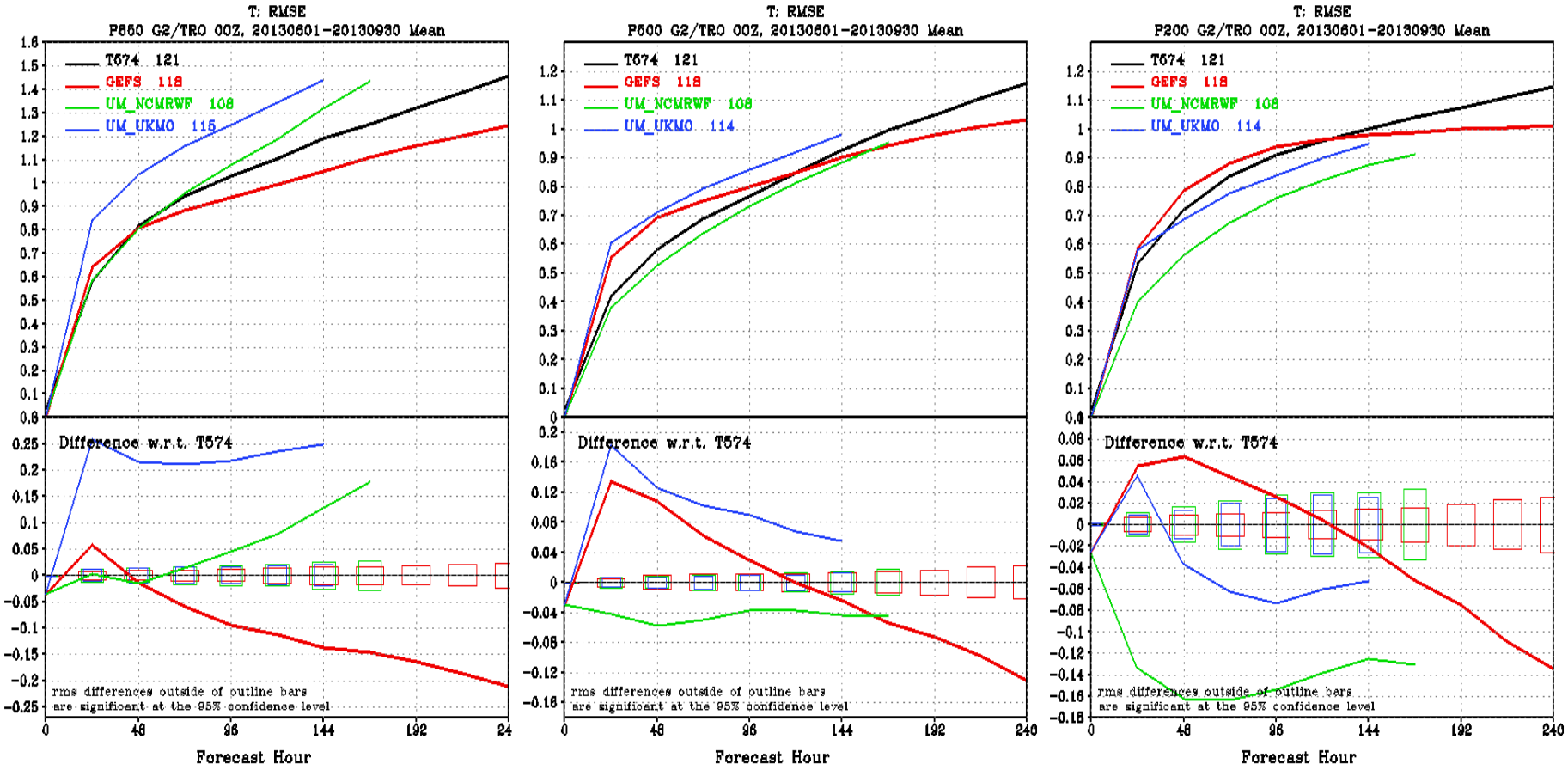

Figure 2: Root Mean Square Error (RMSE) of Temperature at 850, 500 & 200hPa pressure level (upper part) and difference of Mean (RMSE) w.r.t T574L64 and its statistical significance (lower part) over Tropics

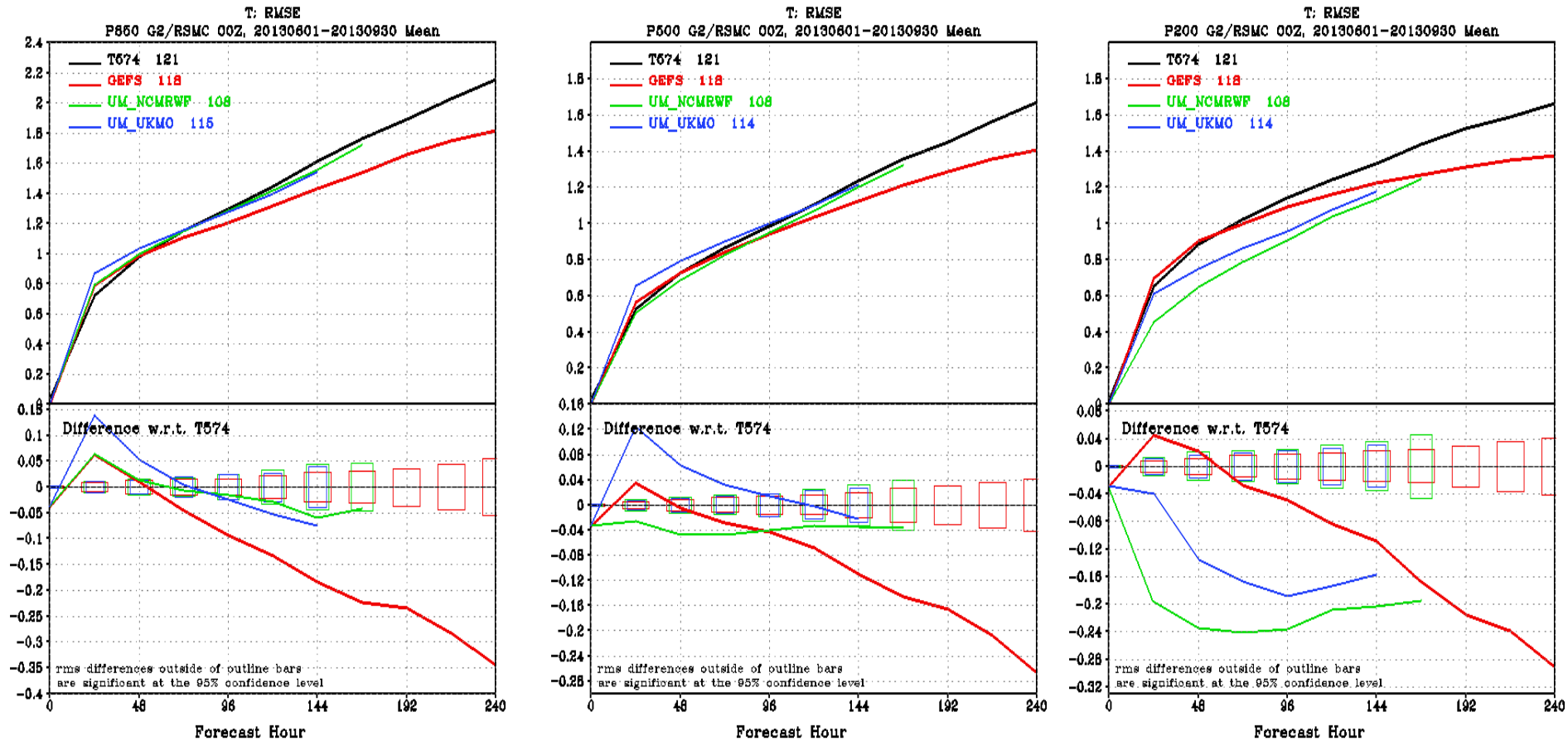

Figure 3: Root Mean Square Error (RMSE) of Temperature at 850, 500 & 200hPa pressure level (upper part) and difference of Mean (RMSE) w.r.t T574L64 and its statistical significance (lower part) over RSMC

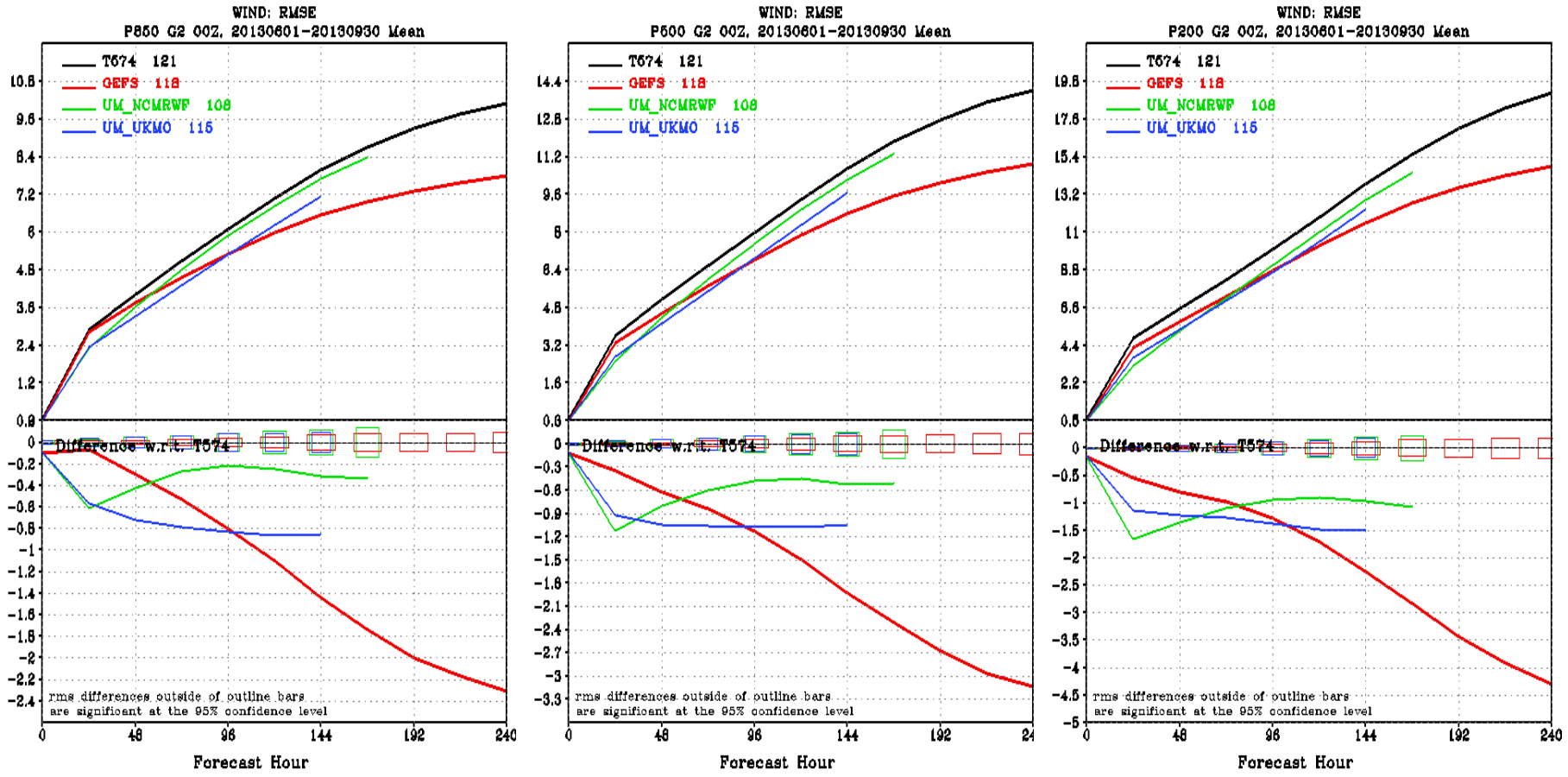

Figure 4: Root Mean Square Error (RMSE) of Wind vector at 850, 500 & 200hPa pressure level (upper part) and difference of Mean (RMSE) w.r.t T574L64 and its statistical significance (lower part) over Globe.

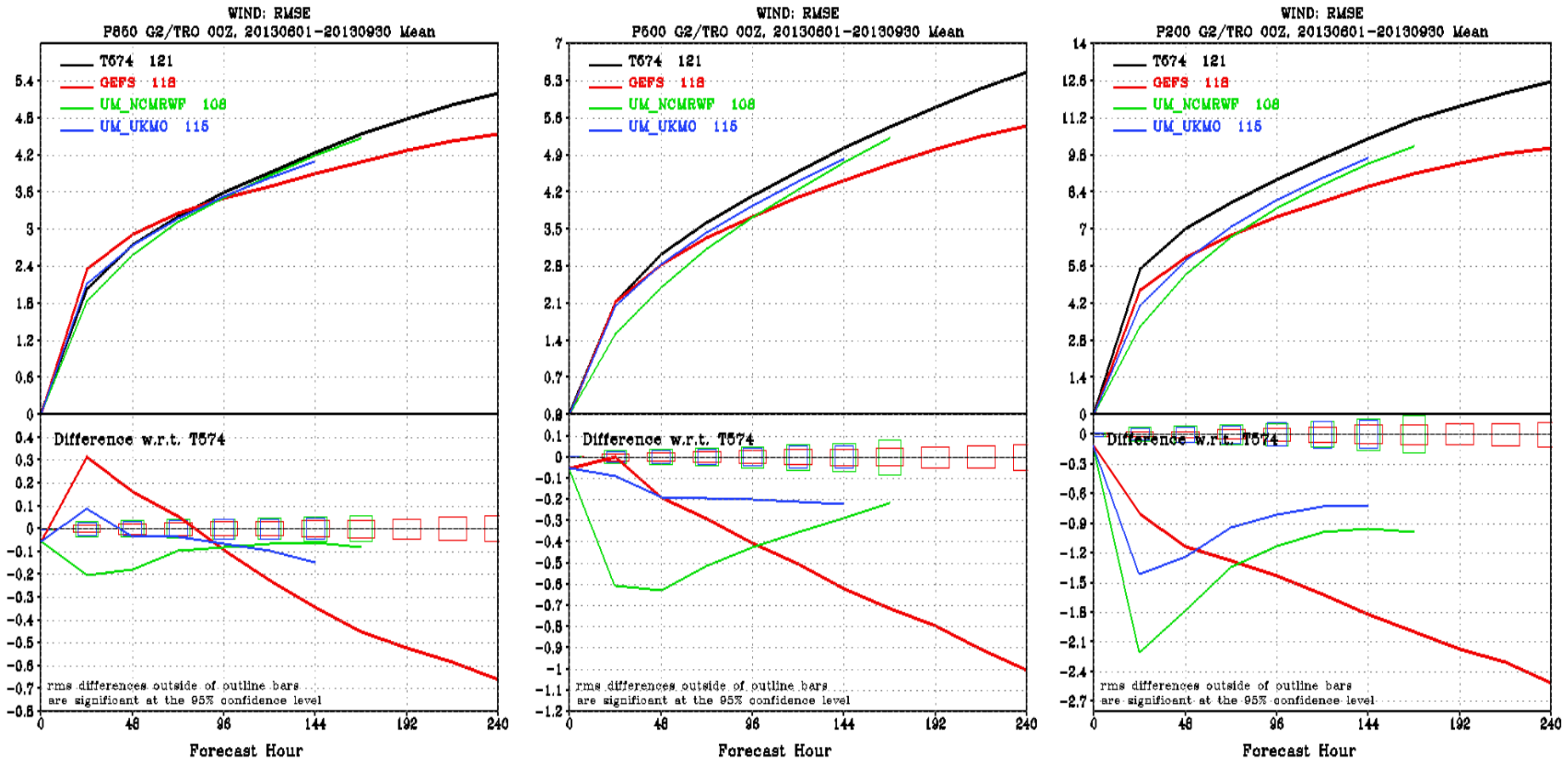

Figure 5: Root Mean Square Error (RMSE) of Wind vector at 850, 500 & 200hPa pressure level (upper part) and difference of Mean (RMSE) w.r.t T574L64 and its statistical significance (lower part) over Tropics.

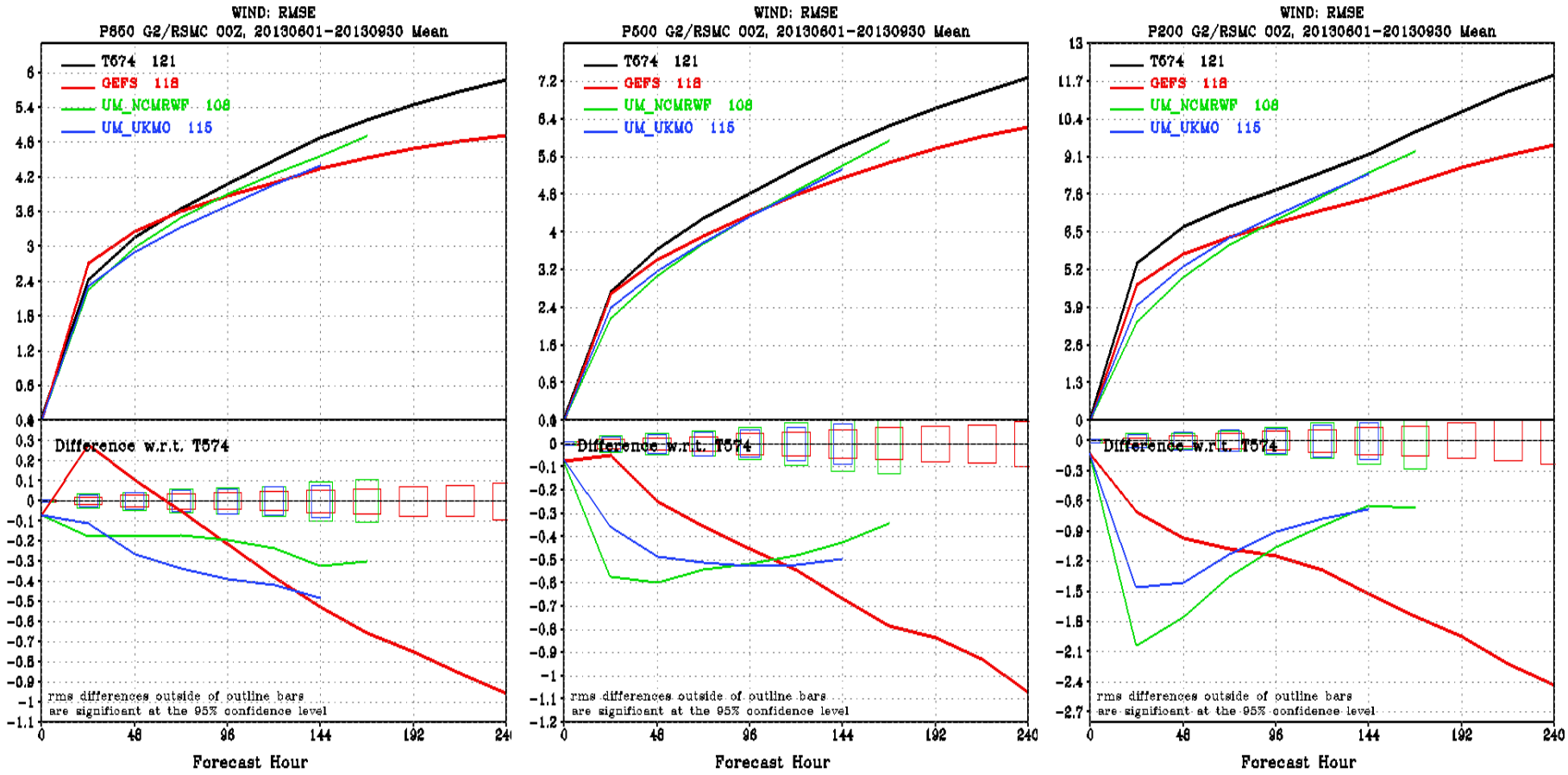

Figure 6: Root Mean Square Error (RMSE) of Wind vector at 850, 500 & 200hPa pressure level (upper part) and difference of Mean (RMSE) w.r.t T574L64 and its statistical significance (lower part) over RSMC.

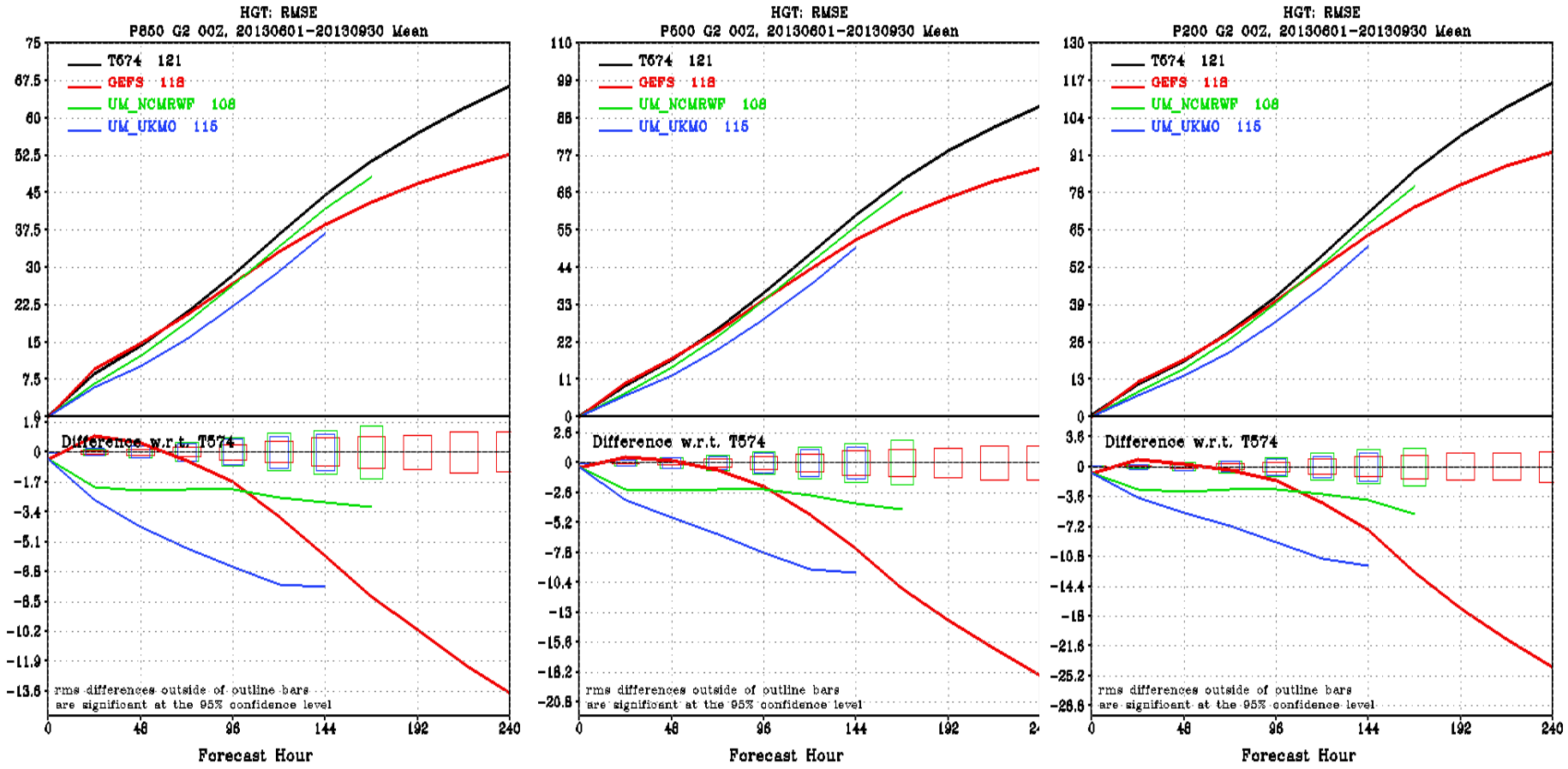

Figure 7: Root Mean Square Error (RMSE) of Geopotential Height at 850, 500 & 200hPa pressure level (upper part) and difference of Mean (RMSE) w.r.t T574L64 and its statistical significance (lower part) over Globe.

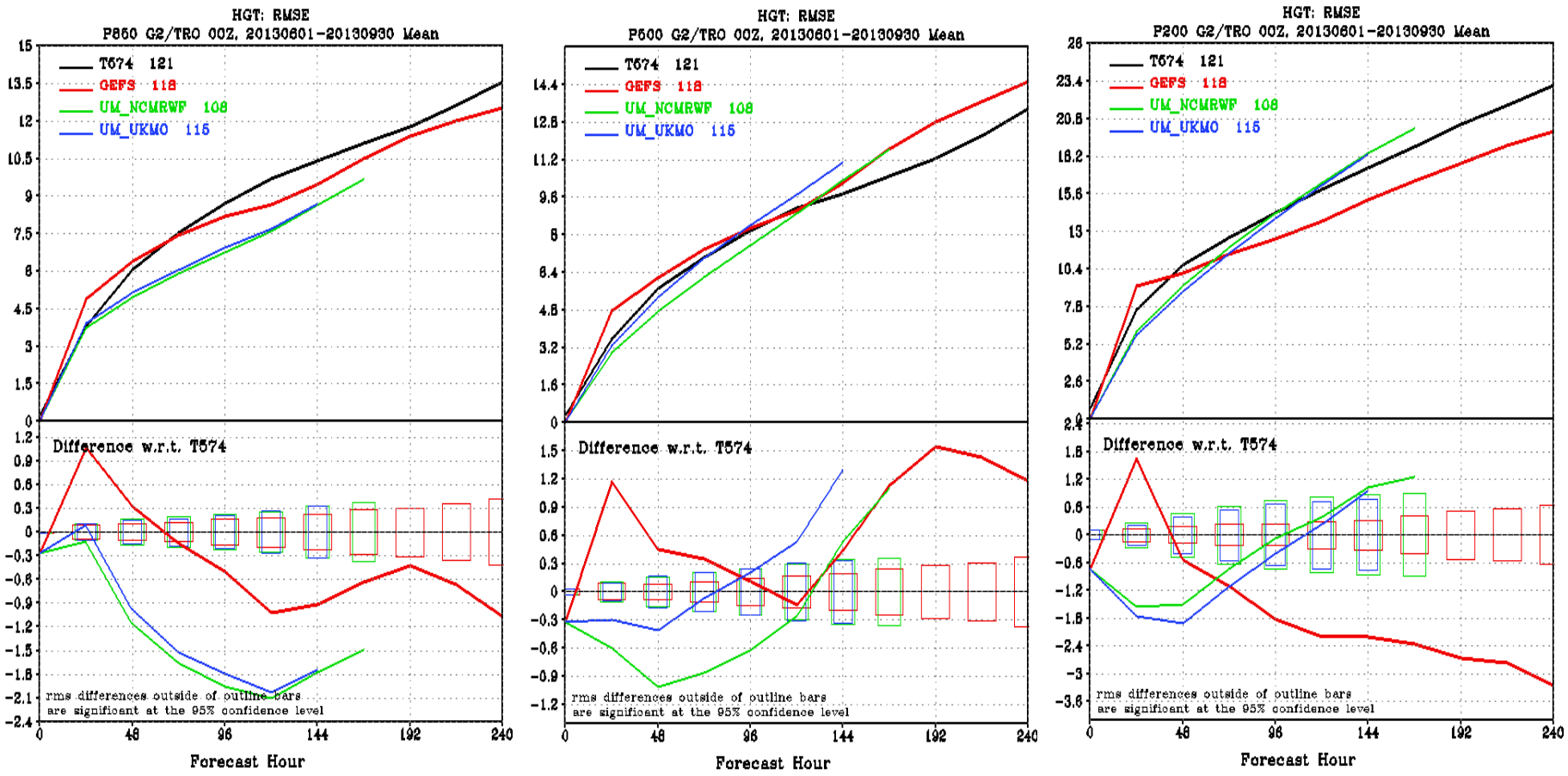

Figure 8: Root Mean Square Error (RMSE) of Geopotential Height at 850, 500 & 200hPa pressure level (upper part) and difference of Mean (RMSE) w.r.t T574L64 and its statistical significance (lower part) over Tropics.

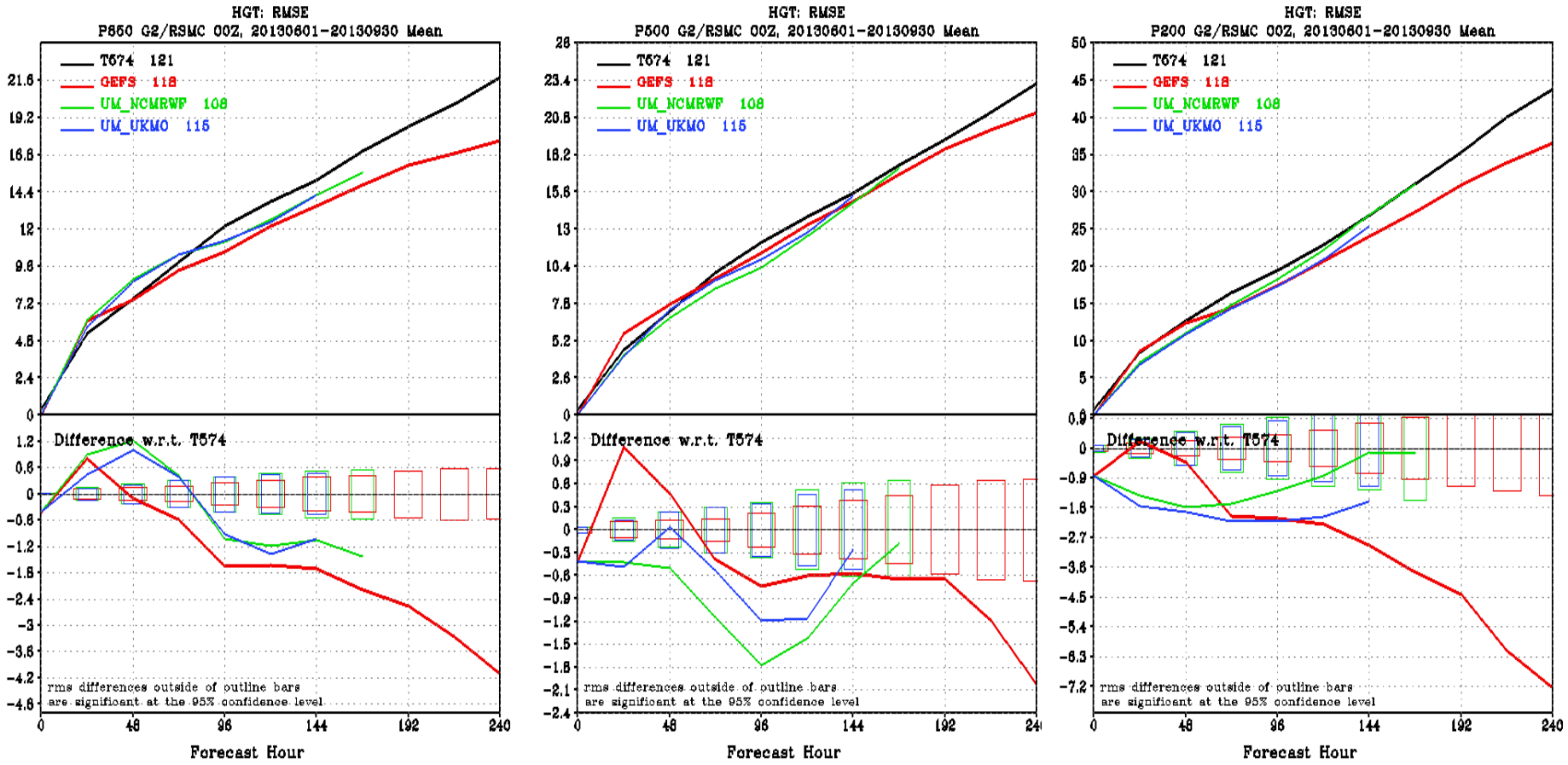

Figure 9: Root Mean Square Error (RMSE) of Geopotential Height at 850, 500 & 200hPa pressure level (upper part) and difference of Mean (RMSE) w.r.t T574L64 and its statistical significance (lower part) over RSMC.

Chapter 3: Rainfall Forecast Verification

Raghavendra Ashrit, Kuldeep Sharma, Anumeha Dube, Gopal R. Iyengar and A. K. Mitra

1. Observed Rainfall data over India

Rainfall analysis based on quality controlled observations is very useful and critical for verification of the NWP forecasts. In this study we use the IMD-NCMRWF merged daily rainfall data available at 0.5°, denoted NMSG. The NMSG objectively analyses the IMD daily rain gauge observations onto a 0.5° grid using a successive corrections technique with the TRMM 3B42 satellite precipitation providing the first guess field. In the NMSG product merging of the IMD's gauge data not only corrects the mean biases in satellite estimates but also enhances the satellite information over India, which is affected by temporal sampling errors (Mitra et al. 2009). The real time rainfall analysis at 0.5° grid resolution is used from 1st June to 30th September 2013. The data analysis and verification is carried out for all the grids on the Indian land regions. Grids over the ocean and Himalayas are masked.

2. Average frequency of rainfall events

A comparison of the observed and forecast average frequency of rainfall in different thresholds is tabulated in Figure 1. The frequency of occurrence is computed for each day during JJAS 2013 and average is worked out for both models (GFS and NCUM). The wet bias in both the model forecasts is evident from the tabulated values in Figure 1. The histogram of difference (%) in the frequency is also presented in Figure 1. It is evident that the bias in the rainfall frequency is large in NCUM compared to that in GFS forecasts. It can be concluded that the NCUM overestimates (*underestimates*) the frequency of low (*high*) rainfall amounts. The NCUM prominently show higher frequency (by about 30-40%) of low rainfall amounts (1-10 and 10-20mm/day range) at all lead times. For 40 mm threshold the NCUM forecasts have lower frequency (by about 20-50%) at all lead times. The GFS forecasts have higher frequency (by about 6-9%) only for 1 mm rainfall threshold at all lead times. For other rainfall thresholds GFS forecast rainfall has lower frequency (by about 0-10%) at all

lead times. It must be noted that average frequency of rainfall events in the forecasts highlights the overall health of the forecast system; it has no bearing on the forecast skill of the model. Analysis of the forecast skill is presented in the next section.

3. Rainfall Forecast Skill

Firstly the verification results are presented in terms of standard categorical verification scores used in evaluating precipitation, namely, Probability of Detection (POD), Success Ratio (SR), Probability of False detection (POFD), Extreme Dependency Score (EDS) (Stephenson et al. 2008), Equitable Threat Score (ETS), Accuracy and Hanssen and Kuipers Score (HK Score), all computed over the full domain covering India. Description of each of the scores is provided in **Appendix-I**. Details of these scores can also be found in references on statistical methods like Jolliffe and Stephenson (2012) and Wilks (2011). This is followed by verification using the CRA method to quantify the systematic errors.

3.1 Categorical Verification of Rainfall Forecasts

The categorical verification scores are computed for each rainfall threshold based on all the observation/forecast pairs of each day during the monsoon season. The performance of the model forecasts (Day-1, Day-3 and Day-5) are summarized using box and whisker plots in Figures 2-4.The averages of each of the scores are tabulated in Table 1. The accuracy (fraction correct) and success ratio (SR) for both models suggest similar performance of the two models with no clear separation. By and large higher values of POD, BIAS and POFD in the NCUM compared to GFS are consistent with the wet bias in NCUM discussed in the last section. However the FAR values in both the models are mostly same. ETS, HK Score and EDS indicate higher average skill in the NCUM forecasts.

The skill scores based on each day of the season are summarized using box and whisker plots. The left panels in Figure 2 show the Probability of Detection (POD) and right panels show Success Ratio (SR). Both the scores indicate very good skill for rainfall thresholds below 20 mm/day. For 1 and 10 mm/day thresholds NCUM has higher POD (left panels) and marginally lower SR (right panels). Lower SR for NCUM than in GFS suggests NCUM forecasts feature higher false alarms than in GFS

forecasts for these rainfall thresholds. For 20 mm/day threshold NCUM shows higher POD in Day-1 (and in Day-3 marginally) forecast along with higher SR in all Day-1, Day-3 and Day-5 forecasts. Similarly for 40 mm/day threshold the NCUM forecasts show lower POD and higher SR compared to GFS forecasts.

This means for higher rainfall thresholds NCUM has lower hit rate and also lower false alarms. Both models show low POD and SR for higher rainfall thresholds (80 mm/day) indicating poor skill along with increasing number of outliers for higher rainfall thresholds.

The panels in Figure 3 show Probability of False Detection (POFD) on left and Extreme Dependency Score (EDS) on right. The box and whisker plots showing the POFD indicate that NCUM forecasts have high false alarms compared to GFS forecasts. For all thresholds up to 20 mm/day the NCUM forecasts show higher EDS.

Similarly the panels in Figure 4 show the box and whisker plots for two summary scores, the Equitable Threat Score (ETS) and Hanssen and Kuipers Score (HK Score). With rather low ETS values both models have moderate skill. NCUM does a better job in separating ‘yes’ events from ‘no’ events for 1, 10 and 20 mm/day thresholds.

3.2 CRA Verification of Rainfall Forecasts

The CRA method is an object-oriented verification procedure suitable for gridded forecasts that was developed for estimating the systematic errors in forecasts for rainfall systems (Ebert and McBride, 2000; Ebert and Gallus, 2009). It was one of the first methods to measure errors in predicted location and to separate the total error into components due to errors in location, volume and pattern. The steps involved in CRA technique are described in Ebert and Gallus (2009). A brief summary of the procedure is given here.

Firstly a CRA is defined for an observation/forecast pair based on a user-specified isohyet (rain rate contour) in the forecast and/or the observations. It is the *union* of the forecast and observed rain entities as illustrated in Figure 5. The forecast and observed entities need not overlap, but they must be associated with each other, that is, they must be nearby and associated with a common synoptic situation. During the monsoon season large parts of India regularly receive rainfall in the range up to 10

mm/day. It was found that choice of 1, 2 and 5 mm/day contours spread the CRA across large geographical areas, merging unrelated rain systems. CRAs defined by higher thresholds of 10, 20, 40 and 80 mm/day were used to identify and isolate the events of higher rainfall amounts.

In the next step a pattern matching technique is used for estimating the location error. Here the forecast field is horizontally translated over the observed field in a series of iterations until the best match is obtained. The location error is then simply the vector displacement of the forecast.

The best match between the two entities can be determined either: (a) by maximizing the correlation coefficient, (b) by minimizing the total squared error, (c) by maximizing the overlap of the two entities, or (d) by overlaying the centres of gravity of the two entities. For a good forecast all of the methods will give very similar location errors. In the present study the best match is determined by maximizing the correlation. The mean squared error (MSE) and its decomposition (location error, volume error and pattern error) are computed as shown below (see Grams et al. 2006, for details of the derivation).

$$MSE_{Total} = MSE_{Displacement} + MSE_{Volume} + MSE_{Pattern} \quad (1)$$

where the component errors are estimated as

$$MSE_{Displacement} = 2\boldsymbol{s_F s_O}\,(r_{OPT} - r),$$

$$MSE_{Volume} = (\boldsymbol{F' - O'}), \quad (2)$$

$$MSE_{Pattern} = 2\boldsymbol{s_F s_O}\,(1 - r_{OPT}) + (\boldsymbol{s_F} - \boldsymbol{s_O})^2$$

In the above expressions $\boldsymbol{F'}$ and $\boldsymbol{O'}$ are the mean forecast and observed precipitation values after shifting the forecast to obtain the best match, $\boldsymbol{s_F}$ and $\boldsymbol{s_O}$ are the standard deviations of the forecast and observed precipitation, respectively, before shifting. The spatial correlation between the original forecast and observed features (r) increases to an optimum value (r_{OPT}) in the process of correcting the location via pattern matching.

The CRA verification on any typical observation-forecast pair starts with detailed QPF statistics for rainfall above 1mm as shown in Figures 6-7 for Day-3 forecasts by GFS and NCUM. **The panels show the starting date of 24 hour rainfall accumulation**. The figure shows the GFS Day-3 forecast valid for 17th June 2013 along with detailed statistics. The statistics for this observation-forecast pairs indicate NCUM (compared to GFS) has higher number of raining grids 641 (453) and

lower average rain rate of 31 mm/day (48 mm/day), lower maximum rain rate 105 mm/day (288 mm/day). This is mainly due to the high rainfall amounts along the west coast of India which is captured in the GFS forecasts and is missed in the NCUM forecasts. However, NCUM (compared to GFS) has lower mean absolute error (MAE) of 10.5 mm/day (13 mm/day), lower RMSE of 20 mm/day (29 mm/day) and higher (lower) correlation 0.48 (29). This is because in the GFS forecasts the rainfall over the west coast is spread over larger area in Maharastra (and completely missed in Gujarat) compared to observations. Although the POD is higher in NCUM, the comparable fraction of false alarms in both models leads to higher bias score in NCUM. With higher values of ETS and HK Score NCUM shows higher skill compared to GFS in this observation-forecast pair.

The CRA verification is shown in Figures 8-9 for 17th June 2013 in both models using the 40 mm/day threshold. The spatial maps show the observed and forecast rainfall associated with the Uttarakhand flood disaster. The 40 mm/day contour is shown in bold to represent the area covered with 40 mm/day rain amount. The scatter plot on the right indicates the agreement in observed and forecast rainfall after the shifting the forecast rainfall to obtain best match with observation. The numbers below the scatter plot show (i) number of grids with rainfall excess of 40 mm/day (ii) average rain rate (mm/day) (iii) maximum rain (mm/day) and (iv) rain volume (km^3) in the observations and forecasts. In the GFS forecasts the maximum rain (highest rain amount) is very high (204 mm/day) and comparable to the observed value (248 mm/day). Since the number of grids with rainfall exceeding 40 mm/day in the forecasts is 15 as against 65 in observations, the average rain and rain volume are 29 mm/day and 6 km^3 as against 73 mm/day and 15 km^3. In the NCUM forecasts (Figure 9), the highest rainfall amount is 105 mm/day which is lower compared to the observed value of 248 mm/day. Since there are 55 grids with rainfall exceeding 40 mm/day the average rain rate and rain volume are 42 mm/day and 12 km^3 as against 56 mm/day and 17 km^3. Thus due to better spatial distribution of rainfall, NCUM forecast shows improved predicting of average rain and rain volume.

GFS forecast have RMSE of 72 mm/day which is mainly contributed by volume (39%) and patter errors (44%). Displacement error contribution is only 17%. However

in the NCUM forecast the RMSE is 55 mm/day which is chiefly contributed by pattern error (67%). Displacement error (26%) and volume error (7%) have lower share.

Similar analysis is presented for Day-5 forecasts showing the QPF statistics (Figures 10 and 11) for rainfall above 1mm and CRA Verification for 40 mm/day threshold (Figures 12-13). The all India statistics indicate NCUM and GFS forecast skill are comparable although NCUM underestimate the highest rainfall amounts, while it has better spatial distribution compared to GFS forecast. The CRA analysis shows that a large part of RMSE in the GFS forecasts is due to volume and pattern errors. In the NCUM Day-5 forecasts displacement and pattern errors mainly contribute to the RMSE.

The CRA analysis and the error decomposition are meaningful only for cases where the displacement is correct. For all the cases where the correlation is not significant or if the CRA is shifted out of domain, the displacement is considered *incorrect*. This is indicated in the Figures 8, 9, 12 and 13 just above the 'Error Decomposition'. Analysis of the error decomposition is purely based on the CRAs involving cases with *correct* displacement ('*good*' CRA). A forecast is considered '*good*' when observation-forecast pair match very well (are similar). For all such '*good*' cases, the CRA error decomposition is easily done since it involves '*good*' CRAs. A forecast is considered '*bad*' when the observation-forecast pair do not match well (are different). For all such '*bad*' cases CRA error decomposition is difficult since very often the CRA is shifted out of domain (loss of information). Such CRAs involving '*bad*' forecasts are all rejected for Eror decomposition. In the analysis carried out for the whole season, the fraction of rejected CRAs is direct indicator of the model performance. Better performing models should have relatively lower rejection of CRAs. The number of '*good*' CRAs along with total number of CRAs (in bracket) in the Day-1, Day-3 and Day-5 forecasts of both models is shown in Table 2. NCUM forecasts generally have higher number of 'good' CRAs. For 10 mm/day CRA, GFS forecasts have about 83%, 84% and 89% of total CRAs rejected in the Day-1, Day-3 and Day-5 forecasts respectively. For the same 10 mm/day CRAs, NCUM forecasts have about 70%, 80% and 79% of rejections in the Day-1, Day-3 and Day-5 forecasts respectively. For 20 mm/day CRA GFS (NCUM) has 95% (89%), 95% (91%) and 97% (93%) of rejections in Day-1, Day-3 and Day-5 forecasts respectively.

The contribution from displacement error, pattern error and volume error are assessed for 10, 20 and 40 mm/day cases listed in Table 3 and in box plots (Figure 14). The mean values of the x-err, y-err, td, tv and tp for GFS and NCUM are presented in Table 3 for all lead times. The positive x-err (in degree lon) indicate that on an average the forecast are found to the east of observed location. This is common to both the models. The negative y-err (in degree lat) indicate that on an average the forecasts are found to the south of observed location which is prominent in GFS forecasts. The td, tv and tp values in Table 3 (and Figure 14) indicate very similar feature for both the models. The contribution from the volume error is least. For 10 and 20 mm/day CRAs the contribution from pattern error is highest in all forecasts. For 40 mm/day CRA the contribution from displacement error (td) is highest in all the forecasts.

4. Conclusions

- A comparison of observed and forecast frequency of rainfall occurrence in 1 mm, 10 mm, 20 mm and 40 mm thresholds suggests-
    - NCUM overestimates (*underestimates*) the frequency of low (*high*) rainfall amounts. The NCUM prominently show higher frequency (by about 30-40%) of low rainfall amounts (1-10 and 10-20 mm/day range) at all lead times. For 40 mm threshold the NCUM forecasts have lower frequency (by about 20-50%) at all lead times.
    - The GFS forecasts have higher frequency (by about 6-9%) only for 1mm rainfall threshold at all lead times. For other rainfall thresholds GFS forecast rainfall has lower frequency (by about 0-10%) at all lead times.
- POD, POFD, EDS and HKscores clearly indicate higher forecast skill in NCUM in Day-1, Day-3 and Day-5 forecasts. It is noted that NCUM does a better job in separating ‘yes’ from ‘no’ events for 1, 10 and 20 mm/day thresholds.
- NCUM forecasts generally have higher number of ‘good’ CRAs. For 10 mm/day CRA, GFS forecasts have about 83%, 84% and 89% of total CRAs rejected in the Day-1, Day-3 and Day-5 forecasts respectively. For the same 10 mm/day CRAs, NCUM forecasts have about 70%, 80% and 79% of rejections in the Day-1, Day-3

and Day-5 forecasts respectively. For 20 mm/day CRA GFS (NCUM) has 95% (89%), 95% (91%) and 97% (93%) of rejections in Day-1, Day-3 and Day-5 forecasts respectively.

- GFS forecasts show higher RMSE compared to NCUM forecasts for 10 and 20 mm/day. However in both models the contribution from pattern error is over 60-80% followed by contribution from displacement error 20-40%. Contribution from volume error is consistently below 15% in both the models for all thresholds and at all lead times.

References:

Ebert, E.E. and J. L. McBride, 2000: Verification of precipitation in weather systems: Determination of systematic errors. J. Hydrol., 239, 179-202.

Ebert, E.E. and W. A. Gallus Jr, 2009: Towards better understanding of Contiguous Rain Areas (CRA) method of spatial verification, Weather and Forecasting, 24, 1401-1415

J Jolliffe, I.T. and Stephenson, D.B., 2011: Introduction, in Forecast Verification: A Practitioner's Guide in Atmospheric Science, Second Edition (eds I. T. Jolliffe and D. B. Stephenson), John Wiley & Sons, Ltd, Chichester, UK. doi: 10.1002/9781119960003.ch1

Wilks, D. S., 2011: Statistical Methods in the Atmospheric Sciences. International Geophysical Series Vol. 100, Academic Press.

Table 1: Average of verification scores (1st June-30th Sept 2013) for GFS and NCUM forecasts for 4 rainfall thresholds

		Day1				Day-2				Day-3				Day-4				Day-5			
		1	*10*	*20*	*40*	*1*	*10*	*20*	*40*	*1*	*10*	*20*	*40*	*1*	*10*	*20*	*40*	*1*	*10*	*20*	*40*
Accuracy	**GFS**	0.7	0.8	0.9	0.9	0.7	0.8	0.9	0.9	0.7	0.8	0.9	0.9	0.7	0.8	0.9	0.9	0.7	0.8	0.8	0.9
	NCUM	0.7	0.8	0.9	1.0	0.7	0.8	0.9	1.0	0.7	0.8	0.9	1.0	0.7	0.7	0.9	1.0	0.7	0.7	0.9	1.0
SR	**GFS**	0.7	0.5	0.3	0.2	0.7	0.4	0.3	0.2	0.7	0.4	0.3	0.2	0.7	0.4	0.3	0.1	0.7	0.4	0.3	0.1
	NCUM	0.6	0.4	0.3	NA	0.6	0.4	0.3	0.2	0.6	0.4	0.3	0.2	0.6	0.4	0.3	0.2	0.6	0.4	0.3	NA
POD	**GFS**	0.8	0.4	0.3	0.2	0.7	0.4	0.3	0.2	0.7	0.4	0.3	0.2	0.7	0.4	0.3	0.1	0.7	0.4	0.3	0.1
	NCUM	0.9	0.6	0.4	0.2	0.9	0.6	0.3	0.1	0.9	0.6	0.3	0.1	0.9	0.5	0.3	0.1	0.9	0.5	0.3	0.1
FAR	**GFS**	0.3	0.6	0.7	0.8	0.3	0.6	0.7	0.8	0.3	0.6	0.7	0.8	0.3	0.6	0.7	0.9	0.3	0.6	0.7	0.9
	NCUM	0.4	0.6	0.7	NA	0.4	0.6	0.7	0.8	0.4	0.6	0.7	0.8	0.4	0.6	0.7	0.8	0.4	0.6	0.7	NA
BIAS	**GFS**	1.1	1.0	1.0	1.5	1.1	1.0	1.0	1.4	1.1	1.0	1.1	1.5	1.1	1.0	1.1	1.4	1.1	1.0	1.1	1.5
	NCUM	1.5	1.5	1.2	1.2	1.4	1.4	1.1	1.2	1.4	1.4	1.1	1.2	1.4	1.3	1.1	1.3	1.4	1.4	1.0	1.2
ETS	**GFS**	0.3	0.2	0.1	0.1	0.3	0.2	0.1	0.1	0.3	0.2	0.1	0.1	0.3	0.2	0.1	0.1	0.2	0.1	0.1	0.1
	NCUM	0.3	0.2	0.2	0.1	0.3	0.2	0.1	0.1	0.3	0.2	0.1	0.1	0.3	0.2	0.1	0.1	0.2	0.2	0.1	0.0
HKSCORE	**GFS**	0.4	0.3	0.2	0.2	0.4	0.3	0.2	0.2	0.4	0.3	0.2	0.1	0.4	0.3	0.2	0.1	0.4	0.2	0.2	0.1
	NCUM	0.4	0.4	0.3	NA	0.4	0.4	0.2	0.1	0.4	0.3	0.2	0.1	0.4	0.3	0.2	0.1	0.4	0.3	0.2	NA
EDS	**GFS**	0.4	0.3	0.3	0.2	0.4	0.3	0.3	0.2	0.4	0.3	0.3	0.2	0.4	0.3	0.3	0.1	0.4	0.3	0.2	0.1
	NCUM	0.8	0.5	0.4	0.2	0.7	0.5	0.3	0.0	0.7	0.4	0.3	0.0	0.7	0.4	0.3	-0.1	0.7	0.4	0.2	-0.1
POFD	**GFS**	0.3	0.1	0.1	0.0	0.3	0.2	0.1	0.0	0.3	0.2	0.1	0.0	0.3	0.2	0.1	0.0	0.3	0.2	0.1	0.0
	NCUM	0.5	0.2	0.1	0.0	0.5	0.2	0.1	0.0	0.5	0.2	0.1	0.0	0.5	0.2	0.1	0.0	0.5	0.2	0.1	0.0
OR	**GFS**	7.1	5.1	6.0	11.1	7.0	5.0	5.2	NA	6.5	4.7	5.1	7.7	6.2	4.3	4.4	5.8	5.9	3.9	4.1	4.9
	NCUM	14.0	7.3	7.6	NA	11.6	6.1	6.5	13.8	11.0	5.7	6.1	10.6	10.0	5.2	5.7	7.2	9.6	4.9	5.1	NA
ORSS	**GFS**	0.7	0.6	0.7	0.6	0.7	0.6	0.6	0.6	0.7	0.6	0.6	0.5	0.7	0.6	0.6	0.4	0.7	0.5	0.5	0.4
	NCUM	0.8	0.7	0.7	NA	0.8	0.7	0.6	0.4	0.8	0.7	0.6	0.4	0.8	0.6	0.6	0.3	0.8	0.6	0.6	NA

Table 2: The total number of CRAs (values in bracket) for 3 thresholds in GFS and NCUM forecasts and the number of CRAs with correct displacements

	Day-1	Day-3	Day-5
10 mm/day(NCUM)	86 (287)	65 (324)	64 (310)
10 mm/day(GFS)	66 (389)	60 (377)	40 (364)
20 mm/day(NCUM)	46 (414)	37 (421)	31(432)
20 mm/day(GFS)	24 (461)	21 (458)	12 (457)
40 mm/day(NCUM)	8 (363)	3 (367)	4 (366)
40 mm/day(GFS)	3 (395)	5 (422)	4 (433)

Table 3: Average displacements (*x and y*) in the forecasts rainfall CRAs along with the % share in total error from three components displacement error (*Td*), volume error (*Tv*) and pattern error (*Tp*)

GFS	Day-1			Day-2			Day-3			Day-4			Day-5		
	10	20	40	10	20	40	10	20	40	10	20	40	10	20	40
x-err	0.8	0.6	2.2	1.3	0.9	1.5	1.4	1.2	1.1	1.8	1.1	-0.2	1.1	1.6	0.7
y-err	-0.8	-0.8	-1.3	-0.4	-0.1	-1.4	0.2	0.4	-0.1	-0.4	0.1	-0.8	-0.4	-0.7	0.9
Td	24	36	63	28	35	66	29	42	65	32	43	43	32	41	57
Tv	4	8	22	4	11	1	4	6	1	6	6	22	6	8	13
Tp	71	56	15	67	54	33	67	52	34	62	51	35	62	51	30

NCUM	Day-1			Day-2			Day-3			Day-4			Day-5		
	10	20	40	10	20	40	10	20	40	10	20	40	10	20	40
x-err	0.9	1.3	1.2	1.1	1.1	0.8	1.2	1.3	0.6	1.1	1.5	3.0	0.8	1.4	1.3
y-err	0.2	0.0	-0.2	0.0	0.2	0.7	0.2	0.2	-0.3	0.1	0.1	-1.7	-0.3	-0.4	-1.9
Td	16	28	58	16	27	58	24	36	47	33	43	74	31	50	70
Tv	5	9	7	4	7	11	3	10	13	5	9	5	7	8	6
Tp	79	63	35	79	66	30	72	54	40	62	49	21	62	43	24

	Day-1				Day-2				Day-3				Day-4				Day-5			
	1	*10*	*20*	*40*	*1*	*10*	*20*	*40*	*1*	*10*	*20*	*40*	*1*	*10*	*20*	*40*	*1*	*10*	*20*	*40*
Obs	**921**	**405**	**210**	**71**	**921**	**405**	**210**	**71**	**921**	**405**	**210**	**71**	**921**	**405**	**210**	**71**	**921**	**405**	**210**	**71**
GFS	**1002**	**384**	**190**	**67**	**992**	**392**	**197**	**69**	**977**	**397**	**200**	**72**	**981**	**394**	**201**	**72**	**989**	**404**	**209**	**76**
NCUM	**1321**	**572**	**231**	**56**	**1286**	**546**	**209**	**46**	**1270**	**528**	**201**	**42**	**1262**	**521**	**193**	**40**	**1262**	**528**	**190**	**35**

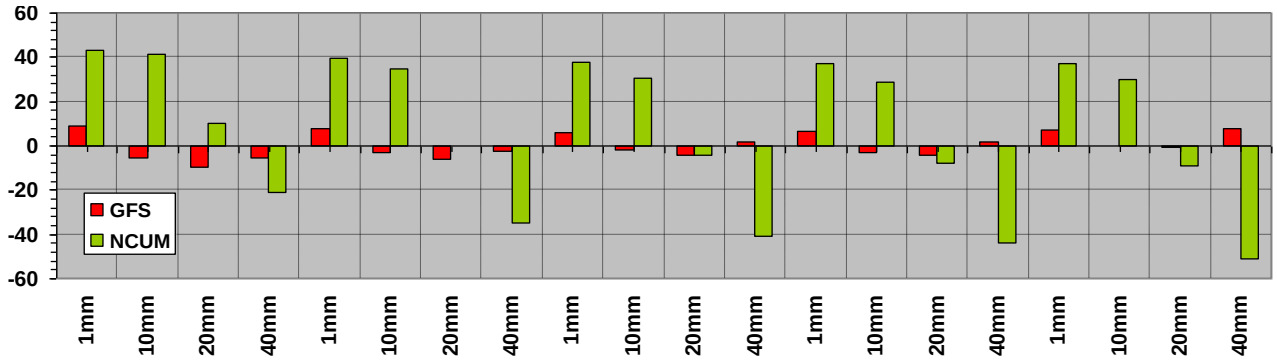

Figure 1: Observed and forecast frequency of occurrence of rainfall for different thresholds (values in table) and the bar chart shows difference (%) in the two model forecast frequencies against the observations

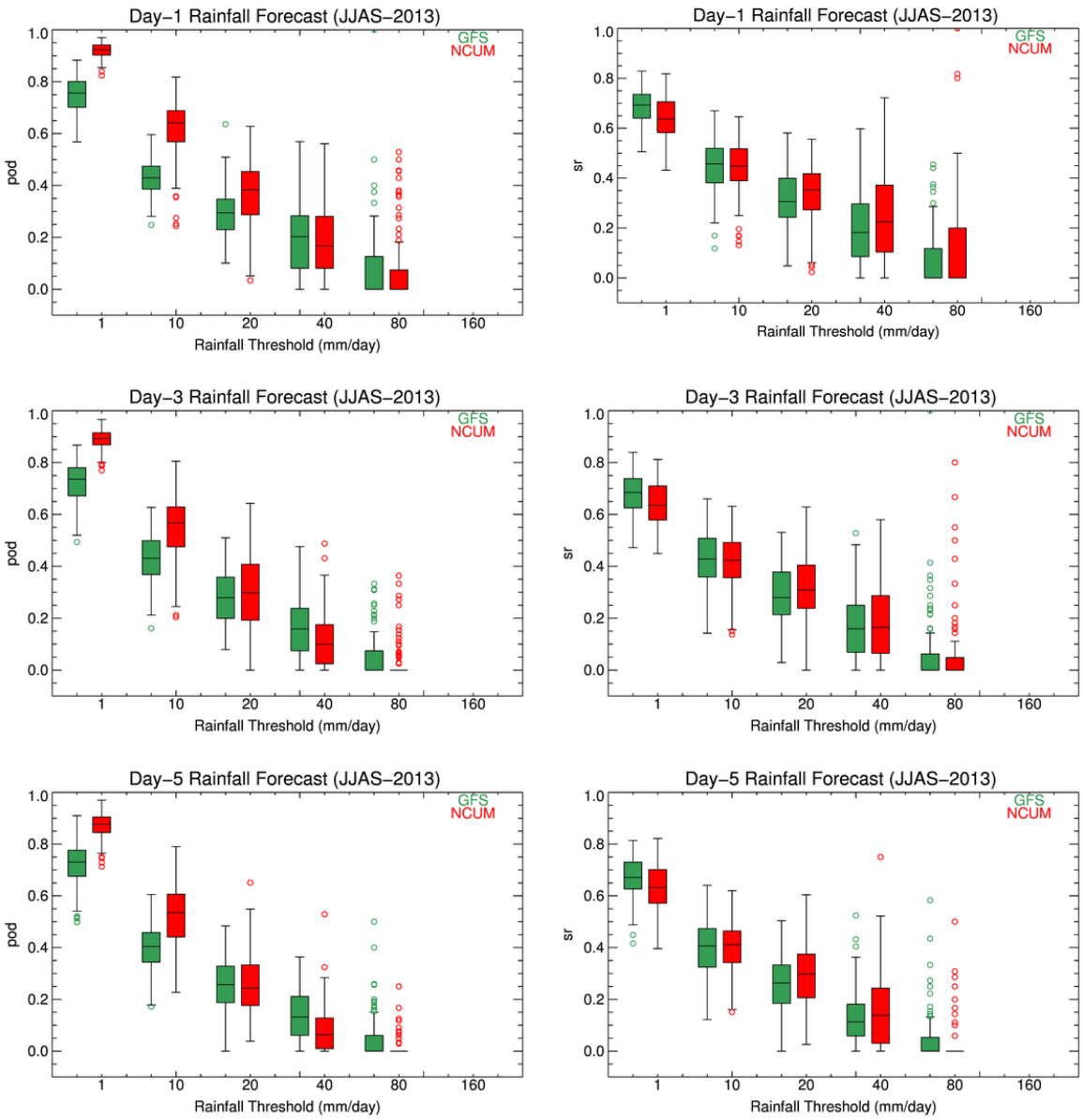

Figure 2: Probability of detection (POD; left) and Success Ratio (SR; right) in the Day-1, Day-3 and Day-5 forecasts of two models GFS and NCUM for various rainfall thresholds

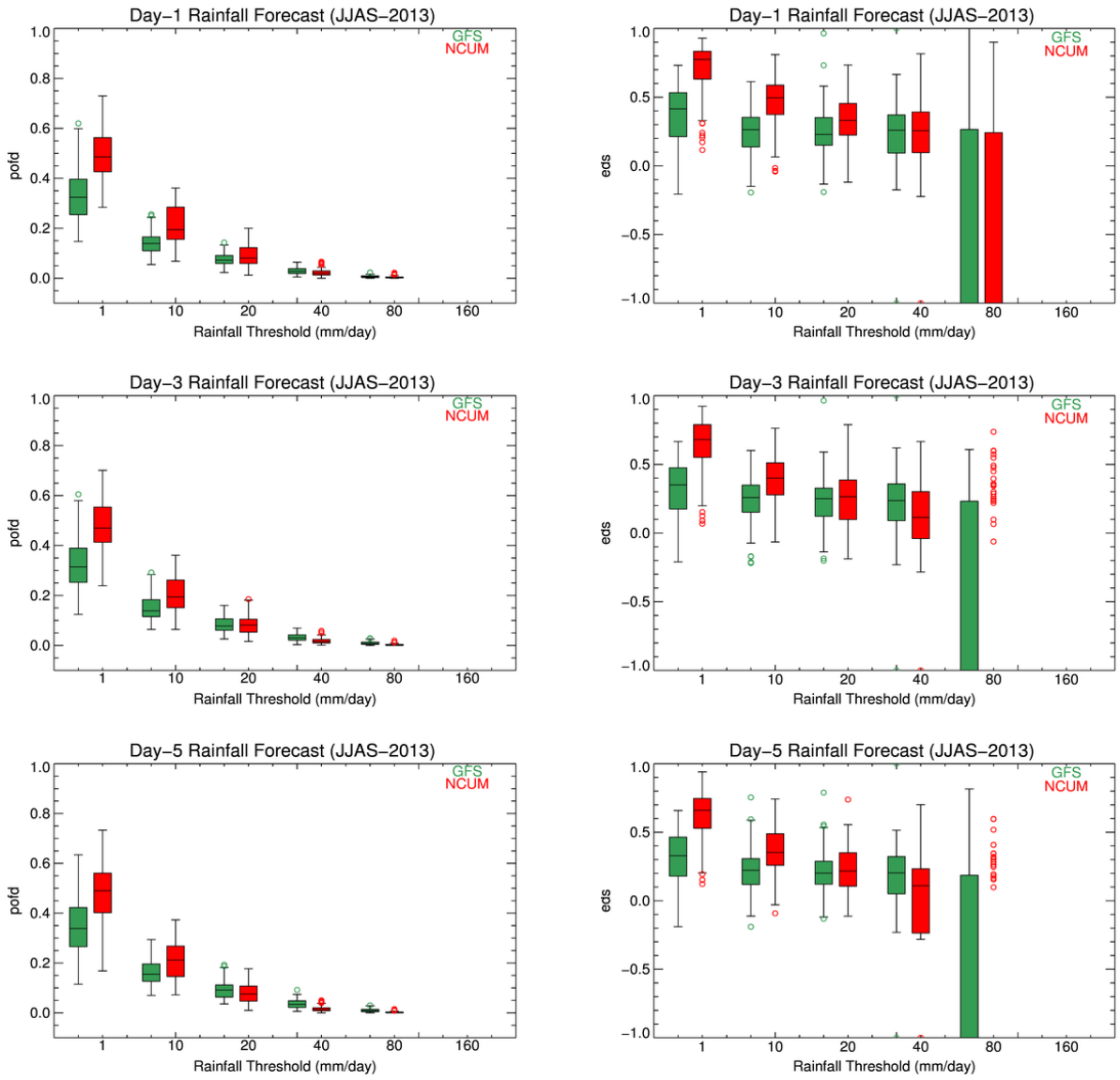

Figure 3: Probability of false detection (POFD; left) and Extreme dependency score (EDS; right) in the Day-1, Day-3 and Day-5 forecasts of two models GFS and NCUM for various rainfall thresholds

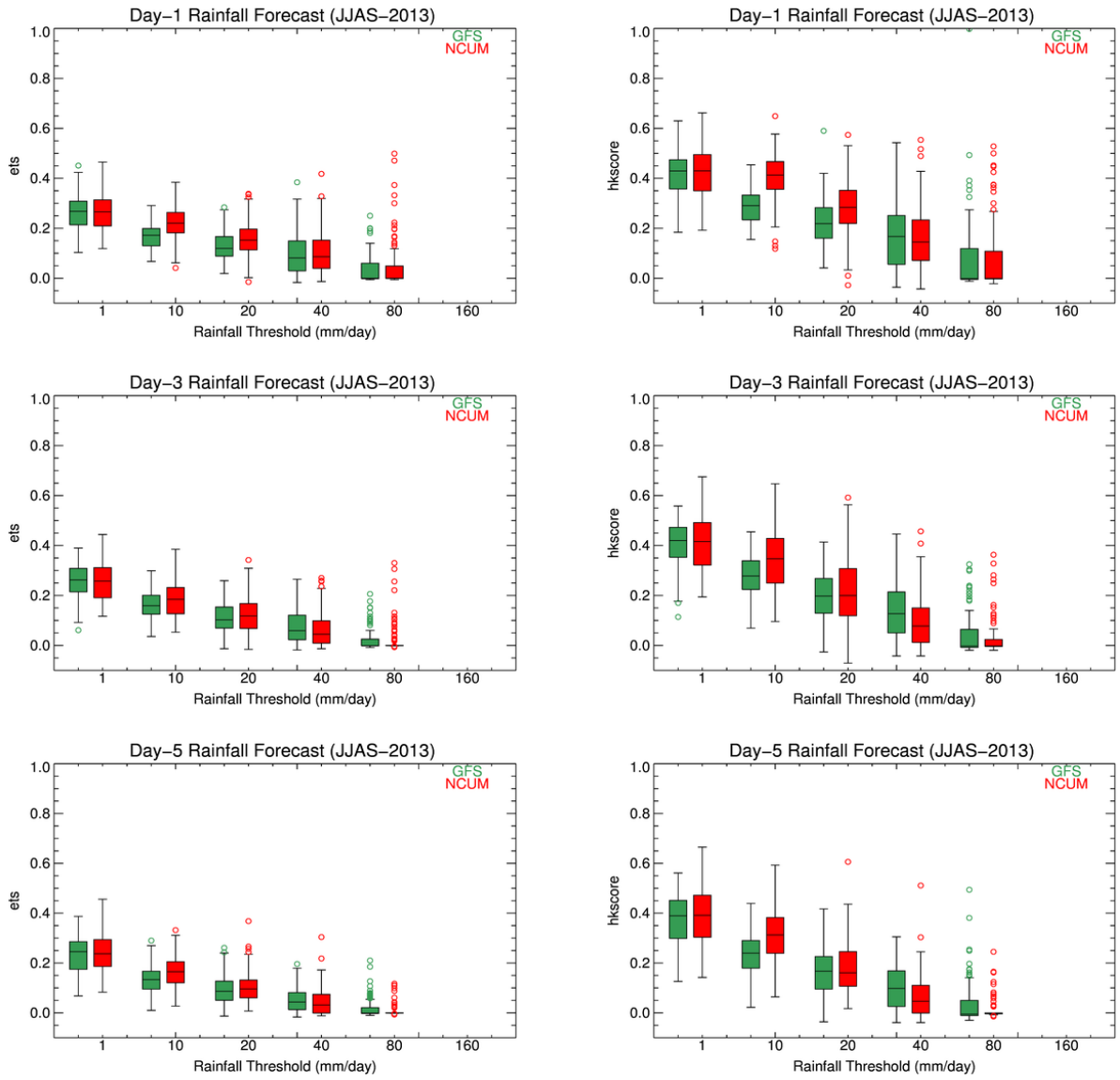

Figure 4: Equitable Threat Score (ETS; left) and Hanssen and Kuipers Score (HK Score; right) in the Day-1, Day-3 and Day-5 forecasts of two models GFS and NCUM for various rainfall thresholds

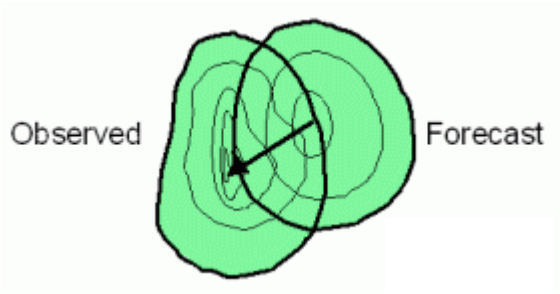

Figure 5: CRA formed by overlap of forecast and observations

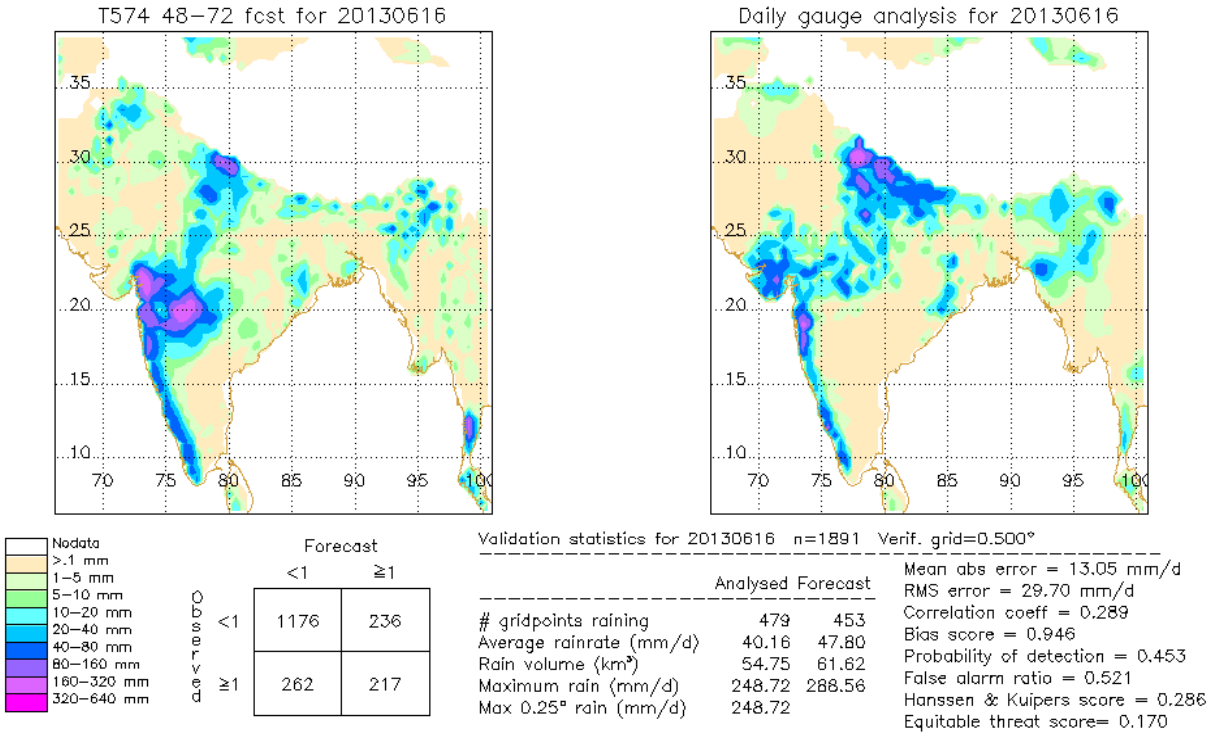

Figure 6: Verification of GFS Day-3 rainfall forecasts valid for 17th June 2013

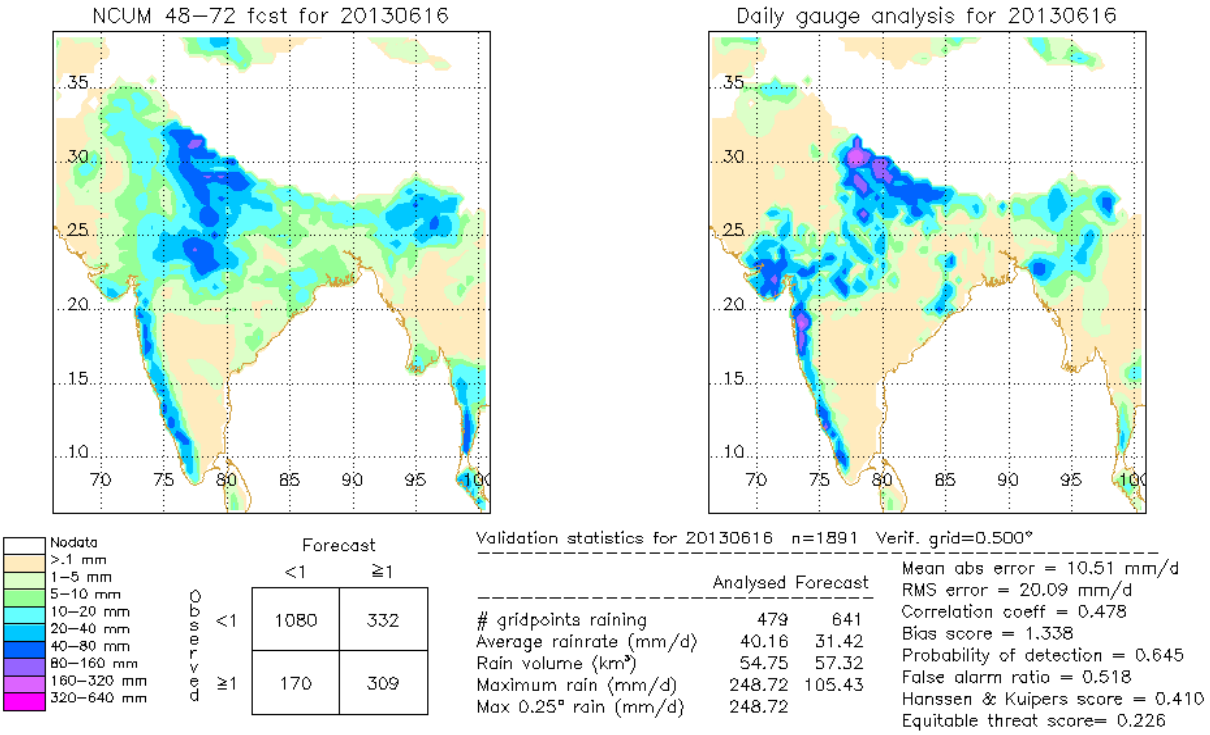

Figure 7: Verification of NCUM Day-3 rainfall forecasts valid for 17th June 2013

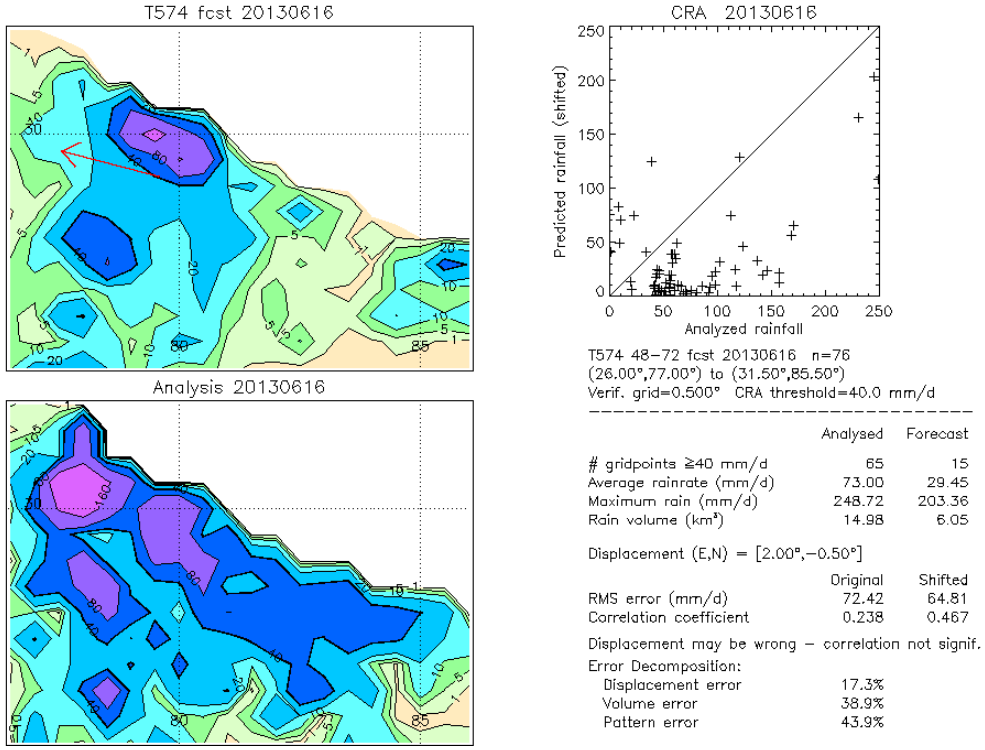

Figure 8: CRA (40 mm) verification of GFS Day-3 rainfall forecasts valid for 17th June 2013

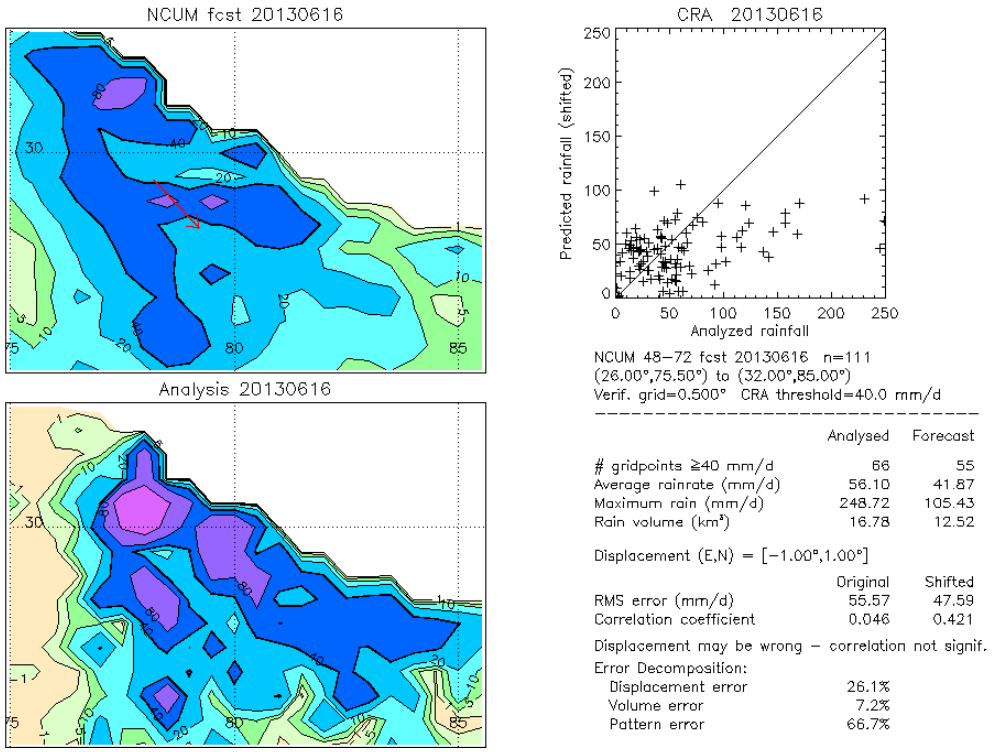

Figure 9: CRA (40 mm) verification of NCUM Day-3 rainfall forecasts valid for 17th June 2013

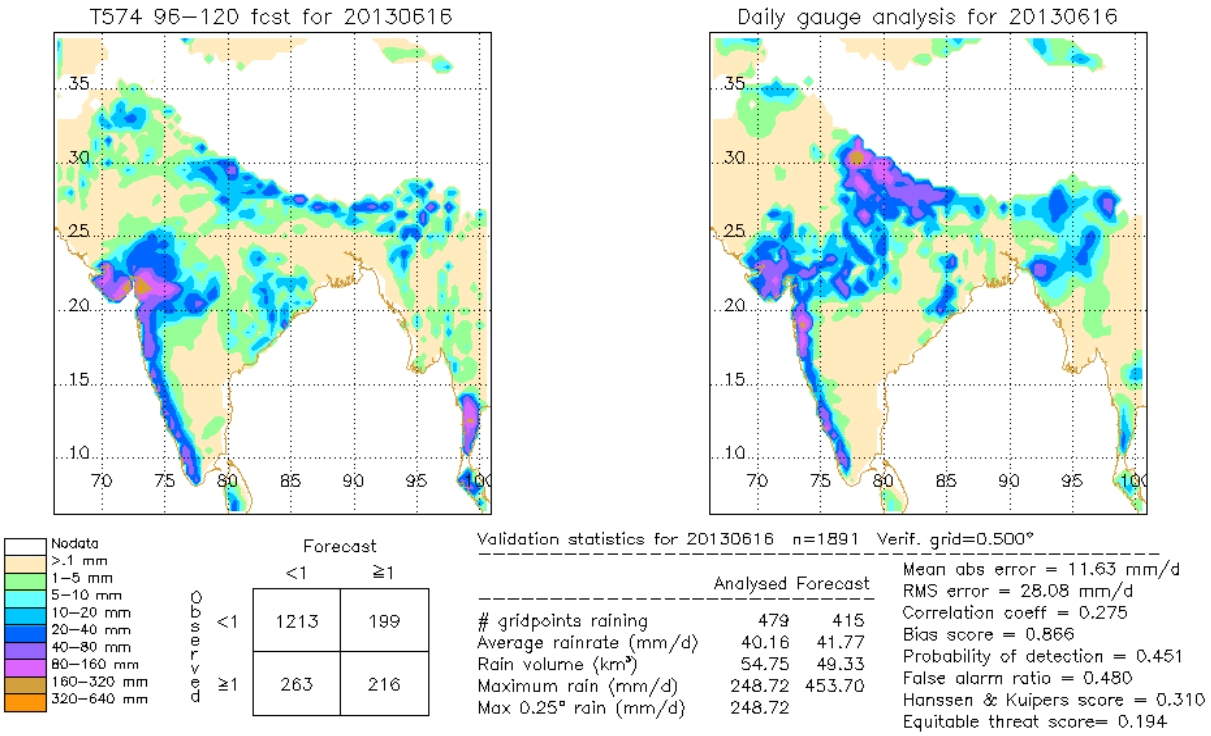

Figure 10: Verification of GFS Day-5 rainfall forecasts valid for 17th June 2013

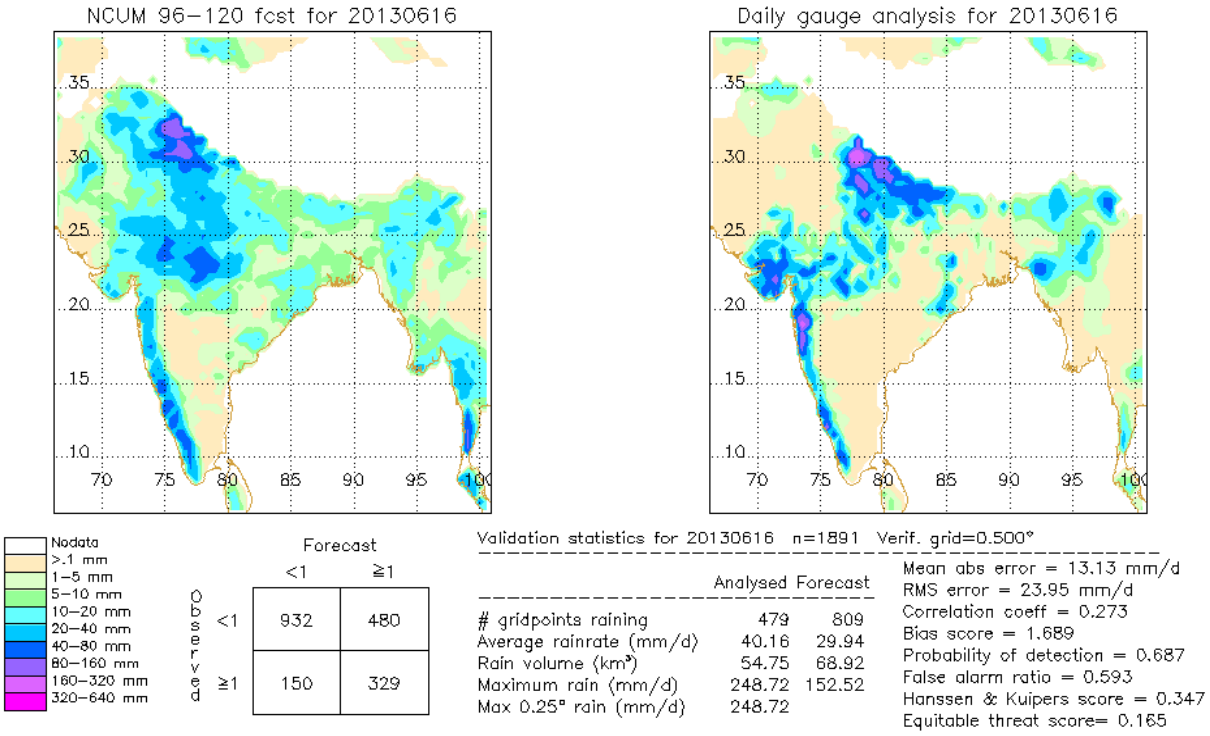

Figure 11: Verification of NCUM Day-5 rainfall forecasts valid for 17th June 2013

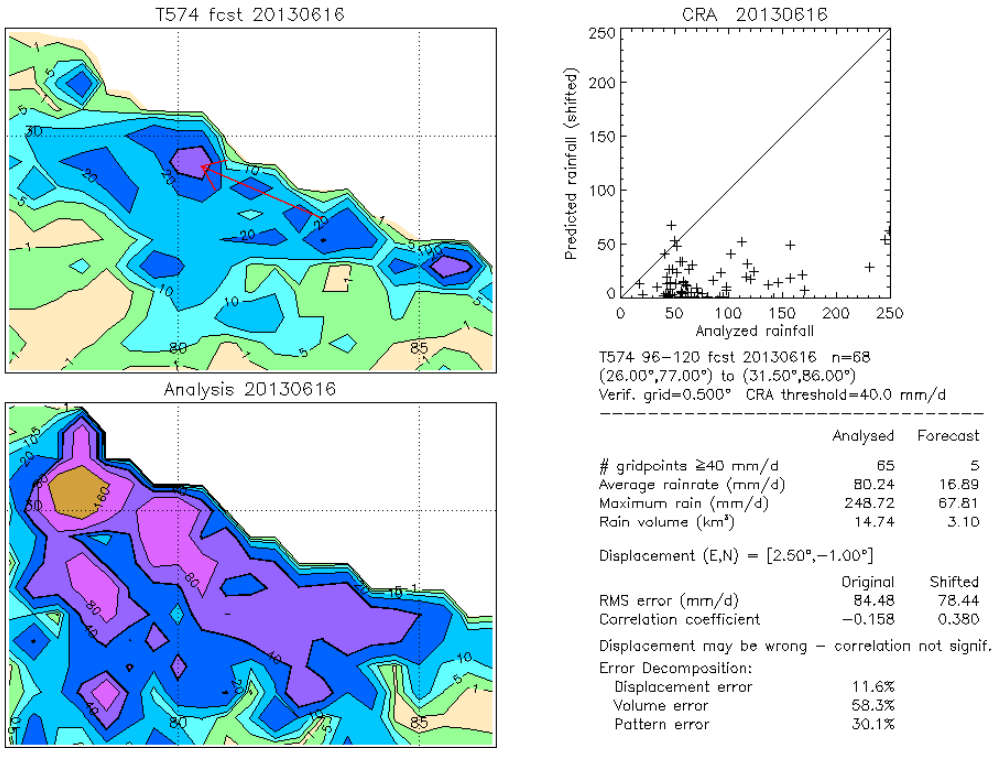

Figure 12: CRA (40 mm) verification of GFS Day-5 rainfall forecasts valid for 17th June 2013

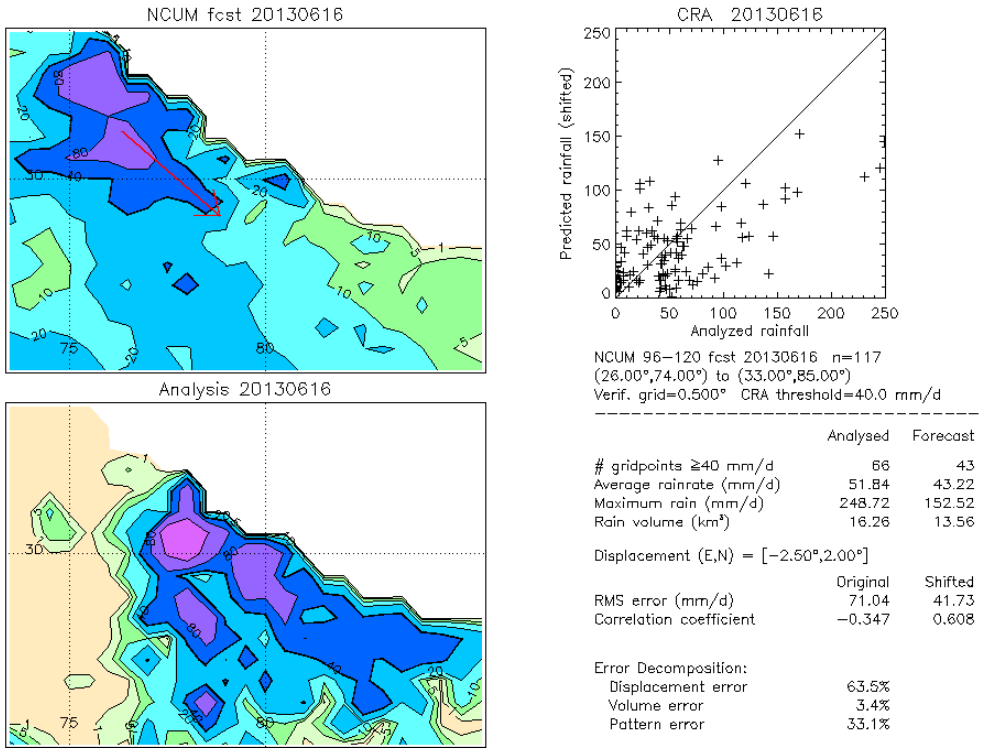

Figure 13: CRA (40 mm) verification of NCUM Day-5 rainfall forecasts valid for 17th June 2013

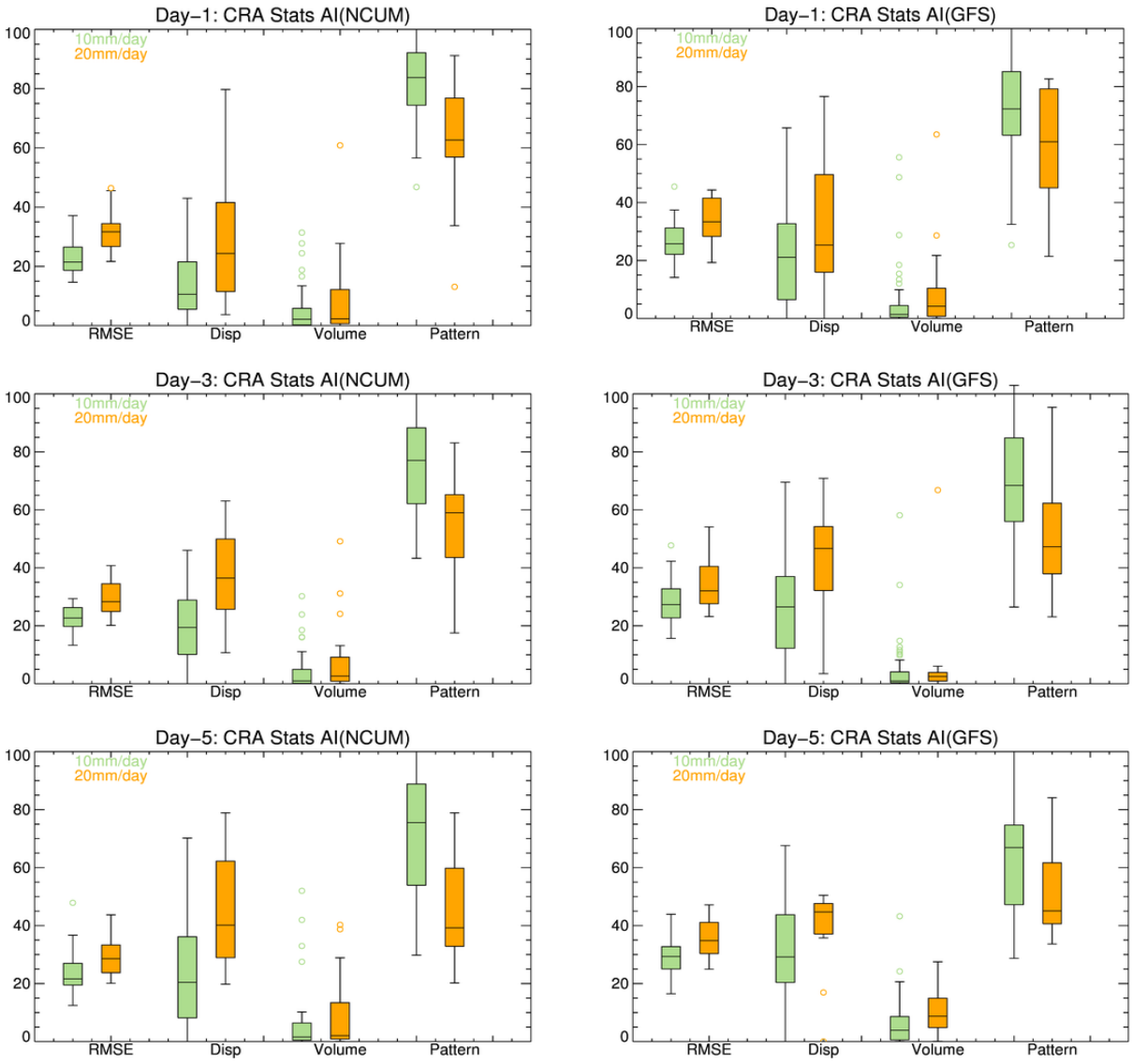

Figure 14: RMSE in the NCUM (*left*) and GFS (*right*) forecast rainfall along with the contribution from displacement error, volume error and pattern error in the Day-1 (*top*), Day-3 (*middle*) and Day-5 (*bottom*) forecasts

Chapter 4: All- India and Sub-divisional Rainfall Forecasts

Saji Mohandas

This section describes the spatial and temporal characteristics of global model rainfall predictions with respect to the long period average of observed rainfall provided by Northern Hemispheric Analysis Centre (NHAC), India Meteorological Department, New Delhi, in terms of subdivisional and All India Rainfall (AIR) for JJAS 2013. The Figures 1-2 describe the spatial pattern of AIR in terms of area averaged subdivisional rainfall for T574 and NCUM. The observed (actual) rainfall distribution shows that Monsoon-2013 was mostly normal or excess for the entire country except for northeast, Bihar, Jharkhand and Haryana, where it was deficient. None of the subdivision was scanty. The Day-1, Day-3 and Day-5 forecasts of T574 shows in general mostly normal or excess rainfall except for a few subdivisions over north and eastern parts of India. None of the forecasts could bring out the deficient rainfall over north eastern states. Day-1 forecast shows entire range of subdivisions over the sub-Himalayan belts is either deficient or scanty and Day-3 is closer to the observations. As far as NCUM is concerned, there is more mismatch from observed distribution as most of the subdivisions over the south peninsula are in red color while in general most of the subdivisions over north India are excess. Thus NCUM apparently tries to forecast the track of the monsoon systems more northward compared to T574.

Figures 3-4 show the All India daily rainfall in millimeters for JJAS 2013, Seasonal rainfall, Monthly rainfall and weekly rainfall predicted by T574 model and Figures 5-6 show the corresponding charts based on NCUM model forecasts, against the observed rainfall (OBSV) provided by India Meteorological Department (IMD). The seasonal, monthly and weekly rainfall values also show the long period averages (CLIM) and the weekly rainfall is the 7 days prediction from the single initial condition every week.

Daily mean All India rainfall for Monsoon-2013 started with a weak note but with a sudden and explosive onset spell peaking at about 14 mm by the end of the second week of June. However, during the third week of June there was a short break, and the monsoon activity gathered momentum again after 23rd June, which continued for next two

months without much significant breaks. During this period the average rainfall remained 8-9 cm per day with occasional events of heavy AIR. The peak record of the season was observed near 20th July (~16 mm). From the last week of August, the activity remained relatively sublime with daily AIR hardly crossing 6 mm most of the period. The second part of July is apparently the most active spell as observed from the IMD panel.

Day-3 forecast of T574 is able to generate the intraseasonal modulations as described above in All India daily rainfall closest to the observed, though with a slight underprediction. Day-1 and Day-5 rainfall are much more underpredicted than Day-3. The peaks in observed All India daily rainfall are around 15th June (14 mm), 25th June (13 mm), 20th July (16 mm) and 1st August (15 mm) and 16th August (14 mm). Overall, all the forecasts relatively underpredict these spells. However, Day-3 forecast correctly predicted the first spell. In the case of NCUM, Day-1 forecasts show the best skill in the All India Rainfall in the prediction of the peaks both in quantity as well as timing. However, in the Day-3 to Day-5 forecasts, AIR shows systematic underprediction in NCUM.

Seasonal AIR from T574 shows lower values for all the forecasts compared to the observations. Day-3 forecast AIR is the maximum compared to Day-1 and Day-2 and hence more close to the observation though it is still a significant underprediction. However, NCUM shows large overprediction of Day-1 seasonal rainfall and it drastically reduces as the forecast lead time increases towards Day-5. In the case of NCUM, Day-3 seasonal rainfall is very close to the observed estimate and Day-5 shows an underprediction. Monthly mean AIR shows maximum long period average (CLIM) for July month and the global models show the similar characteristics as CLIM or OBSV in terms of monthly All India Rainfall. In T574, Day-3 AIR is found to be more close to the observed in general while for June and July NCUM Day-1 forecasts show some overprediction and there is a gradual reduction in AIR from Day-1 to Day-5. The weekly AIR curves show more agreement with observation for NCUM. T574 curve generally undershoots the observed curve, whereas NCUM curve show overprediction of weekly rainfall during the first two weeks of June. Both the models could not predict the low activity during the break period coinciding with the end of August and beginning of September as the forecast curves overshoots the observation curves.

Summary

- The T574 forecasts for Day-1, Day-3 and Day-5 shows in general normal or excess rainfall amounts except over subdivisions in the north and eastern parts of India.
- None of the forecasts could bring out the deficient rainfall over north eastern states.
- T574 Day-3 forecast is able to generate the intra seasonal modulations as described above in All India daily rainfall closest to the observed, though with a slight underprediction.
- NCUM, Day-1 forecasts show the best skill in the All India Rainfall in the prediction of the peaks both in quantity as well as timings. However, from Day-3 to Day-5, AIR shows systematic underprediction in NCUM forecasts.

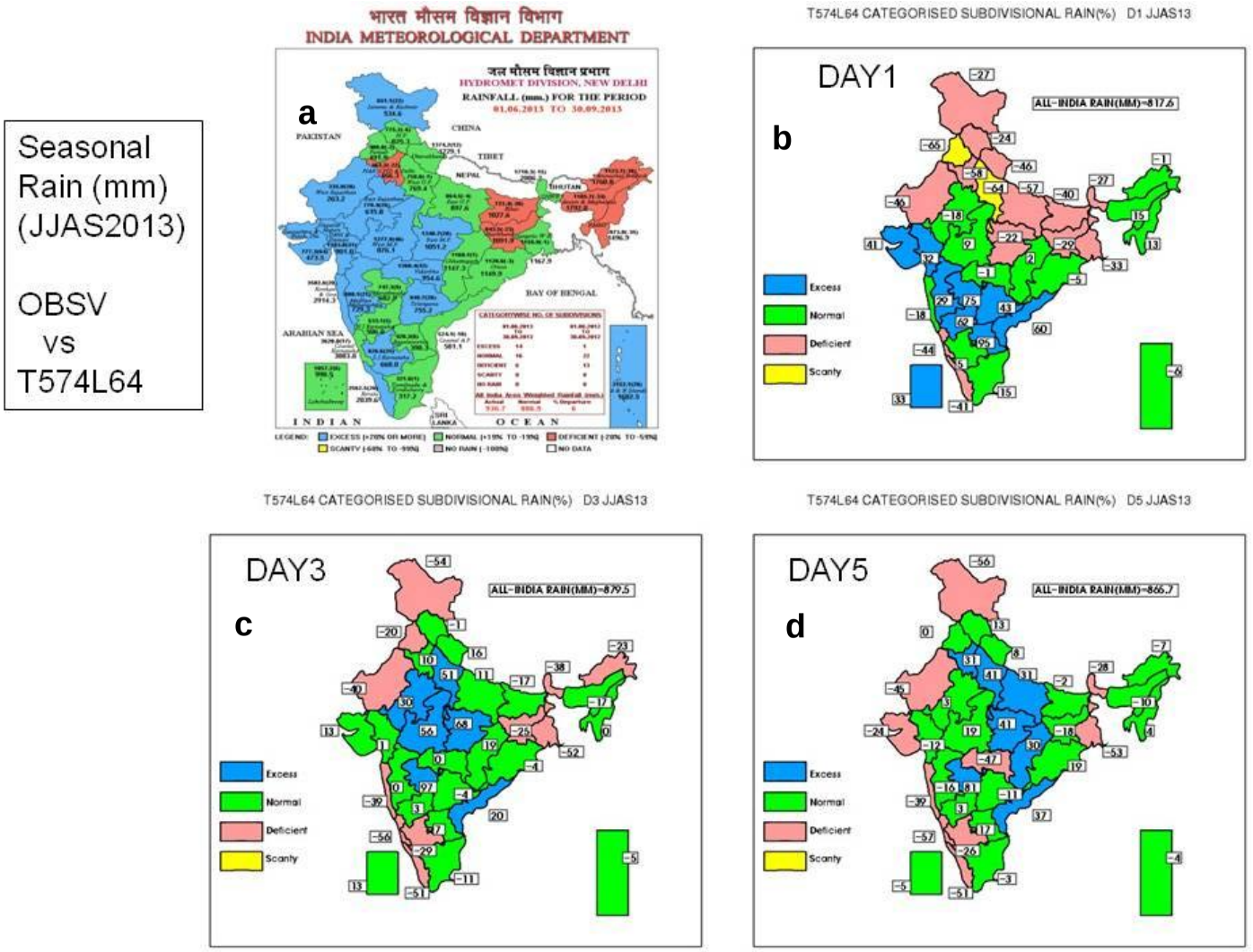

Fig. 1: All India and subdivisional rainfall (mm) for JJAS 2013 categorized into Excess, Normal, Deficient and Scanty; (a) observed (b) Day-1 forecast (c) Day-3 forecast and (d) Day-5 forecast by GFS model.

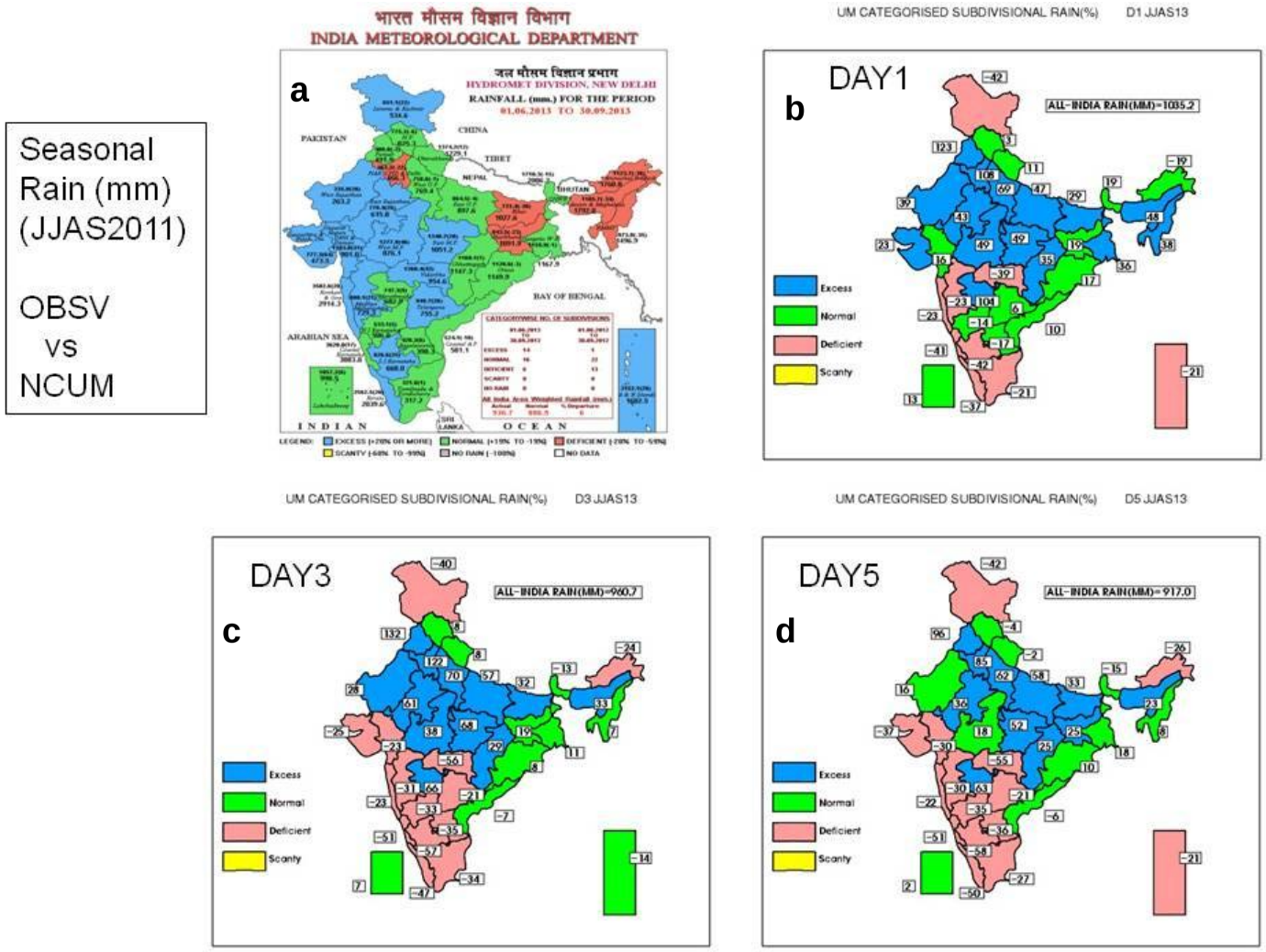

Fig: 2 All India and subdivisional rainfall (mm) for JJAS 2013 categorized into Excess, Normal, Deficient and Scanty; (a) observed (b) Day-1 forecast (c) Day-3 forecast and (d) Day-5 forecast by NCUM model.

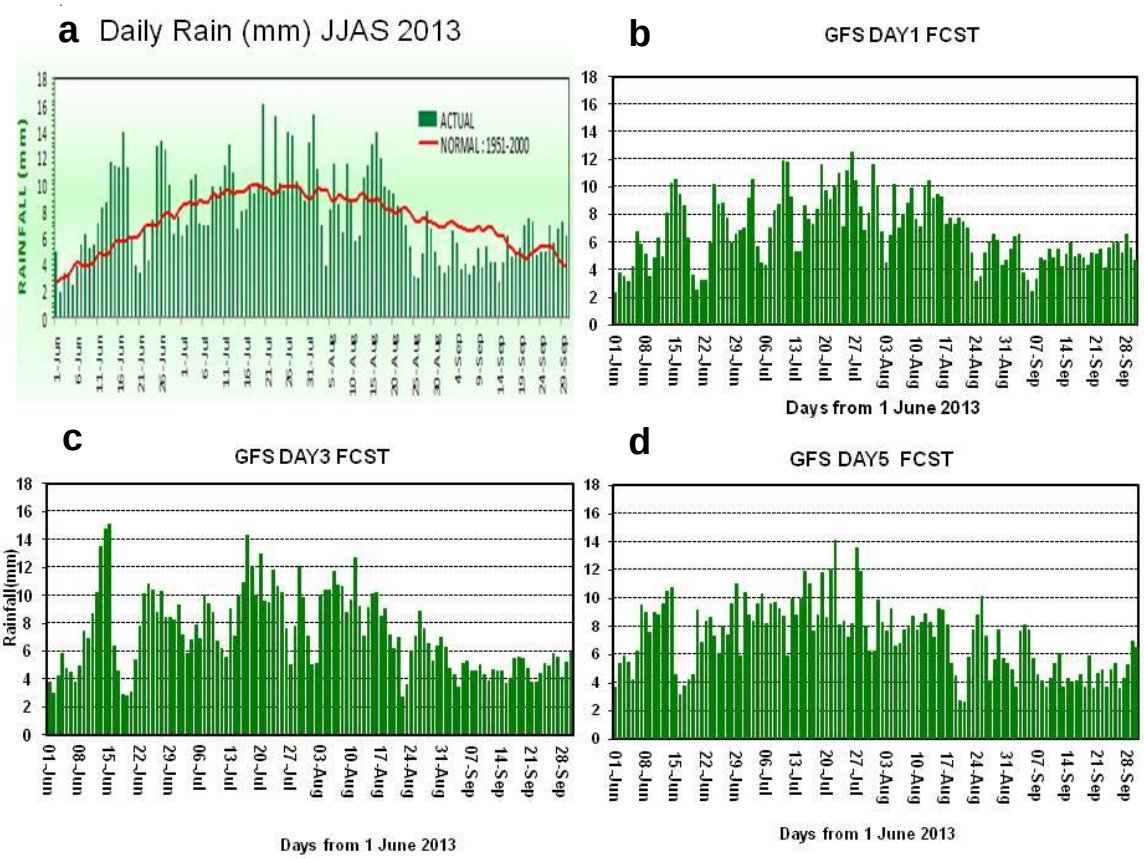

Fig. 3: All India daily rainfall (mm) for JJAS 2013; (a) observed (b) Day-1 forecast (c) Day-3 forecast and (d) Day-5 forecast from GFS model

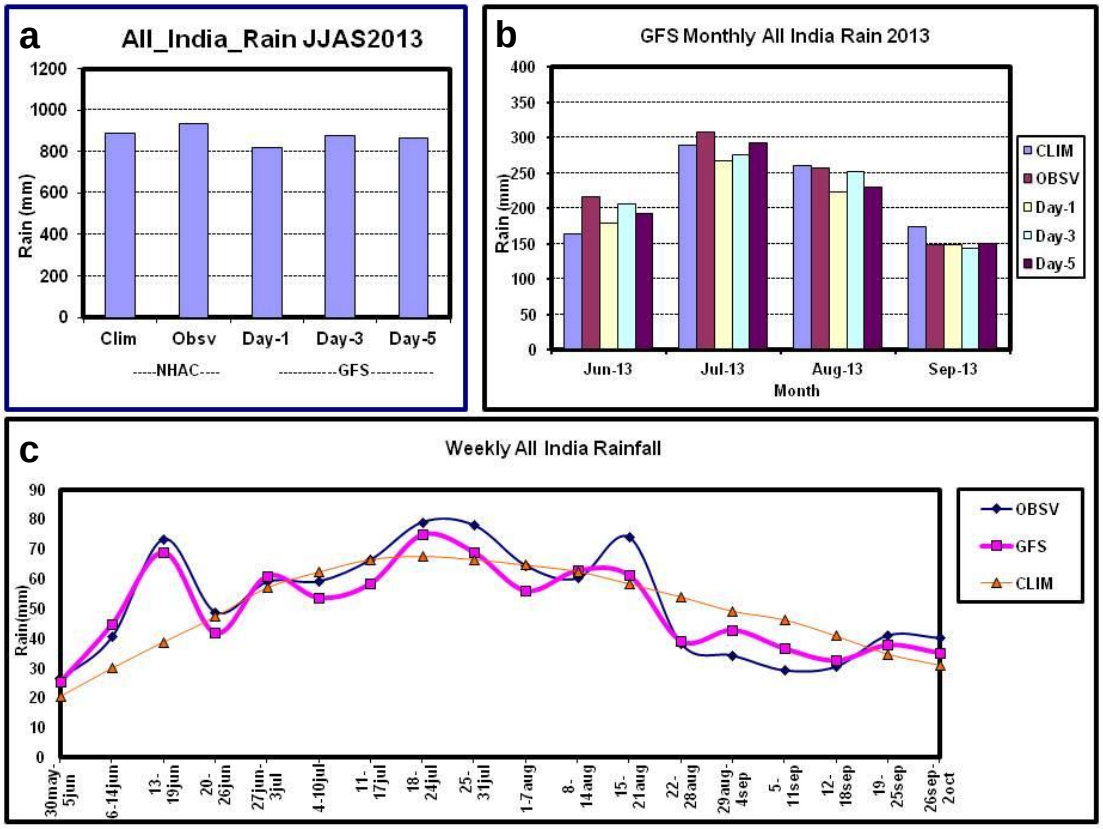

Fig. 4: Seasonal (a), Monthly (b) and weekly (c) rainfall (mm) predicted by GFS for Monsoon-2013 against observed (OBSV) and long period average (CLIM). Weekly rainfall is accumulated 7-day forecast from single initial conditions of every week

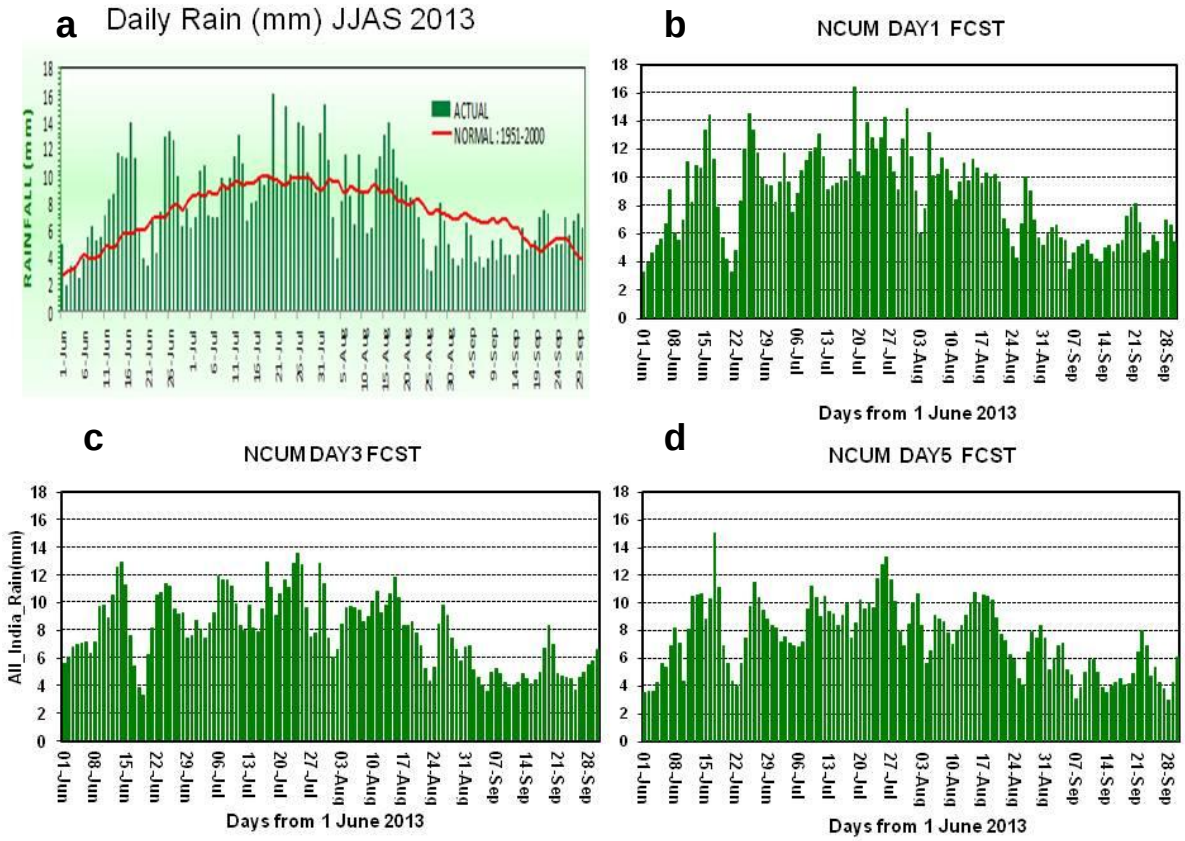

Fig. 5: All India daily rainfall (mm) for JJAS 2013; (a) observed (b) Day-1 forecast (c) Day-3 forecast and (d) Day-5 forecast by NCUM model

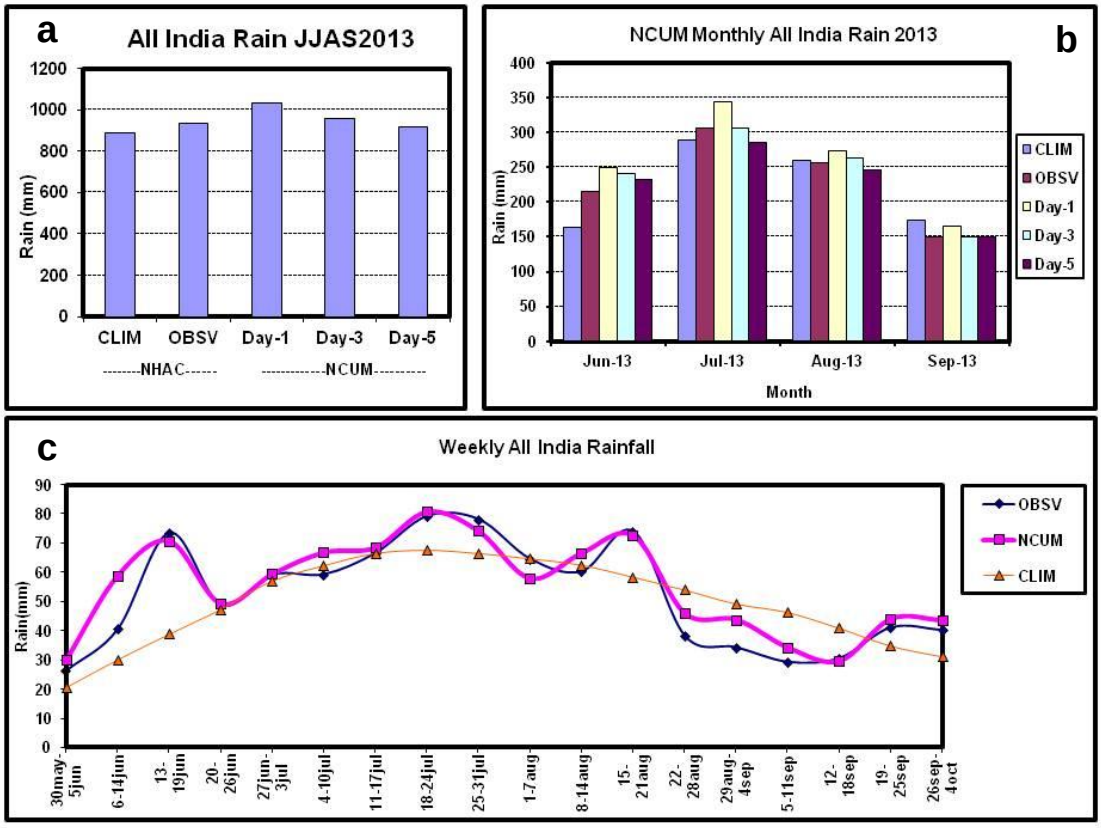

Fig. 6: Seasonal (a), Monthly (b) and weekly (c) rainfall (mm) predicted by NCUM model for Monsoon-2013 against observed (OBSV) and long period average (CLIM). Weekly rainfall is accumul1ated 7-day forecast from single initial conditions of every week

Chapter 5: Dynamical Monsoon Onset Indices

D. Rajan and Gopal R. Iyengar

1. Introduction

The onset of the Indian summer monsoon across the southern tip of Indian peninsula marks the beginning of the principal rainy season for India. The onset of the Indian summer monsoon represents one of the most dramatic transitions in the regional circulation pattern. The dynamic characteristics of the Asian summer monsoon during the onset phase over the Indian Peninsula and its variability have been examined by many authors; but still there is no consensus on the theory.

Precipitation in India has clear seasonal variation and the onset of the Indian summer monsoon is of great interest not only as a research problem but also a socio-economic factor for water resources in India. Due to distinct spatial features of monsoon and the diverse ways of representing monsoon, it is difficult to derive ‘universal index' to measure the variability of the monsoon over Asian continent. The onset date of the monsoon has been defined by various methods in past research studies.

The variability of the continental tropical convergence zone and the large-scale monsoon rainfall is linked to the variability of convection over the equatorial Indian Ocean and the surrounding seas i.e., Arabian Sea and the Bay of Bengal. The onset and withdrawal of the broad scale Asian monsoon occur in many stages and represent significant transitions in the large-scale atmospheric and ocean circulations (Fasullo and Webster 2003), which can be examined by analyzing various monsoon indices. Useful indices provide a simple characterization of the state of the monsoon during different epochs and the inter-annual variability. While there is no widely accepted definition of these monsoon transitions at the surface, the onset is recognized as a rapid, sustained increase in rainfall over a large scale while the withdrawal marks the return to dry, quiescent conditions, hence the 850 hPa level flow patterns are examined.

2. Background

In early nineties the India Meteorological Department (IMD) determined the normal onset and withdrawal dates of summer monsoon with 180 rain-gauges stations

across British India from 'characteristic monsoon rise/fall in pentad rainfall', and prepared charts showing normal onset and withdrawal dates across the Indian sub-continent. These old chronological dates are being revised in the department.

The arrival of the summer monsoon over the Kerala coast is found to be reasonably regular towards the end of May or beginning of June (Climatological Atlas for Airmen 1943; Rao, 1976; Reddy, 1977; Ramesh et al. 1996; Taniguchi and Koike, 2006, Goswami and Gouda, 2010). It is established that the onset of South west monsoon occurs through its Arabian Sea and Bay of Bengal branches striking the Kerala coast (southern tip of India) and Northeast India (Assam and neighborhood) around 1st June.

Many studies show the declaration is best when the occurrence of the onset/withdrawal is dramatic and declaration is worst when it is feeble. The monitoring and forecasting of the summer monsoon onset over the Indian subcontinent is very important guidelines for the operational forecaster as a reference. This migration and location of the heat source associated with summer monsoon has important implications for the withdrawal of monsoon over South Asia. However, to date there has been no systematic investigation of the retreat of the monsoon system despite its key contribution to total rainfall variability. However, it is well proved that, in terms of rainfall, the onset is better defined than the withdrawal.

An objective manner of declaring the onset of the southwest monsoon over Indian main land is described in this chapter. Three global analysis and forecasts systems (a) GFS (b) NCUM (c) UKMO that are available at NCMRWF have been used to compute various monsoon indices to monitor the onset phase of the monsoon during May – June 2013.

3. Monsoon circulation indices for onset, strength and withdrawal

The Kerala state situated in the southwest part of the Indian sub-continent is the gateway for the Indian summer monsoon. Based on Kerala rainfall, the mean onset date occurs around 1 June and varies with a standard deviation of 7-9 days from year to year. Moreover, given the relatively small scale of Kerala (that is less than 200 km in breadth), sensitivity of any onset or withdrawal declaration based solely on the district's rainfall to spatial intricacies in the monsoon transitions is also likely to be large.

Generally IMD declares the official onset date based on rainfall, wind, temperature, moisture, cloud pattern, and the state of the sea, etc. The basis for declaring the onset on this particular date is discussed below. Ananthakrishnan et al. (1968) have discussed various synoptic conditions (Rainfall, wind field and outgoing long wave radiation) associated with the onset of monsoon over Kerala. Based on this, a set of objective criteria is being followed by the India Meteorological Department since 2006, to declare the monsoon onset over Kerala.

Recently IMD has started experimenting with a revised methodology for dates of onsets by taking rainfall data with 569 stations during the period 1971- 2000. The number of continuous rainy days, number for each 3 day, 5 day and 7 day moving average are also computed. (IMD Forecast Review Manual 2010).

Even though for a forecaster it is a challenging task to declare the date of onset because all the above parameters are highly variable in space and time. It is difficult to quantify these parameters precisely and so the experience of the forecaster plays a key role in declaring the date of monsoon onset subjectively for individual years (Wang et al. 2009).

During this year; as per IMD's daily weather bulletins the arrival of southwest monsoon current occurred two-three days in advance over the South Bay of Bengal and South Andaman Sea as compared to the normal date. This early arrival is due to the development of convection over the region and it set in over the Andaman region during 17-19 May 2013. It further advanced to the southern part of the South-West Bay of Bengal during 20-25 May. Subsequently monsoon entered over the East Central Bay of Bengal almost near the normal date. After a few days IMD had declared the onset date over Kerala as 1 June, on the normal onset date.

Ramesh et al. (1996), recommended the following characteristics for the evolution of the onset over the Arabian Sea covering the area of 0° – 19.5° N and 55.5°E – 75°E: (i) the net tropospheric (1000 – 300 hPa) moisture build-up, (ii) the mean tropospheric (1000 – 100 hPa) temperature increase, (iii) sharp rise of the kinetic energy at 850 hPa.

Goswami et al. (1999), defined the index based on the meridional wind (V) shear between 850 hPa and 200 hPa over the south Asian region 10°N–30°N, 70°E – 110°E which is related to the Hadley cell features. This index can be used to examine the onset and advancement phases of the monsoon. It is observed that the strength of the low-level

Somali jet and upper tropospheric tropical easterly jet increase rapidly during the time of evolution of the summer monsoon over India.

Wang et al. (2001) introduced a dynamical index based on horizontal wind (*U*) shear at 850 hPa called the circulation index. They recommend that the circulation index computed with the mean difference of the zonal winds (*U*) between the two boxes; one for southern region and the other for the northern region, i.e. 5°N – 15°N, 40°E – 80°E and 20°N – 30°N, 70°E – 90°E can be used as the criteria for identifying the onset date. The southern region box is taken over South Arabian Sea and the northern region box is taken over northern land region. This circulation index describes the variability of the low-level vorticity over the Indian monsoon trough, thus realistically reflecting the large scale circulation.

Fasullo and Webster (2003) defined the onset date in terms of vertically integrated moisture transport derived from reanalysis datasets. As per their results the inter-annual variation in the onset date modestly agreed with reality.

A daily circulation index (Syroka and Toumi, 2002, 2004) was defined as the difference in average 850 hPa zonal winds between a southern region 5°N – 15°N, 50°E – 80°E and a northern region 20°N – 30°N, 60°E – 90°E. The index changes sign, reflecting both the changing intensity of the low-level westerly monsoon flow and the vorticity associated with the monsoon trough and synoptic activity. This daily circulation index may be used to define both the dates of onset and withdrawal of the Indian summer monsoon from these regions. The daily circulation index exhibits substantial noise, so a centered 7-day running average is taken. The date of onset of the monsoon is defined as the first of seven consecutive days for which the index becomes positive. The 7-day period was found to be the smallest time interval which smoothed synoptic noise sufficiently to define the dates more easily.

Taniguchi and Koike (2006) for the first time emphasized on the relationship between the Indian monsoon onset and abrupt strengthening of low-level wind over the Arabian sea 7.5°N – 20°N, 62.5°E – 75°E. They used three variables, namely, (i) vertically integrated water vapor (ii) moisture transport and (iii) low-level wind in an objective manner to determine the onset date. This gives a measure of the strength of the low-level jet over South Arabian Sea and indicates the strength of the monsoon over India. They showed that Indian summer monsoon onset is brought mainly by

enhancement of low-level wind over the Arabian Sea. They have proved that this relationship holds good for the declaration of onset dates for many years.

Wang et al. (2009) found that the onset date can be objectively determined by examining of the sustained 850 hPa zonal wind (*U*) averaged over the southern Arabian Sea (5°N – 15°N, 40°E – 80°E). In the recent studies this criterion is referred as objective circulation index. The rapid establishment of the steady westerlies is an excellent parameter to correlate with the abrupt commencement of the rainy season over the southern tip of Indian peninsula. The date of onset is defined as the first day when onset circulation index exceeds 6.2 m/sec with the provision that the onset circulation index in the ensuing consecutive six days also exceeds 6.2 m/sec. The requirement of the onset circulation index greater than 6.2 m/sec for a period of six consecutive days is to ensure that the strong westerly is not induced by a synoptic event; rather it reflects a steady establishment of the strong southwest monsoon over the southern Arabian Sea. This definition of onset circulation index meets the requirements: simple, objective, and representative of both the Kerala rainfall and large scale circulation changes during the onset.

These widely used monsoon dynamical indices of the South Asian summer monsoon are listed in the Table 1 with their corresponding brief definition and their references. These monsoon indices are based on circulation features associated with convection centers related with rainfall during the summer monsoon for the Indian region. In this study we have computed the above described circulation indices based upon the various definitions that are tabulated in Table 1.

4. Results and discussions

The daily outputs of GFS, NCUM and UKMO analyses and forecasts (up to 7 days) from 11 May to 10 June 2013 is used in this study. Due to non-availability of data, the UKMO products were used up to 5-days only. The details of the assimilation and forecast systems for the above three models have been documented in the NCMRWF reports published earlier. The IMD diagnostics Bulletin (2013) daily/seasonal reports have been referred for the observation of rainfall, flow patterns, the dates of the northern limit of monsoon, strength of the monsoon, etc. during the entire period of this study.

(a) Daily Wang & Ding zonal index

Figures 1-4 show the objective circulation indices based on Wang et al. (2009) for the analyses followed by 1-day, 3-day, 5-day and 7-day forecasts from the GFS, NCUM and UKMO respectively.

It is seen from Figure 1 that the GFS analysed zonal wind (*u*) exceeded the threshold value of 6.2 m/s on 30 May. It continued to exceed the threshold value for the next six days and more. Hence according to this index, 30 May was the onset date over Kerala as seen by the GFS analyses values. The NCUM and UKMO analyses show the early onset dates as 25 May and 26 May respectively by exceeding the threshold value of 6.2 m/s.

It is seen from Figure 2 that GFS 1-day, 3-day, 5-day and 7-day forecasts fields mark the onset date as 25 May, 26 May, 28 May and 29 May 2013 respectively. From the Figure 3 it is seen that NCUM 1-day, 3-day, 5-day and 7-day forecasts fields show onset dates as 23 May, 24 May, 26 May and 28 May 2013 respectively. From the Figure 4 it is seen that UKMO 1-day, 3-day and 5-day forecasts fields show onset date as 21 May, 19 May and 21 May respectively.

Thus it is concluded that only the GFS analysis show the onset date as 30 May which is near to the observed onset date; all other analyses and their corresponding forecasts show the early onset during the period 19 May-29 May.

After 1 June it was observed that the south west monsoon has further advanced into entire South Arabian Sea, some parts of central Arabian Sea, entire Kerala, most parts of Tamil Nadu and some more parts of south west and west central Bay of Bengal. The above observation can be correlated with the sharp rise of these indices values as shown in the figures 1 to 4 after the onset dates.

(b) Goswami Hadley vertical index

Figures 5-8 show the Hadley cell indices/vertical shear of the (*v*) suggested by Goswami et al. (1999) for the onset phase from the analysis and 1-day, 3-day, 5-day and 7-day forecasts obtained from the GFS, NCUM and UKMO respectively. From the Figure 5 it is seen that all the three analysed value of the vertical shear exceeded the threshold value of 0 m/s (change of sign) on 19 May. But this date cannot be taken as the onset

date over Kerala. From the Figures 6 - 8 it is seen that the computed value of the vertical shear exceeded the threshold value of 0 m/s during 19 May to 22 May. But these dates cannot be considered as the onset date. Hence it is concluded that this Hadley cell index could not bring out the onset date during this year.

(c) Syroka & Toumi vertical index

Figures 9-12 show the circulation indices based on Syroka and Toumi (2004) theory for the onset phase of the monsoon from the GFS, NCUM and UKMO models respectively. The Figure 9 which is based on the GFS analysis, this index changes its sign on 21 May, which cannot be defined as the onset date. According to NCUM analysis, this index changes its sign on 19 May, which also cannot be taken as the onset date. Based on the UKMO analysis, this index changes its sign on 25 May, which can be defined as the onset date.

The Figure 10 shows the indices values obtained from GFS forecasts; as per this it is noted that the onset dates vary from 26-29 May. Similarly from the figures 11 and 12; the NCUM and UKMO model show the onset date as 20 to 27 May and 22 to 26 May 2013 respectively. Thus it is concluded that this index is also not able to bring the onset date correctly.

5. Summary

Three popular monsoon indices have been used to study the onset of monsoon during 2013 season. In general, the indices are able to represent the onset, variability in strength of monsoon and the withdrawal in a reasonable way. As per these indices, the actual date of monsoon onset over the main land is during 24-30 May. The indices used with medium range forecasts from the global models (GFS, NCUM & UKMO) indicate that the same could be used to forecast the changes in phases of the monsoon system within the season. These monsoon indices have to be refined with more years of data from higher resolution models. In future use thermodynamic parameters from the models will also add up the value to the monitoring of monsoon by such indices.

Acknowledgements

The observed rainfall available from IMD's web site is used in this study.

References

Ananthakrishnan, R. Srinivasan V., Ramakrishnan A.R. and Jambunathan R. 1968: Synoptic features associated with onset of South-West monsoon over Kerala, Forecasting manual unit Report IV-18.2., India Meteorological Department.

Climate Diagnostic Bulletin of India South West Monsoon Near Real Time.

India Meteorological Department, 1943, 'Climatological Atlas for Airmen'.

Fasullo. J. and P. J. Webster, 2003: A hydrological definition of Indian monsoon onset and withdrawal. *J. Climate*, 16(14), 3200-3211.

Goswami. B.N., V. Krishnamurthy and H. Annamalai, 1999: A broad scale circulation index for interannual variability of the Indian summer monsoon. *Quart. J. Roy. Meteor. Soc.,* 125, 611-633.

Goswami. P. and K.C. Gouda 2010: Evaluation of a dynamical basis for advanced forecasting of date of onset of monsoon rainfall over India. *Monthly Weather Review.*

Ramesh K. J., Swati Basu and Z. N. Begum 1996: Objective determination of onset, advancement and withdrawal of the summer monsoon using large-scale forecast fields of a global spectral model over India. *Meteo. and Atmospheric physics*, 61, 137-151.

Rao, Y.P., 1976: Southwest monsoon Meteorological Monograph IMD, New Delhi

Reddy, S.J., 1977: Forecasting the onset of southwest monsoon over Kerala. *Indian J. Met. Hydrol. and Geophys.*, 28, 1, 113-114

Syroka, J., and R. Toumi 2002: Recent lengthening of the south Asian summer monsoon season. *Geophy. Res. Lett.,* 29, (DOI: 10.1029/2002/ GL015053).

Syroka, J., and R. Toumi 2004: On the withdrawal of the Indian summer monsoon. *Quart. J. Roy. Meteor. Soc.,* 130, 989-1008.

Taniguchi. K., and T. Koike 2006: Comparison of definitions of Indian summer monsoon onset: better representation of rapid transitions of atmospheric conditions. *Geo. Res. Lett.,* 33, L02709, 5 pages.

Taniguchi. K., D. Rajan and T. Koike 2010: Effect of the variation in the lower tropospheric temperature on the wind onset of the Indian summer monsoon. *Meteorology and Atmospheric Physics*, 106, 75-94.

Wang, B., Q. Ding and V. Joseph 2009: Objective definition of the Indian summer monsoon onset using large-scale winds. *J. Climate* 22, 3303–3316.

Wang. B., R.Wu and K.M. Lau 2001: Inter-annual variability of the Asian summer monsoon: Contrasts between the Indian and Western North Pacific-East Asian monsoons. *J. Climate*, 14, 4073-4090.

Table 1: Indices computed in this study

	Type of Index	**Domain of application**	**Definition in terms of regions**	**Reference**
Goswami	Meridional wind	South Asia	*V*850 – *V*200 over (10°N – 30°N, 70°E –110°E)	Goswami et al. (1999)
Wang and Ding	Circulation zonal wind	Tropical South Asia	*U*850 averaged over (5°N – 15°N, 40°E–80°E)	Wang et al .(2009)
Syroka and Toumi	Circulation zonal wind	Tropical Asia	*U*850 (5°N – 15°N, 50°E –80°E) – *U*850 (20°N – 30°N, 60°E – 90°E)	Syroka and Toumi (2002, 2004)

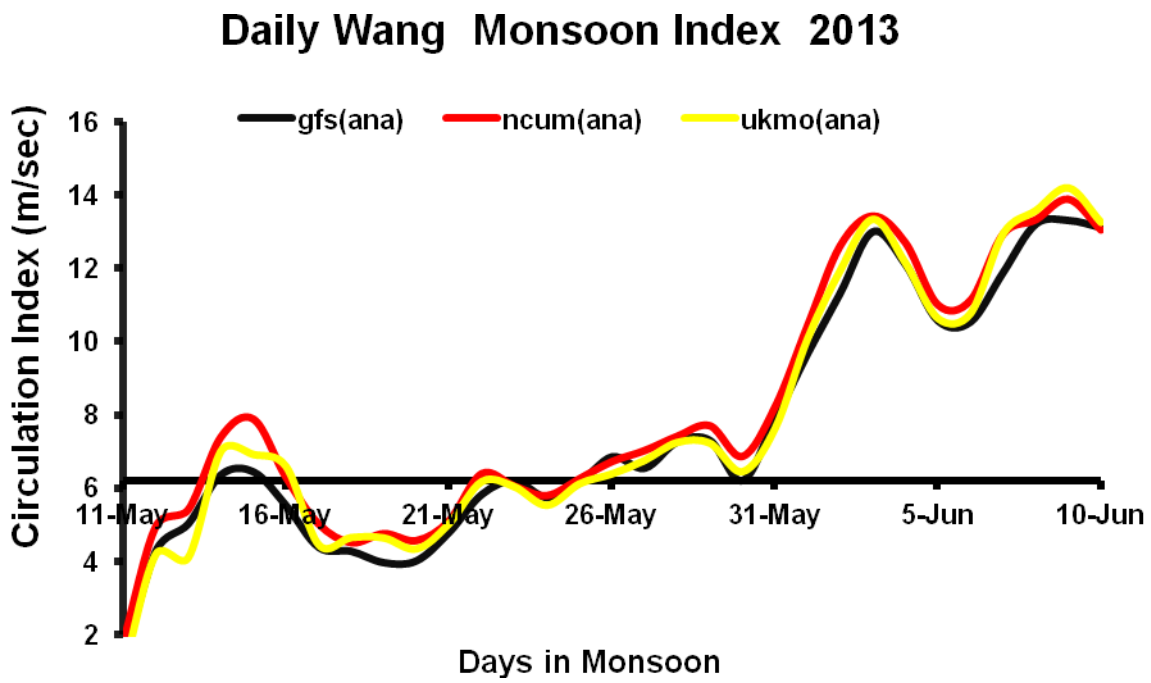

Figure 1: Daily Wang & Ding circulation zonal index from GFS-ana, NCUM-ana, and UKMO-ana

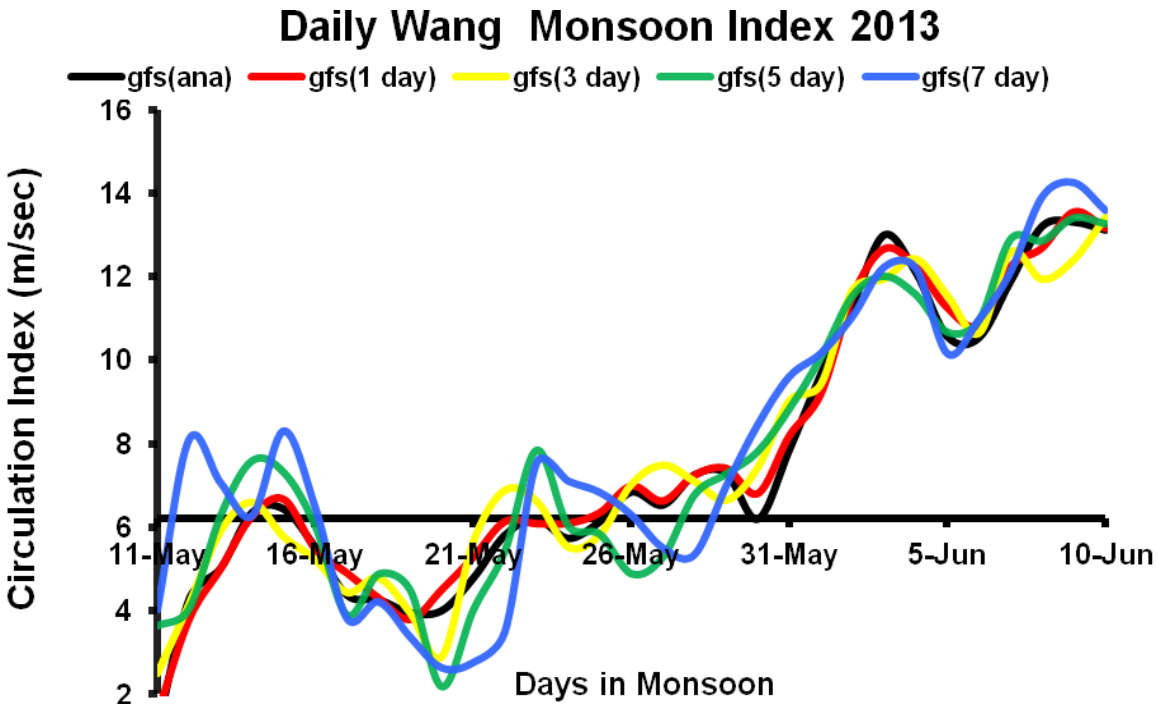

Figure 2: Daily Wang & Ding circulation zonal index from GFS-ana, GFS (1 day), GFS (3 day), GFS (5 day) and GFS (7 day)

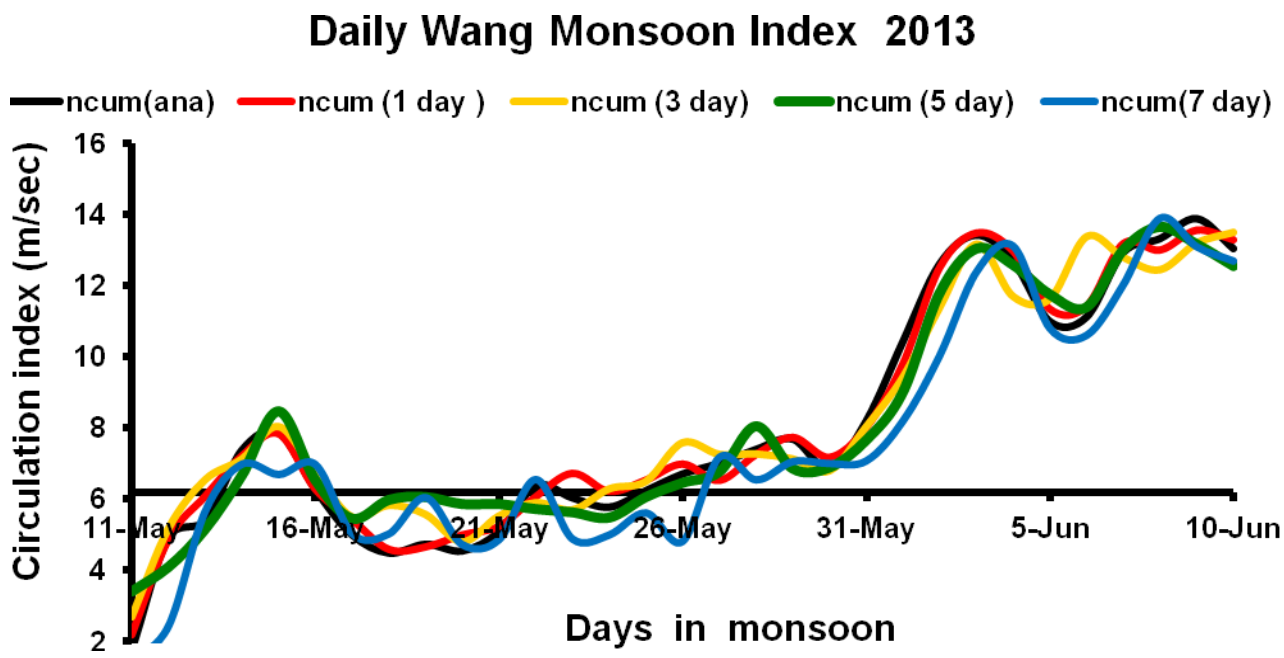

Figure 3: Daily Wang & Ding circulation zonal index from NCUM-ana, NCUM (1 day), NCUM (3 day), NCUM (5 day) and NCUM (7 day)

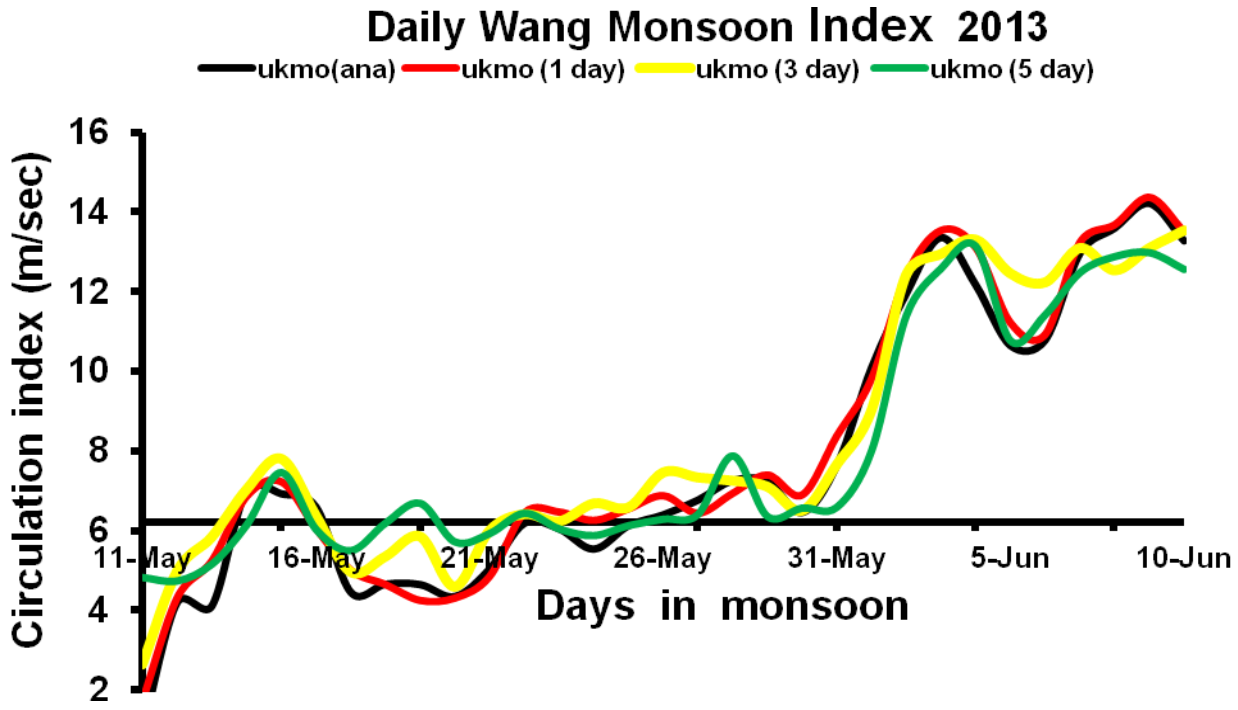

Figure 4: Daily Wang & Ding circulation zonal index for UKMO-ana, UKMO (1 day), UKMO (3 day) and UKMO (5 day)

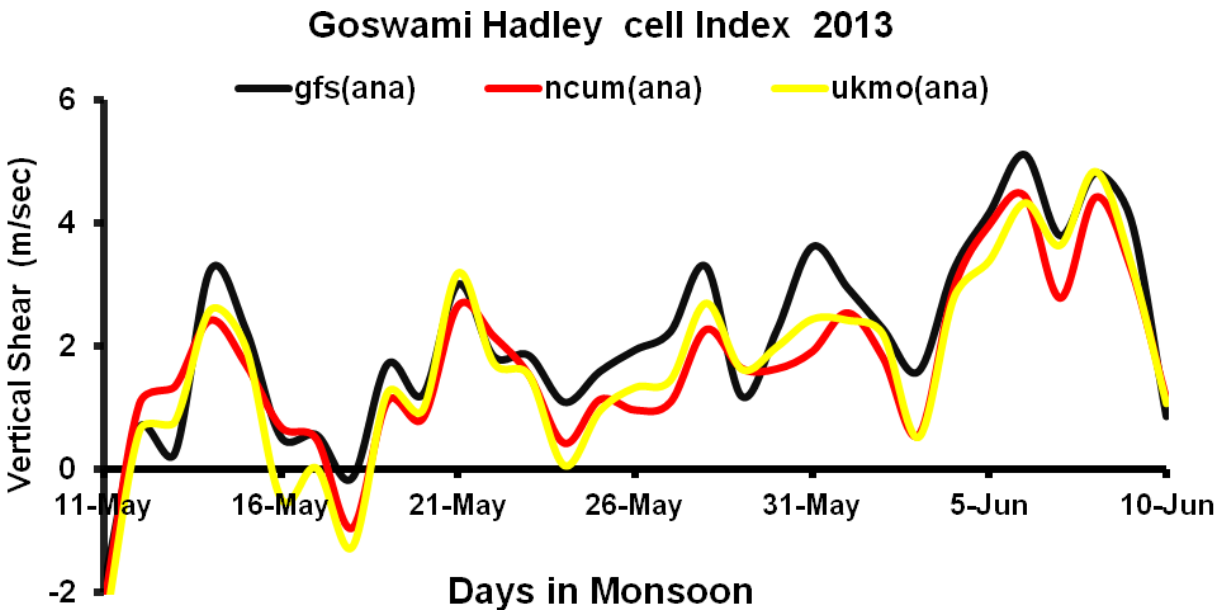

Figure 5: Daily Goswami Hadley Cell index for GFS-ana, NCUM-ana and UKMO-ana

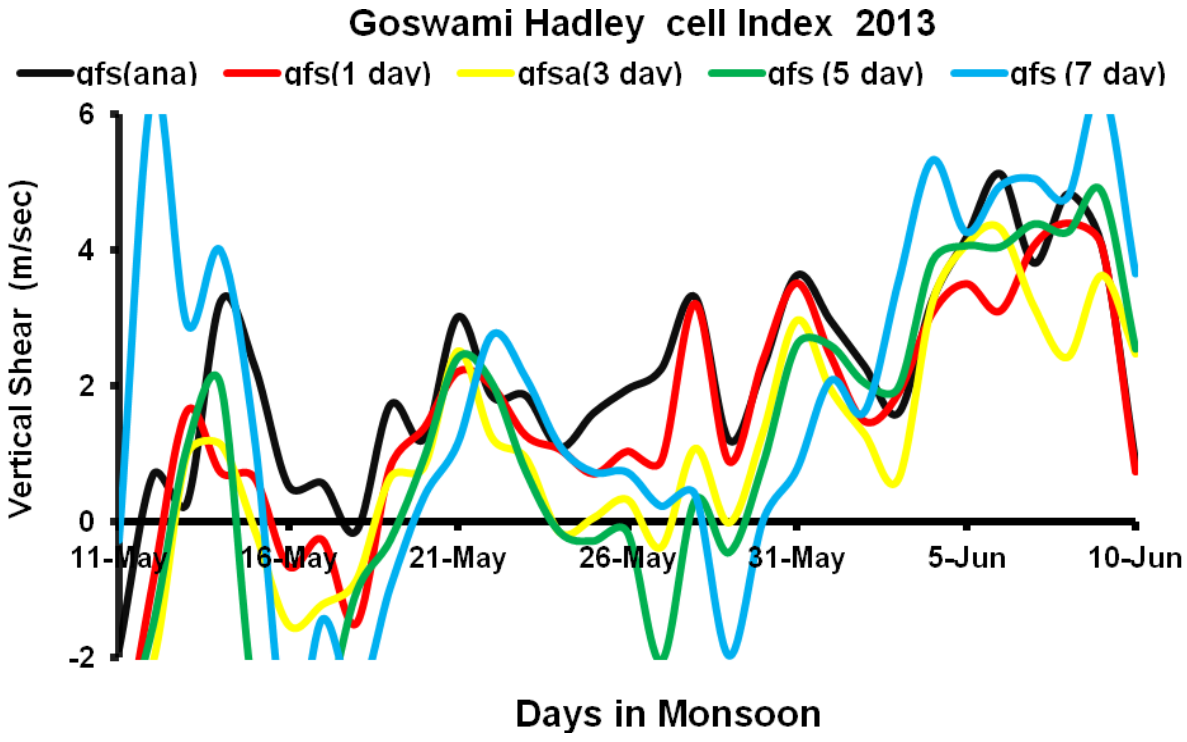

Figure 6: Daily Goswami Hadley ell index for GFS-ana, GFS (1 day), GFS (3 day), GFS (5 day) and GFS (7 day)

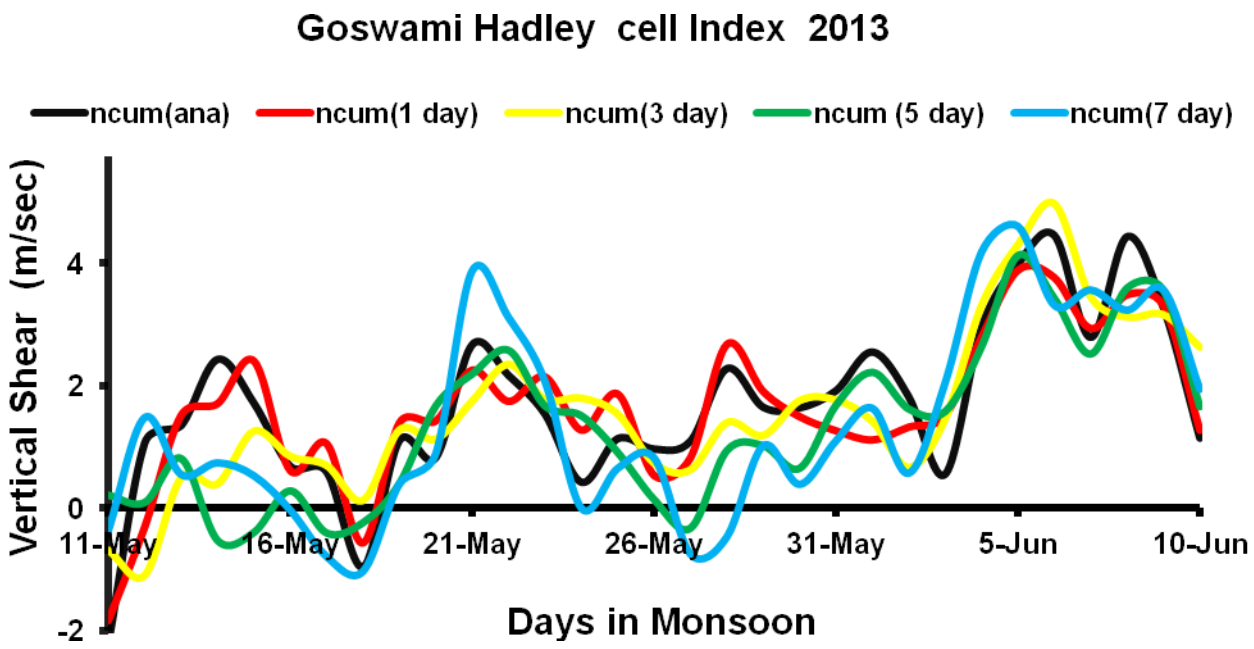

Figure 7: Daily Goswami Hadley Cell index for NCUM-ana, NCUM (1 day), NCUM (3 day), NCUM (5 day) and NCUM (7 day)

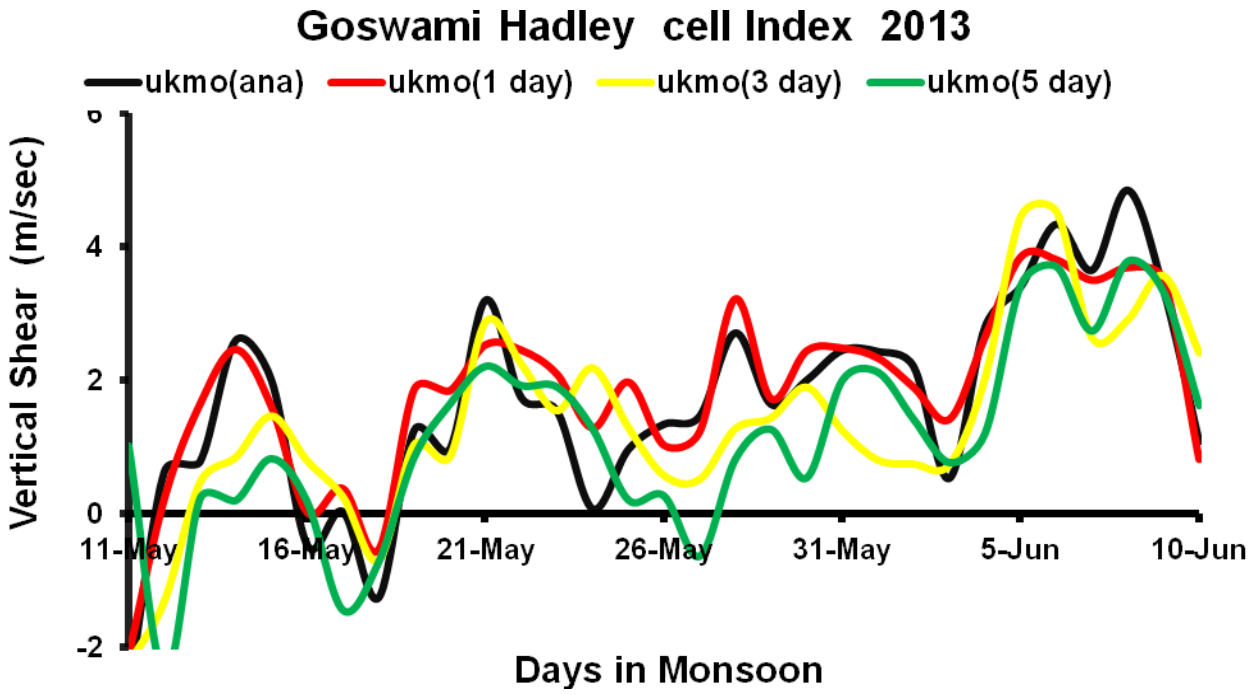

Figure 8: Daily Goswami Hadley Cell index for UKMO-ana, UKMO (1 day), UKMO (3 day), and UKMO (5 day)

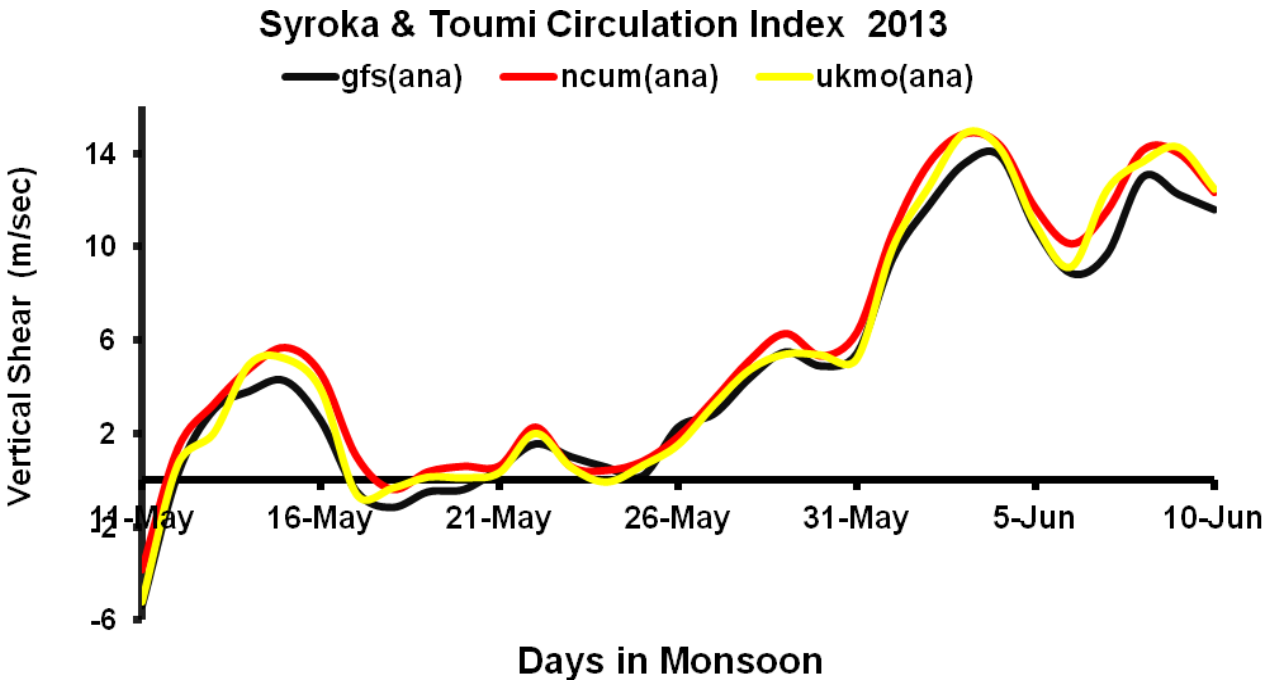

Figure 9: Daily Syroka & Toumi index for GFS-ana, NCUM-ana and UKMO-ana

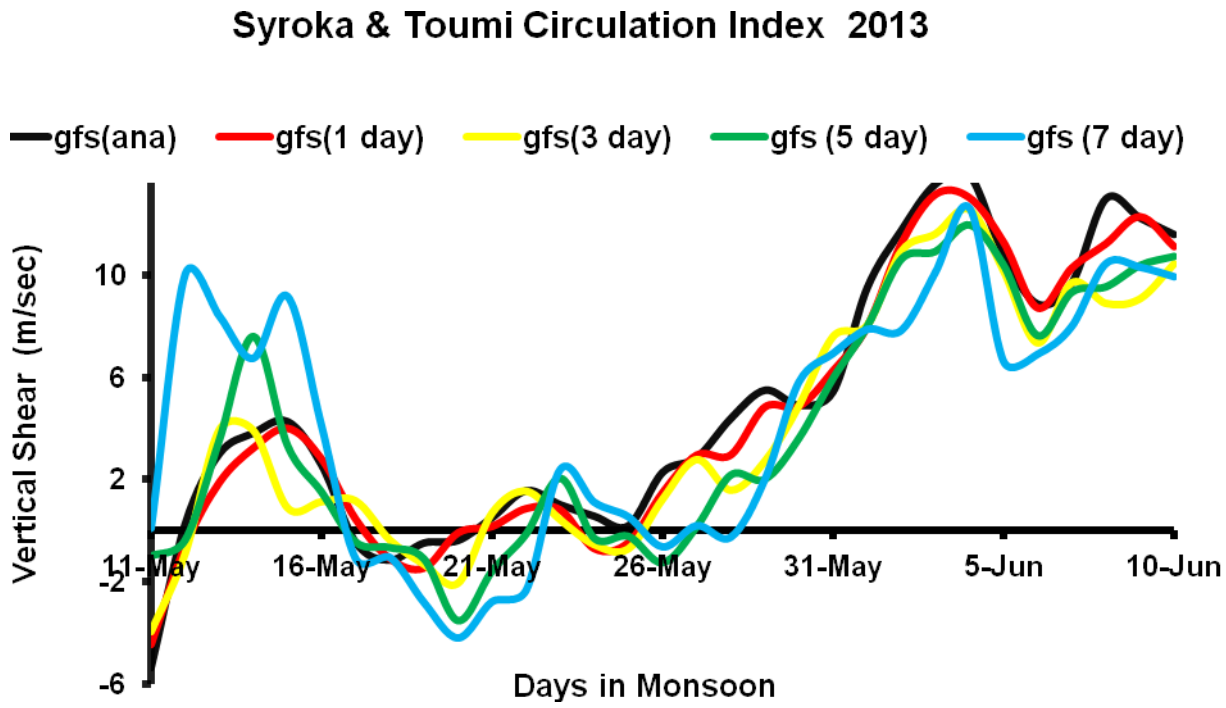

Figure 10: Daily Syroka & Toumi index for GFS-ana, GFS(1 day), GFS (3 day), GFS (5 day) and GFS (7 day)

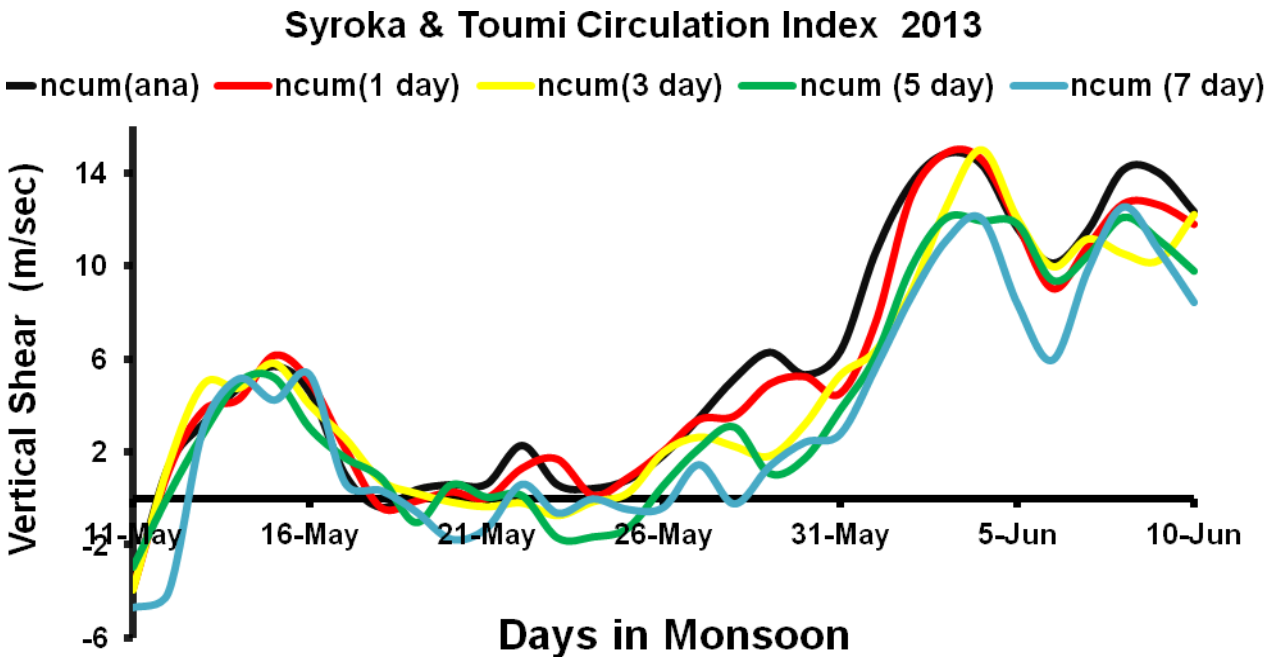

Figure 11: Daily Syroka & Toumi index for NCUM-ana, NCUM (1 day), NCUM (3 day), NCUM (5 day) and NCUM (7 day)

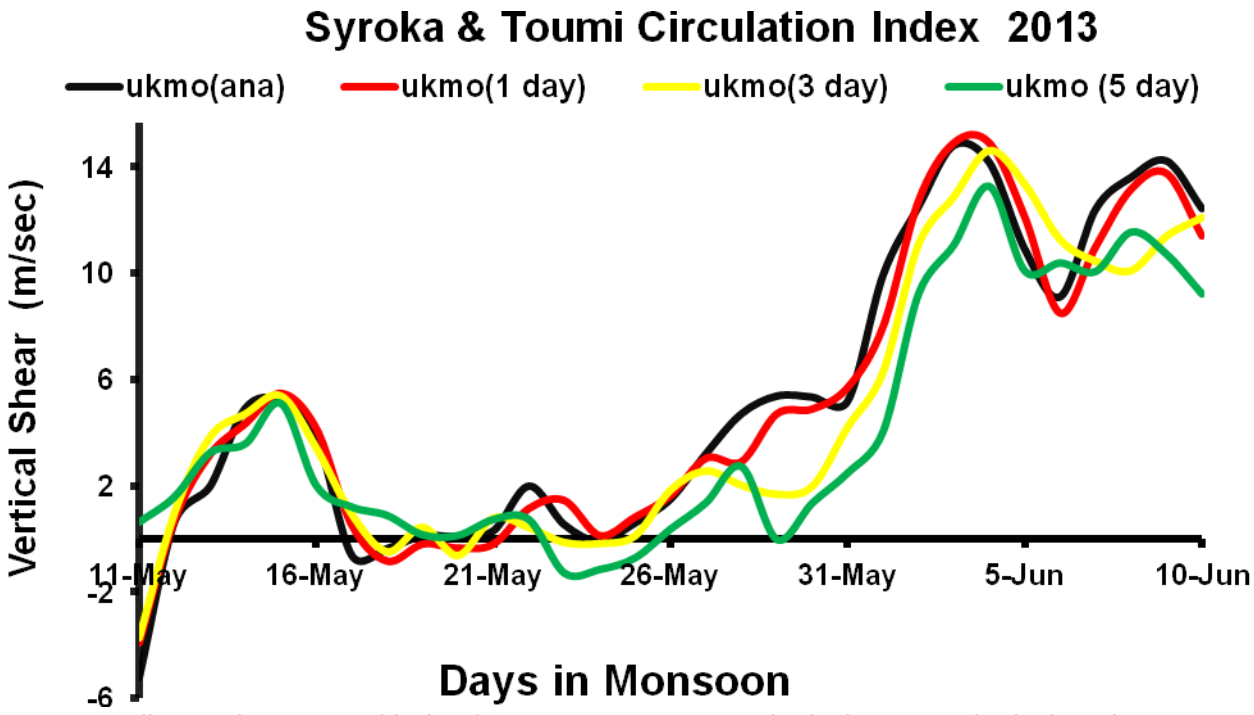

Figure 12: Daily Syroka & Toumi index for UKMO-ana, UKMO(1 day), UKMO (3 day) and UKMO (5 day)

Chapter 6: Monsoon Depressions during JJAS 2013

Raghavendra Ashrit, Amit Ashish, Kuldeep Sharma, John P. George and Gopal R. Iyengar

1. Introduction

During the South-West monsoon season of 2013, there were only two monsoon depressions. One formed over the Bay of Bengal during the last week of July (30 July-2 August) and the other formed over Odhisha in the month of August (20-23 August). Both systems had moved westward.

Forecast Verification of circulation features and associated rainfall of two monsoon depressions is presented in this chapter. The verification is presented in terms of the 850 hPa winds, geopotential height and the 24 hour forecast of rainfall distribution. This is followed by Contiguous Rain Area (CRA) verification (described in Chapter 3) for the forecast rainfall. The verification is carried out for three deterministic models forecast of NGFS, UKMO and NCUM. However the intercomparison of NGFS and NCUM are only presented since NCUM and UKMO are basically same models (but different versions) which show only marginal differences in the forecasts.

2. Monsoon Depression (31 July-2 August, 2013)

Figure 1 shows the 850 hPa winds and rainfall valid for 1st August, 2013. The top panels show the circulation associated with the depression given by the analysis of the three models, namely NGFS, UKMO and NCUM. The observed rainfall is also included in these figures (in cm; shaded). The details of the observed rainfall were described in Chapter 3. The panels in the 2nd 3rd and 4th row show the Day-1, Day-3 and Day-5 forecast of rainfall by the three models, valid for 1st August 2013. Day-1 and Day-3 forecasts successfully captured the rainfall bands in the southwest sector of the depression as observed. In the Day-5 forecast by these models, the circulation as well as the rainfall band associated with the depression is not captured well as compared to the observations.

Detailed CRA verification is also carried out in this case. Figure 2 and Figure 3 present the CRA verification results for the Day-3 and Day-5 forecasts. It may be noted that the date mentioned in Figure 2 and Figure 3 represent the starting date of 24 hour rainfall accumulation (as discussed in Chapter 3) and are consistent with the Figure 1.

In the case of Day-3 forecast CRA analysis with 40 mm threshold is presented in Figure 2(a, b). The spatial maps and the scatter plots clearly suggest that NCUM forecast underestimates the average rainfall rate by 45%, maximum rain by 72% and the rain volume by 45%. The NGFS forecasts underestimate the average rainfall rate by 15%, maximum rain by 11% and the rain volume by 15%. The RMSE and correlation (Figure 2a, b) are almost same for both the models. The contribution to total rainfall forecast error is mainly from volume error (32%) and pattern error (51%) in NCUM. In case of NGFS, it is due to pattern error (55%) and displacement error (41%).

Similarly in the Day-5 forecasts (Figure 3a, b) NCUM underestimates the average rainfall rate by 79%, maximum rain by 85% and the rain volume by 79%. The NGFS forecasts underestimate the average rainfall rate by 39% and the rain volume by 40%. The maximum rain in the domain is overestimated in NGFS forecast by 25%. The RMSE and correlation (Figure 2a, b) indicate moderately higher skill of NCUM forecast. The contribution to total rainfall forecast error is mainly from volume error (73%) and pattern error (23%) in NCUM. In case of NGFS it is due to pattern error (42%) and displacement error (52%).

3. Land Depression (22-23 August, 2013)

The panels in Figure 4 show the analysis and forecast of 850 hPa wind and rainfall valid for 23rd Aug 2013. The panels in the 1st, 2nd, 3rd and 4th row show the Analysis, Day-1, Day-3 and Day-5 forecasts respectively, by NGFS, UKMO and NCUM all valid for 23rd Aug 2013. Day-1, Day-3 and Day-5 forecasts by all the three models successfully captured the rainfall band in the western sector of the depression as seen in the observation. In all the forecasts, the circulation as well as the rainfall band associated with the depression is well captured compared to the observations. However the rainfall amounts in the forecast is underestimated in all the model forecasts.

Detailed CRA verification (with 40 mm threshold) for the Day-3 and Day-5 forecasts is presented in Figure 5 and Figure 6. As described in the last section, the date

stamp in Figure 5 and Figure 6 shows the starting date of 24 hour rainfall accumulation (as discussed in Chapter 3) and are consistent with Figure 4.

In the case of Day-3 forecast CRA analysis is presented in Figure 5(a, b). The spatial maps and the scatter plots clearly suggest that NCUM underestimates the average rainfall rate by 40%, maximum rain by 11% and the rain volume by 40% compared to the observations. The NGFS forecasts underestimate the average rainfall rate by 22%, maximum rain by 9% and the rain volume by 22%. The RMSE and correlation (Figure 5a, b) suggest relatively improved performance of NCUM (52mm/day and 0.66) compared to NGFS (76mm/day and 0.17). The relative contribution to total rainfall forecast error is mainly from volume error (42.8%) and pattern error (57.2%) in the NCUM forecast. In case of NGFS, it is due to pattern error (21.6%) and displacement error (73.3%).

Similarly in the Day-5 forecast (Figure-6a, b) of NCUM underestimates the average rainfall rate by 68%, maximum rain by 73% and the rain volume by 68%. The NGFS forecasts underestimate the average rainfall rate by 54%, maximum rain by 42% and the rain volume by 54%. The RMSE and correlation (Figure 6a, b) indicate higher skill of the NCUM forecast (77.18mm/day; 0.4) compared to NGFS (80.59mm/day; -0.3). The contribution to total rainfall forecast error is mainly from volume error (61.2%) and pattern error (38.8%) in the case of NCUM forecast. In case of NGFS, error is mainly due to pattern error (25.3%), volume error (27.9%) and displacement error (46.8%).

4. Conclusions

- The forecasts up to Day-3 by NGFS and NCUM rainfall band in the southwest sector of both depressions. However, in the first depression Day-5 forecasts show widespread nature of the rainfall and weaker circulation whereas in the other case the rainfall amounts are much lower compared to the observations.
- Both the model forecasts (NGFS and NCUM) underestimate the ranfall amounts. NCUM tends to underestimate the rainfall rate by about 40-45% in Day-3 forecast and by about 69-79% in Day-5 forecast. However NGFS underestimate the rainfall rate by about 15-22% in Day-3 forecast and by 39-55% in Day-5 forecast.

- Total forecast error in NCUM is mainly contributed by volume error (32-73%) and pattern error (23-57%) while the NGFS error is due to displacement error (41-73%) and pattern error (21-55%).

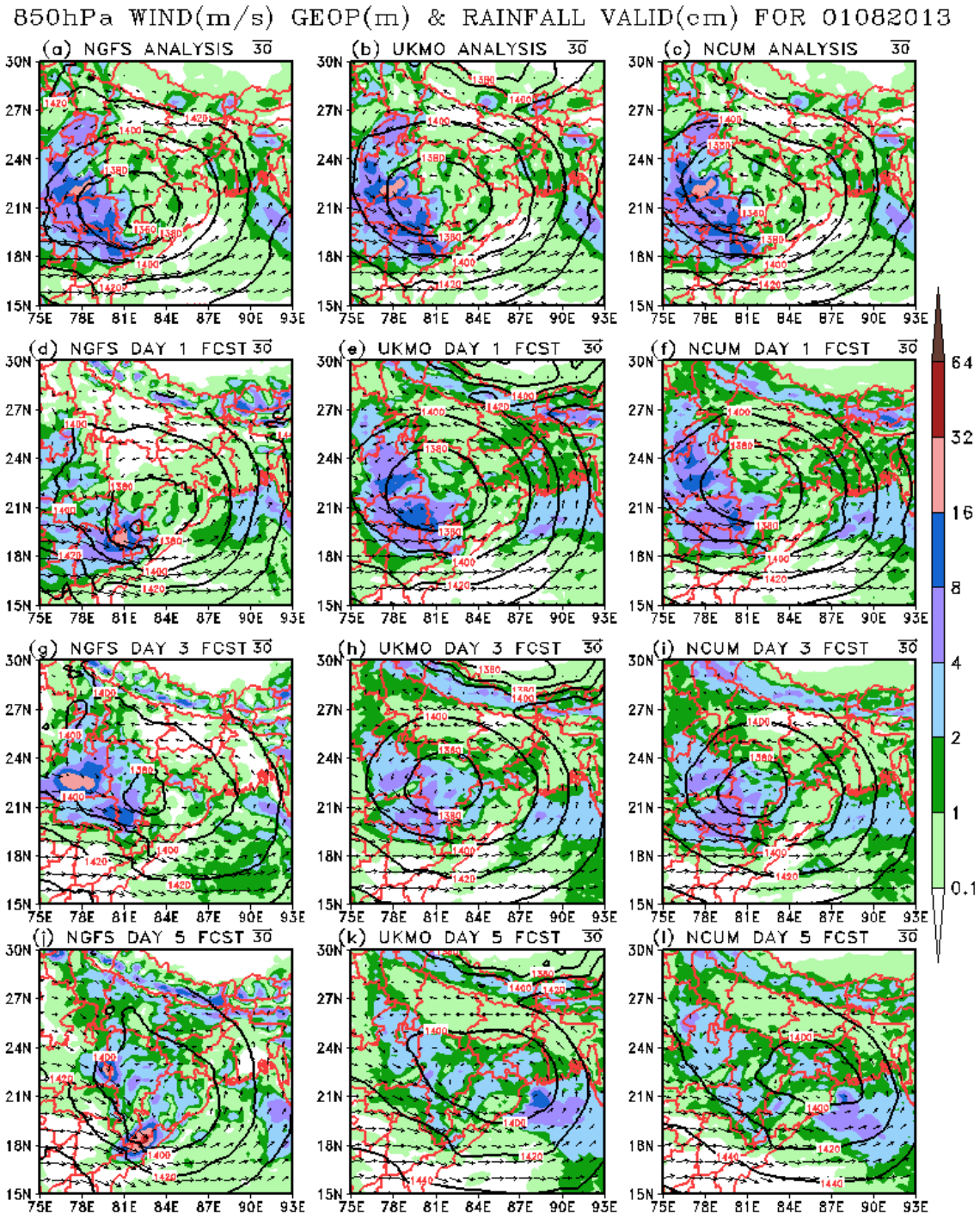

Figure 1: Winds and Geopotential height at 850 hPa of the model analysis along with observed rainfall (24 hour accumulated) valid for 00 UTC of 1st August 2013 from (a) NGFS (b) UKMO and (c) NCUM. Day-1 (d-f), Day-3 (g-i) and Day-5 (j-l) forecast of wind and geopotential at 850 hPa along with the rainfall forecast from the three models valid for the same day

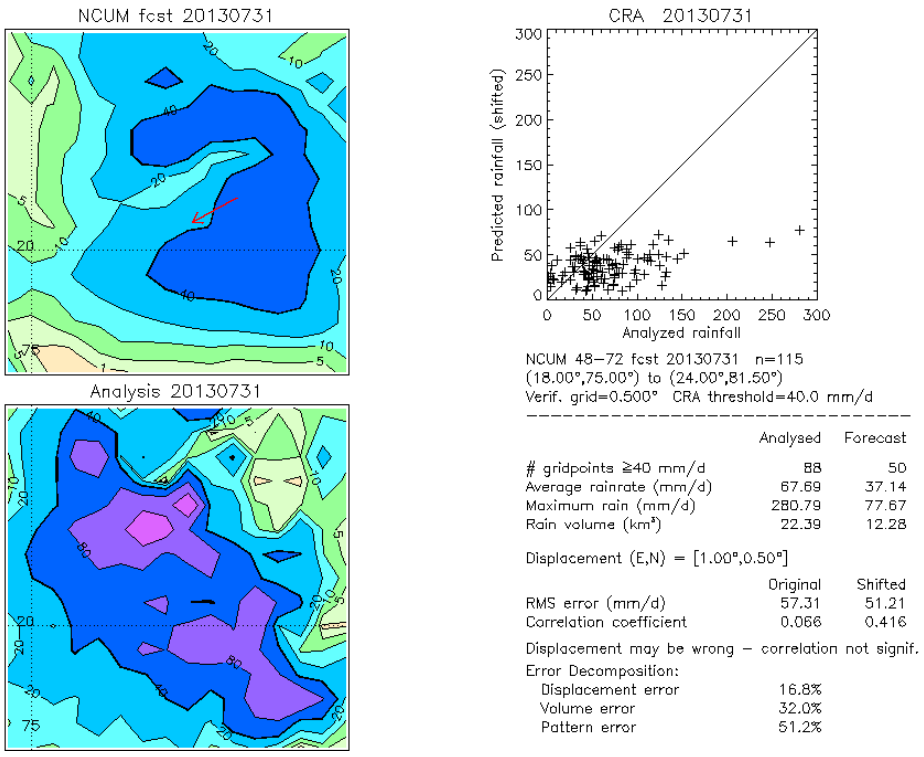

Figure 2a: CRA analysis of Observed and NCUM Day-3 rainfall forecast valid for 1st August 2013

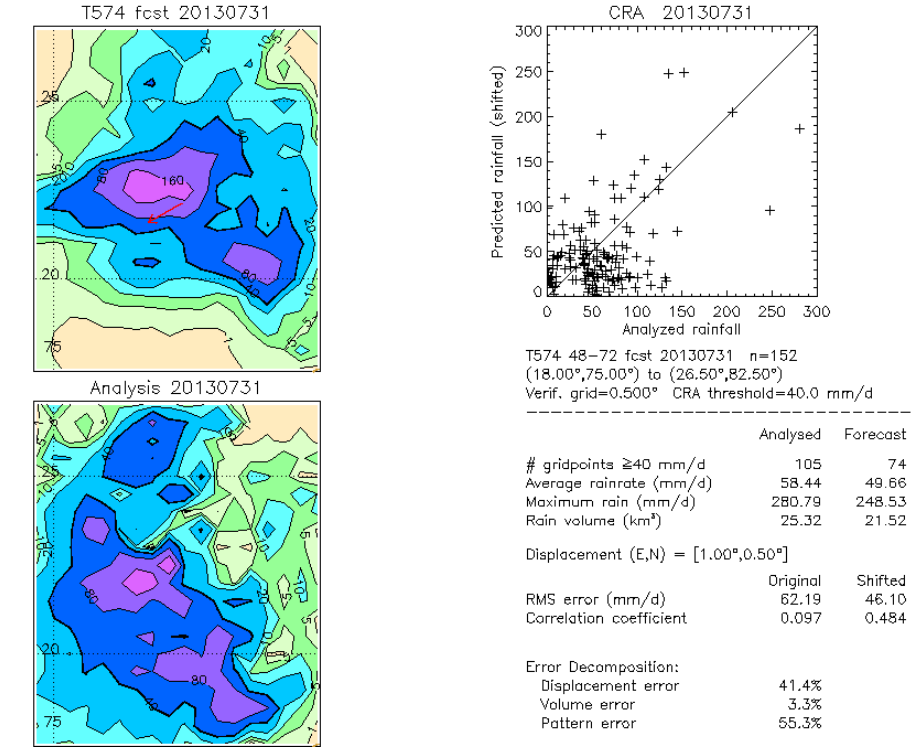

Figure 2b: CRA analysis of Observed and NGFS Day-3 rainfall forecast valid for 1st August 2013.

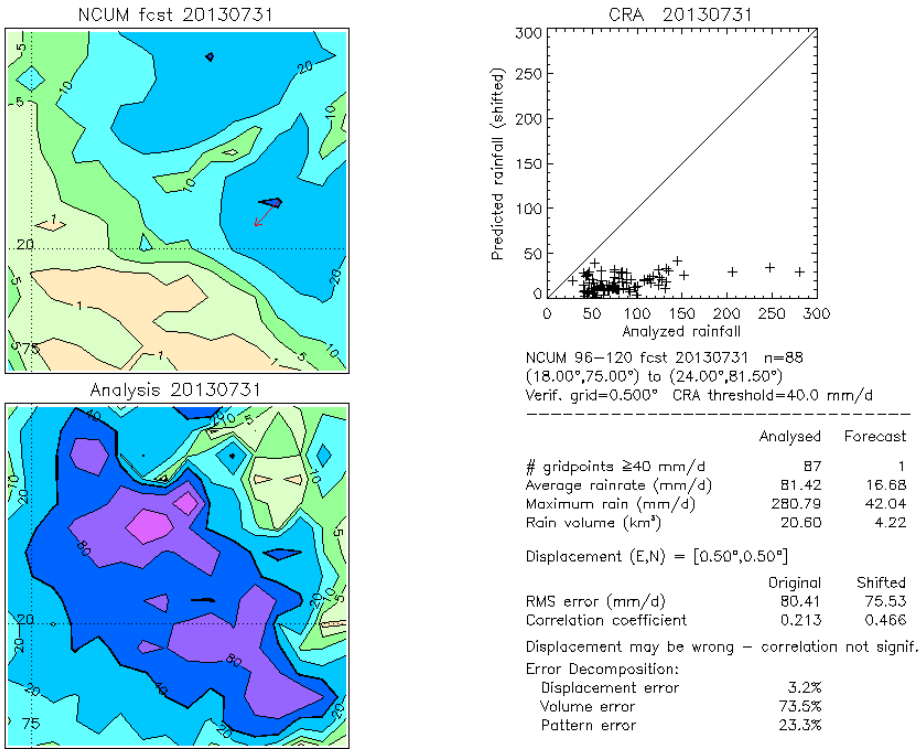

Figure 3a: As in Figure 2a but for Day-5 forecast valid for 1st August 2013

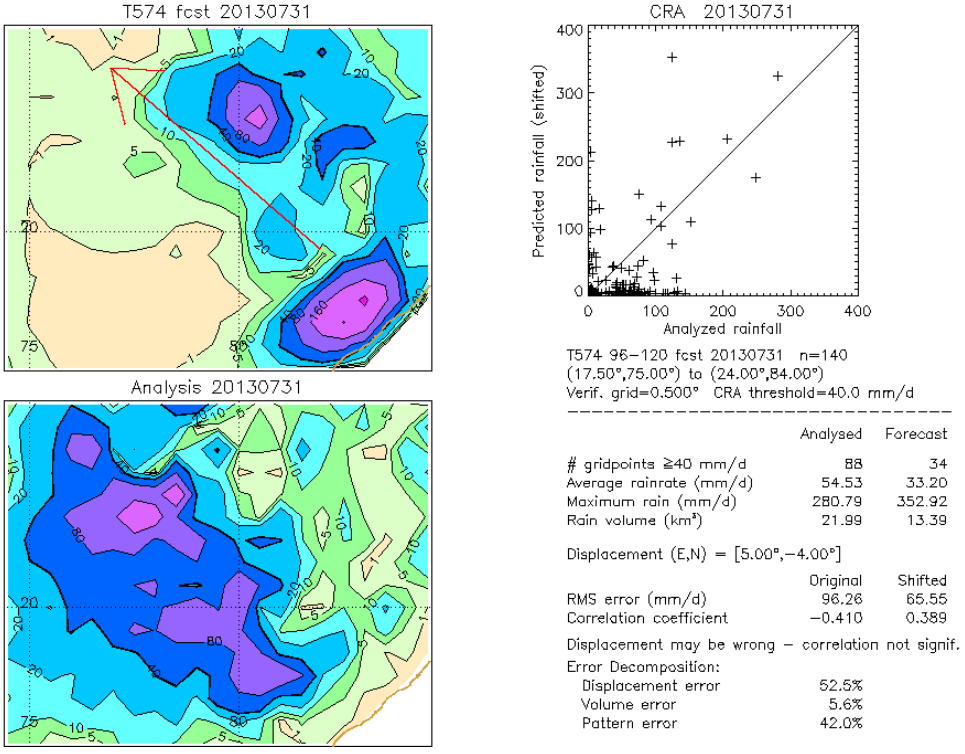

Figure 3b: As in Figure 2b but for Day-5 forecast valid for 1st August 2013

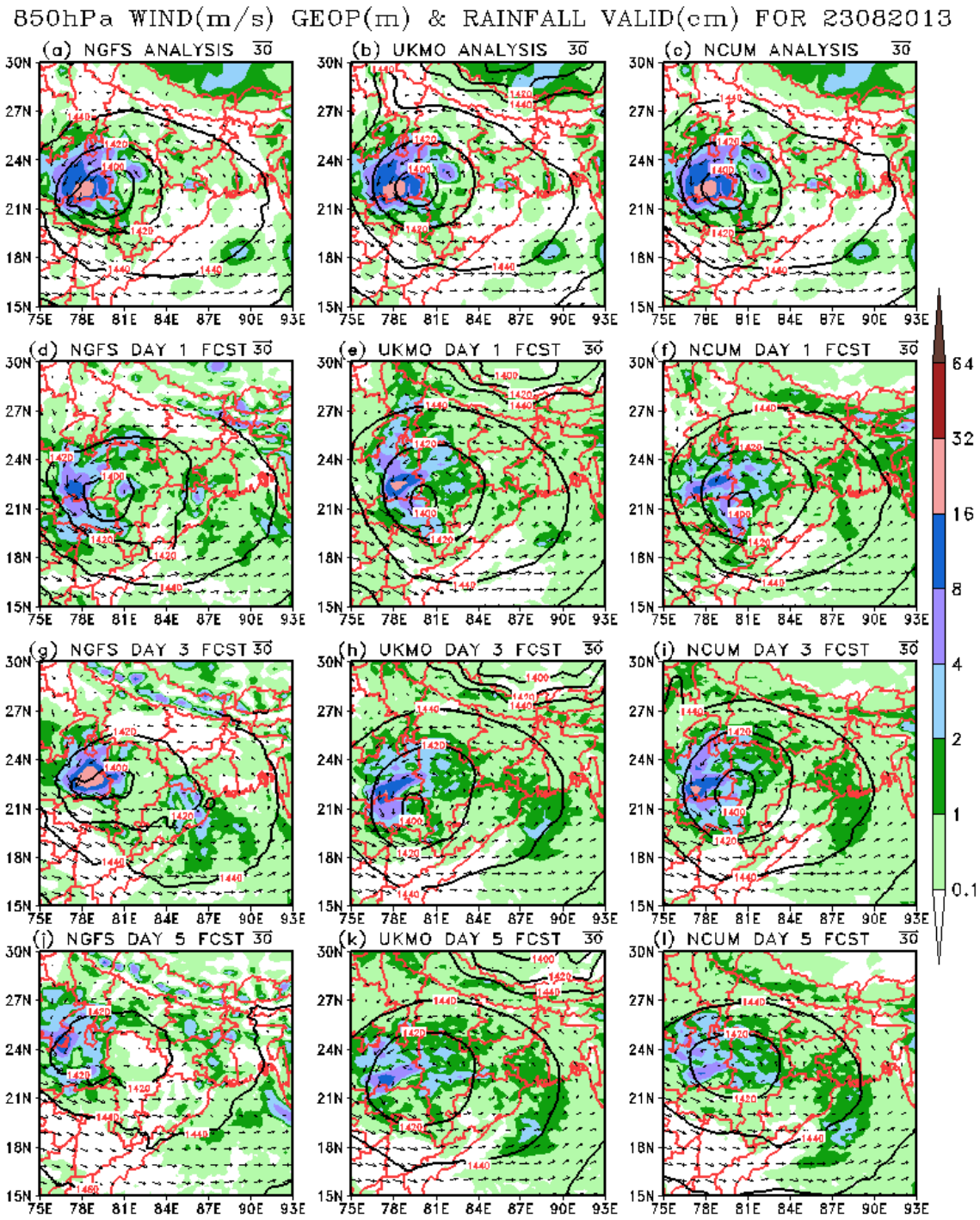

Figure 4: As in Figure 1 but for 23rd August 2013

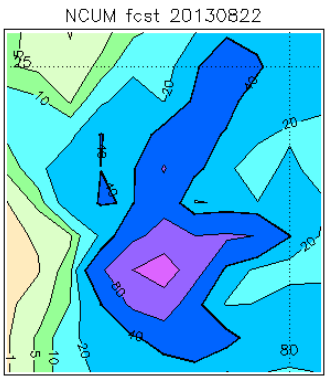

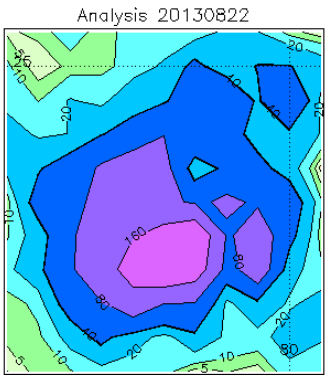

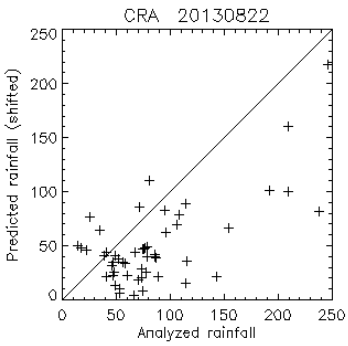

NCUM 48–72 fcst 20130822 n=52
(21.00°,76.00°) to (25.00°,80.00°)
Verif. grid=0.500° CRA threshold=40.0 mm/d

	Analysed	Forecast
# gridpoints ≥40 mm/d	46	27
Average rainrate (mm/d)	84.36	50.07
Maximum rain (mm/d)	245.64	217.28
Rain volume (km³)	12.44	7.38

Displacement (E,N) = [0.00°,0.00°]

	Original	Shifted
RMS error (mm/d)	52.41	52.41
Correlation coefficient	0.662	0.662

Displacement may be wrong – correlation not signif.

Error Decomposition:

Displacement error	0.0%
Volume error	42.8%
Pattern error	57.2%

Figure 5a: As in Figure 2a but for Day-3 forecast valid for 23rd August 2013

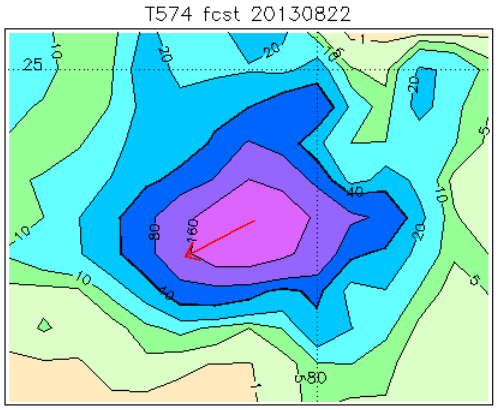

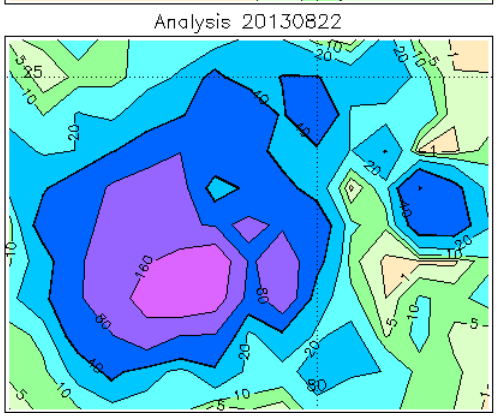

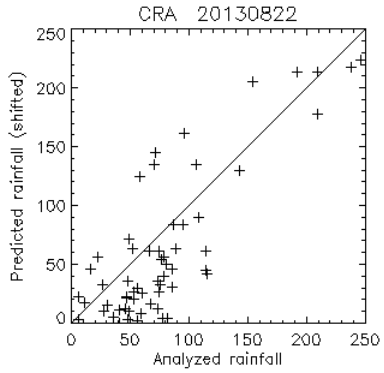

T574 48–72 fcst 20130822 n=60
(21.00°,76.00°) to (25.00°,82.00°)
Verif. grid=0.500° CRA threshold=40.0 mm/d

	Analysed	Forecast
# gridpoints ≥40 mm/d	51	29
Average rainrate (mm/d)	78.36	60.93
Maximum rain (mm/d)	245.64	223.42
Rain volume (km³)	13.33	10.37

Displacement (E,N) = [1.00°,0.50°]

	Original	Shifted
RMS error (mm/d)	76.11	39.56
Correlation coefficient	0.172	0.824

Error Decomposition:

Displacement error	73.3%
Volume error	5.1%
Pattern error	21.6%

Figure 5b: As in Figure 2b but for Day-3 forecast valid for 23rd August 2013

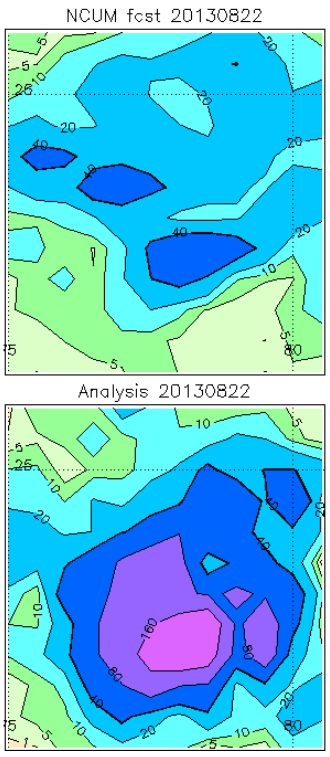

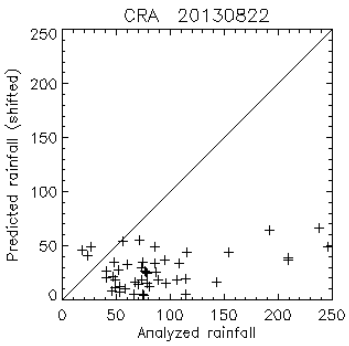

NCUM 96–120 fcst 20130822 n=49
(21.00°,75.50°) to (25.50°,80.00°)
Verif. grid=0.500° CRA threshold=40.0 mm/d

	Analysed	Forecast
# gridpoints ≥40 mm/d	46	11
Average rainrate (mm/d)	87.77	27.41
Maximum rain (mm/d)	245.64	66.24
Rain volume (km³)	12.17	3.80

Displacement (E,N) = [0.00°,0.00°]

	Original	Shifted
RMS error (mm/d)	77.18	77.18
Correlation coefficient	0.409	0.409

Displacement may be wrong – correlation not signif.

Error Decomposition:

Displacement error	0.0%
Volume error	61.2%
Pattern error	38.8%

Figure 6a: As in Figure 5a but for Day-5 forecast valid for 23rd August 2013

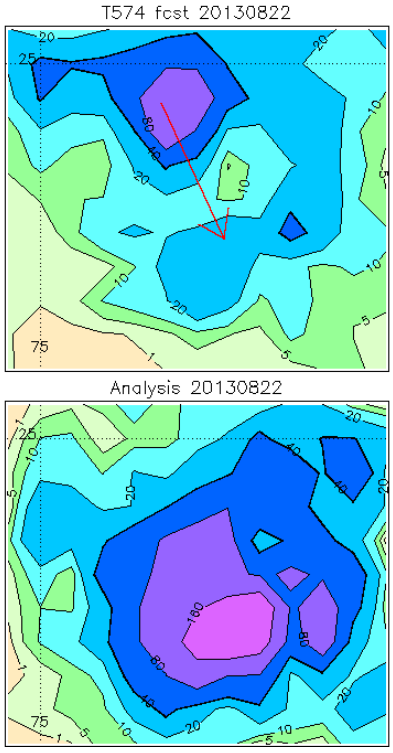

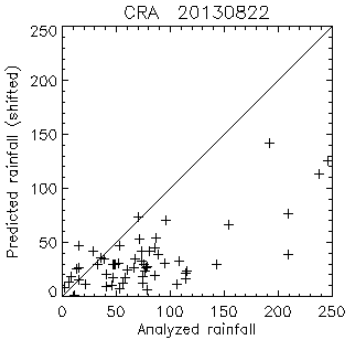

T574 96–120 fcst 20130822 n=60
(21.00°,75.00°) to (25.00°,80.00°)
Verif. grid=0.500° CRA threshold=40.0 mm/d

	Analysed	Forecast
# gridpoints ≥40 mm/d	46	15
Average rainrate (mm/d)	74.79	33.75
Maximum rain (mm/d)	245.64	141.59
Rain volume (km³)	12.72	5.74

Displacement (E,N) = [−1.00°,2.00°]

	Original	Shifted
RMS error (mm/d)	80.59	57.79
Correlation coefficient	−0.293	0.703

Error Decomposition:

Displacement error	46.8%
Volume error	27.9%
Pattern error	25.3%

Figure 6b: As in Figure 5b but for Day-5 forecast valid for 23rd August 2013

Appendix-I

Standard Verification Scores for Rainfall Forecasts (deterministic)

	Forecast yes	***Forecast no***	***Total(o)***
Observed yes	***a [hit]***	***c [misses]***	***a+c***
Observed no	***b [false alarm]***	***d [correct negatives]***	***b+d***
Total(f)	***a+b***	***c+d***	***Total =a+b+c+d***

(a) Accuracy (fraction correct)*: Accuracy= (a+d)/(a+b+c+d)*

It gives the overall fraction of correct forecasts. It ranges from 0 to 1. The perfect score is 1. While being simple and intuitive, this score is heavily influenced by most common category (no rain).

(b) Success Ratio (SR): *SR= a/(a+b)*

It gives the fraction of forecast yes events that realized. It ranges 0 to 1. The perfect score is 1.

(c) Probability of Detection (POD): *POD=a/(a+c)*

It is the fraction of observed events that were correctly predicted. It ranges 0 to 1. The perfect score is 1.

(d)False Alarm Ratio (FAR): *FAR=b/(a+b)*

It is the fraction of forecast events that were observed to be non-event. It ranges from 0 to 1 and the perfect score is 1.

(e)Bias Score (BIAS): *BIAS=(a+b)/(a+c)*

Also called the *frequency bias*, it is the ratio of forecast rain frequency to observed rain frequency. It ranges from 0 to ∞ the perfect score being 1. This score measures the ratio of the frequency of forecast events to the frequency of observed events. Indicates whether the forecast system has a tendency to underforecast (*BIAS*<1) or overforecast (*BIAS*>1) events. Does not measure how well the forecast corresponds to the observations, only measures relative frequencies

(f)Equitable threat score (Gilbert skill score): It is the fraction of all events forecast and/or observed that were correctly diagnosed, accounting for the hits that would occur purely due to random chance.

$$ETS = \frac{(a - arandom)}{(a + b + c - arandom)}$$

where $$arandom = \frac{1}{n[(a+b)(a+c)]}$$

(g) Hansen and Kuipers Score (HKScore): *HKScore =[a/(a+c)]-[b/(b+d)]*

Also called the True Skill Score (TSS) and Peirce Skill Score (PSS), it ranges form -1 to 1 with 1 as perfect score and 0 indicating no skill. Uses all elements in contingency table and does not depend on climatological event frequency. The expression is identical to *HK = POD - POFD*, but the Hanssen and Kuipers score can also be interpreted as *(accuracy for events) + (accuracy for non-events) - 1*.

(h) Extreme Dependency Score (EDS): *EDS= 2log[(a+c)/total]/log[a/total]*

This score gives the association between forecast and observed rare events. It ranges from -1 to 1 with 0 meaning no skill and 1 meaning perfect score.

(i) Probability of False Detection (POFD): *POFD= b/(b+d)*

It gives the fraction of observed ‘no’ events that were incorrectly predicted as ‘yes’ events. POFD ranges from 0 to 1 with 0 as perfect score.

(j) Odd Ratio (OR) *: OR = [(a*d)/(b*c]*

This score is the ratio of the odds of a "yes" forecast being correct, to the odds of a "yes" forecast being wrong. It ranges from 0 to ∞ with 1 indicating no skill and ∞ indicating perfect score.

(k) Odd Ratio Skill Score (ORSS)*: ORSS=[(a*d)-(b*c)]/[(a*d)+(b*c)]*

ORSS gives improvement of forecast over random chance. It ranges from -1 to 1 with 0 indicating no skill and 1 indicating perfect score.